EVALUATING THE EFFECT OF EARTHQUAKES ON OPEN PIT MINE SLOPES

by

Amin Azhari

A thesis submitted to the Faculty and the Board of Trustees of the Colorado School of Mines in partial fulfillment of the requirements for the degree of Doctor of Philosophy (Mining and Earth Systems Engineering).

Golden, Colorado

Date _____

Signed: _____

Amin Azhari

Signed: _____

Dr. Ugur Ozbay

Thesis Advisor

Golden, Colorado

Date _____

Signed: _____

Dr. Priscilla Nelson

Professor and Head

Department of Mining Engineering

ABSTRACT

Among a few earthquake-induced failure instances in open pit mine slopes, none were significant enough to be recorded as causing operational interruptions or injuries. However, there have been a significant number of intense earthquake-triggered natural slope and tailing dam failures which caused serious damages, injuries and death. This research addresses this dichotomy through studies of earthquakes and associated geological parameters on 177 open pit mines, 95 natural slope failures and 37 tailing dam failures, all over the world. The earthquake parameters include magnitude, epi-central distance, focal depth and intensity, while the geological characteristics considered include failure type, water condition, rock type and topography. After analyzing these parameters, it was concluded that the natural slope failures are triggered mainly by earthquakes with depths and epi-central distances of less than 40 and 100 kilometers, respectively. Only 7 open pit mines in this study were subjected to such earthquakes. Studying the earthquake intensity shows that only 20 mines were subjected to shaking intensities of more than 6.0 in the last 25 years, while for natural slopes and tailing dam failures almost 90 percent were subjected to this range of intensities. Among the geological characteristics, water condition, failure type and topographical effect were found to separate open pit mines from the failed natural slopes and tailing dams due to earthquakes. Particularly, water condition plays a role in nearly all of the natural slope failures and obviously in all tailing dam failures, while open pit mines are relatively less affected due to natural or mechanical dewatering. Most recorded natural slope failures are shallow, which are not considered reportable in open pit mines, unless they cause injury or intense property loss. Natural slope failures are commonly triggered on the hill tops and ridges as a result of a topographical amplification phenomenon, while the absence of this effect due to one-face or valley-shape pit slopes increases the pit slope stability. The top soil layer of natural slopes and the unconsolidated layer of tailing dams are widely subjected to stiffness contrast amplification, whereas pit slope surfaces are frequently cut which reduces this effect. Numerical analyses performed in this research show that the topographical amplification on hill-shaped natural slopes is up to 4 times that of pit slopes. The coupled effect of topography and stiffness contrast may increase the amplification factor to 8 for the top soil layer of natural slopes compared to competent pit slopes.

This research shows that the effect of earthquakes on open pit mines cannot be ignored due to the limited number of endured open pit mines in the vicinity of strong earthquakes. However, site characteristics of pit slopes make them less likely to fail compared to natural slopes and tailing dams.

TABLE OF CONTENTS

LIST OF FIGURES

LIST OF TABLES

LIST OF SYMBOLS

Richter magnitude …….....M

Richter local magnitude ……ML

Modified Mercalli intensity …….....MM

Initial wave angle (degrees) ……i

Reflected/refracted wave angle (degrees) ……..i’

Initial wave velocity ……V1

Reflected/refracted wave angle ……...V2

Factor of safety ……FS

Cohesion (Pa) ……c

Area of sliding ……...……A

Weight (N) ……..……..W

Angle of sliding plane (degrees) ……ψ

Friction angle (degrees) ……φ

Earthquake horizontal acceleration (m/s^2) ……α

Earthquake vertical acceleration (m/s^2) ……β

Water pressure on sliding surface (Pa) ……...u

Water pressure on tension crack (Pa) ……..v

Critical acceleration (m/s^2) …….....ac

Acceleration (m/s^2) ……..a

Gravitational acceleration (m/s^2) ……g

Upstream tailing dam construction method …….UP

Downstream tailing dam construction method ……DS

Centerline tailing dam construction method ……CL

Epi-central distance (km) ……...Δ

Focal depth (km) ……h

Statistical constants for intensity calculations ……b, v, and c

Earthquake intensity (MM) ……*Ii*

Average shear velocity is measured down to 30 meters (m/s) ……...Vs^{30}

Shear wave velocity (m/s) ……...*C_s*

Maximum frequency (Hz) ……*f_max*

Maximum mesh dimension (m) ……*l_max*

Young's modulus (MPa) ……E

Shear modulus (MPa) ……G

Bulk modulus (MPa) ……K

Density (kg/m^3) ……ρ

Poisson's ratio ……*v*

ACKNOWLEDGMENTS

Firstly, I would like to express my sincere gratitude to my advisor Prof. Ugur Ozbay for the continuous support and motivation towards my doctoral studies, and sharing portion of his immense knowledge and experience with me. He guided me carry out my research and helped me conclude my doctorate as this thesis. I could not have imagined having a better advisor and mentor for my graduate studies. Also, I'd like to thank him for giving me an opportunity to work with him as a teacher assistant which was a remarkable learning experience for more than 4 years.

Furthermore, I'd like to thank rest of my thesis committee members: Prof. Vaughan Griffiths, Dr. Hugh Miller, Dr. John Grubb and Dr. Jurgen Brune for their discerning comments which encouraged me to widen my research perspectives.

I don't want to forget my colleagues, Mahmood Arshad, Ryan Garvey, Zoheir Khademian, and Eric Poek for the stimulating discussions we have had in the last four years. Also I would like to thank my dear friends Mohammad Barani, Soroush Shahabi and Seyed Mohammad MirMoezi who helped me in editing and generating figures of this thesis.

Last but definitely not the least, I would like to thank my family: my wife, Rezvan Sadat, who provided a nourishing environment for me to focus on my school while she was missing her family back home. My parents and my sisters were always with me spiritually throughout this journey. My mother-in-law, father-in-law and sisters-in-law for their spiritual support and prayers. My children Zoha and Taha, without whom I cannot imagine my life being so charmingly beautiful, their endearing souls gave me fortification during challenging times.

To my wife, Rezvan Sadat, who has been a constant source of support and inspiration during the challenges of graduate life. I am truly gratified for having you in my life. This work is also dedicated to my parents, Mojtaba Azhari and Maryam Ghodsi, who have always loved me unconditionally and whose good examples have taught me to work hard for the things that I aspire to achieve.

CHAPTER 1

INTRODUCTION

1.1 Motivation for Research

Stability of natural and man-made rock slopes during earthquakes is always a great concern for rock mechanic engineers. Natural slopes are usually stable when they are not disturbed by an external force. However, there are a significant number of instances where failures occurred on natural slopes during seismic activities [1-3]. Although most of these failures are reported to be in a small scale, there were a few cases in which large volumes of rock and soil are involved in the failure that could be a high threat to both buildings and life. Stability of man-made slopes excavated for highways, dams, open pit mines and power plants during earthquakes is also important in civil and mining engineering projects. Tailing dams as one type of the man-made slopes built close to open pit mines, are frequently disturbed by earthquakes due to liquefaction. The failure of tailing dams could lead to significant environmental issues. Stability of open pit mine slopes is crucial for economic and safety concerns, due to the presence of miners, expensive equipment, and production requirements in the mining process. In contrast with natural slopes and tailing dams, none of the earthquake activity observations on open pit mine slopes has been reported as significant interruption to the mining operation or a cause for a serious injury. This dichotomy raises a remarkable question "Why are open pit mine slopes considerably less likely to get affected by earthquakes, whereas a significant number of natural slopes and tailing dams failed?" Is it because the earthquakes in the vicinity of open pit mines were not strong enough to cause failure compared to those in the vicinity of natural slope? Or are there geological and

geomechanical parameters that make open pit mines more stable during earthquakes?" Although there was no reported failure so far in open pit mines, considering the effect of earthquakes on pit slopes should not be ignored due to new mining conditions. As such, advancements in monitoring systems allow the open pit designers to plan deeper and steeper pits, especially in large and deep porphyry deposits mostly located around subduction zones with high seismic activities [4]. These designs lead to lower safety factors in which a small external force (i.e. earthquake) could bring the safety factor to less than 1.0 and cause failures. Moreover, the new mining methods like highwall mining extend the final pit slope life which increases the probability of seismic activities during their life time [1, 2]. These circumstances cause debates about the necessity of performing seismic analysis for open pit slope stability [2]. In his 2016 study, Lorig addressed the effect of earthquakes on open pit mines compared to natural slopes using numerical analysis on the effect of topography and stiffness contrast as the two site effects [1]. However, the effect of earthquake parameters (i.e. epi-central distance and focal depth) and other geological and geomechanical parameters were not taken into account in his study. As according to previous studies there are two sets of parameters involved in earthquake triggered natural slope failures; internal parameters named as site characteristics; and external parameters known as earthquake parameters [5-18]. Keefer and Bommer studied the effect of earthquake parameters such as epi-central distance and focal depth on several historical natural landslides during earthquakes [3, 5]. They found a meaningful correlation between the failure intensity and earthquake epi-central distance, magnitude and focal depth in which larger, closer and shallower earthquakes trigger larger landslides. The effect of site characteristics on seismic stability of slopes is also investigated by several researchers [8-16]. Havenith et al. studied the role of site effects in the rockslide triggered by an earthquake in 1911. His study shows that the greater ground amplification on the crest region

and the presence of the surficial low-velocity layer were the two key factors controlling the ground motion of the landslide [9]. McColl et al. deliberate the effect of stiffness contrast in glacial slopes using numerical analysis. He showed the increase in the topographical amplification on glacial erosion and deglaciation compared to ice capped slopes due to lower stiffness contrast of the former [14]. Gouveia et al. conducted a study on the effect of stiffness contrast on non-horizontal layered grounds using numerical analysis. The study shows that the amplification factor on dipped top soil layer is even more than horizontal layers [15]. The effect of water presence on the slope performance during seismic events was studied by Biscontin et al. [18] and Strasser et al. [19]. These studies show the excess pore pressure caused by seismic waves lowers the safety factor compared to the static safety factor [18, 19]. Derived from these studies, among site characteristics, water condition, topography and material stiffness contrast, are the two main geological dissimilarities of natural slopes and tailing dams against open pit mines. There are two commonly used approaches on the stability of slopes during earthquakes named Pseudo-static and Newmark's method which are not able to realistically model the effect of these factors. These two methods are subjected to significant limitations and simplifications which makes them inappropriate to analyze complex slope conditions [1, 20, 21]. As such, Pseudo static as a quasi-static approach assumes earthquake shaking as a unidirectional permanent body force acting only in the direction that increases the slope instability leading to conservative design. The Newmark's method considers the landslide as a rigid-plastic body force with no internal deformation sliding only downward at constant stress along a discrete basal shear surface when exceeding the constant critical acceleration. These limitations encourage the use of numerical analysis (i.e. distinct element method), with the capability of analyzing complex slope geometries and mechanical properties by

applying more realistic earthquake characteristics, to study these site effects on the stability of the three slope types [22, 23].

1.2 Research Objectives

The objective of this research is to provide a better understanding of the earthquake effects on slope stability in open pit mines. This will be done through the studies of the mechanisms involved during natural slope and tailing dam failures, and then comparing them to the earthquake effects on the open pit mine slope stabilities. The parameters involved include earthquakes, geotechnical conditions, and geological properties. The tasks set to achieve this objective include:

- Review past research on earthquake and geomechanical parameters involved in slope stability under earthquake loads,
- Explore the analytical and numerical methods on analyzing the stability of slopes effected by earthquakes and select the most suitable one,
- List and map all historical natural slope and tailing dam failures impacted by earthquakes,
- List and map all large open pit mines around the world,
- Map and study the characteristics of all the earthquakes triggered natural slope and tailing dam failures and those in the vicinity of open pit mines during their life time,
- Geological and geomechanical properties of earthquake-triggered natural slope and tailing dam failures,
- Study the earthquake parameters in the vicinity of open pit mines, such as epi-central distance and intensity using their location on the map,

- Compare the mechanisms involved in triggering earthquakes in natural slopes and tailing dams against those in open pit slopes,
- Compare the geological and geomechanical parameters of natural slope and tailing dam failures against withstood open pit mines due to earthquakes,
- Use discrete element method to study the most effective geological and geomechanical parameters, topographical and stiffness contrast effects, known as site effect factors, and
- Summarize findings of the dissertation and provide recommendation for future work.

1.3 Thesis Overview

Chapter 2 presents a review on earthquake, geological and geomechanical parameters involved in slope failures during earthquakes, including their failure mechanisms and types. In addition, this chapter investigates the analytical and numerical methods on analyzing the stability of slopes under earthquake loads along with their advantages and limitations.

Chapter 3 includes a comprehensive database developed on natural slope and tailing dam failures along with the large open pit mines all over the world. This database contains the location, earthquake parameters, and geological and geomechanical properties of triggered natural slope and tailing dam failures along with earthquake parameters in the area of endured open pit mines and their locations. The earthquake parameters include earthquake depth, epi-central distance, magnitude and intensity. The geological and geomechanical parameters are slope angle, water condition, failure mode and mechanism.

The database presented in Chapter 3 is studied and analyzed in Chapter 4. In this study, the earthquake, geological and geomechanical parameters involved in natural slope and tailing dam

failures are compared with those in open pit mine slopes. This comparison is illustrated by presenting graphs and tables to show the effectiveness of each parameter on stability of natural slopes and tailing dams during earthquakes and their presence and role in open pit mine slopes.

Chapter 5 analyses the two most effective geological and geomechanical properties involved in slope failures subjected to earthquakes, called topographical and stiffness contrast effects, using discrete element method. A discrete element software, Universal Distinct Element Code (UDEC), is used for these analyses. Several models were developed to investigate the effect of these two parameters on different slope types. These models include, several topographies and different material stiffness with various slope geometries are considered in faulted and continuous slopes, representing natural slopes and open pit mines.

Chapter 6 concludes the remarks of the database investigation and numerical analysis found in Chapters 4 and 5 and presents recommendations for future work.

CHAPTER 2

AN OVERVIEW OF SLOPE AND EARTHQUAKE PARAMETERS

2.1 Introduction

To investigate the effect of earthquakes on different slope types, it is important to initially study the effective parameters involved in slope behaviour and the role of each parameter in stability of slopes in response to earthquakes. This chapter gives an overview on the parameters governing the effect of earthquakes on different types of slopes and their consequences. The effect of earthquakes and their consequences may vary according to different slopes resulting in different types of failure modes due to the slope characteristics and earthquake parameters. First, the different earthquake-triggered failure modes and their characteristics are described for the three slope types. The earthquake parameters associated with slope failures such as magnitude, focal depth, epi-central distance and intensity, are then reviewed. In addition to earthquake parameters, slope characteristics controlling the intensity and type of failure are investigated by considering topography, stiffness contrast, and water condition [5-17, 24, 25]. Lastly, the methods which analyze the stability of slopes under earthquake loads are described with their limitations and advantages.

2.2 Earthquake-Triggered Slope Failure Modes

Natural slopes, tailing dams and open pit mine slopes potentially may fail in different modes during earthquakes. Natural slopes have the most variety of failure modes due to wide range of geological and geomechanical properties [3, 5, 26]. However, on man-made slopes, such as open pit mine slopes and tailing dams, failure modes are less variable because the materials

involved are relatively limited compared to natural slopes. For instance, tailing dam response to earthquake is mostly limited to liquefaction and soil slide [27, 28]. The definition of failure in open pit mines is different with respect to other slopes. Reportable failures in open pit mines are those threatening safety or interrupting production. The following presents common earthquake-triggered failure modes for natural slopes, tailing dams and open pit mine slopes, and involved earthquake parameters.

2.2.1 Natural Slopes

Natural slopes fail in various modes during earthquakes. Keefer studied the failure modes and geological characteristics of natural slopes during earthquakes [26]. His study presents a summary of landslide characteristics and their relationship with the geological environment of these slopes (Table 2-1).

Table 2-1 Summary of landslide characteristics and their relation with geological environment of the slopes [26].

	Name	Type of Movement	Magnitude	Abundance[1]	Slope	Depth
Disrupted Landslides	Rock Falls	Bouncing, rolling, free fall	$M_L \geq 4.0$	Very Abundant	>40º	Shallow
	Disrupted Rock Slides	Translational sliding	$M_L \geq 4.0$	Very Abundant	>35º	Shallow
	Rock Avalanches	Complex, involving sliding, flow, and occasionally free fall	$M_L \geq 6.0$	Uncommon	>25º	Deep
	Soil Falls	Bouncing, rolling, free fall	$M_L \geq 4.0$	Moderately Common	>40º	Shallow
	Disrupted Soil Slides	Translational sliding	$M_L \geq 4.0$	Very Abundant	>15º	Shallow
	Soil Avalanches	Complex, involving sliding, flow, and occasionally free fall	$M_L \geq 6.5$	Abundant	>25º	Shallow
Coherent Landslides	Rock Slumps	Rotational sliding	$M_L \geq 5.0$	Moderately Common	>15º	Deep
	Rock Block Slides	Translational sliding	$M_L \geq 5.0$	Uncommon	>15º	Deep
	Soil Slumps	Rotational sliding	$M_L \geq 4.5$	Abundant	>7º	Deep
	Soil Block Slides	Translational sliding	$M_L \geq 4.0$	Abundant	>5º	Deep
	Slow Earth Flows	Translational sliding and internal flow	$M_L \geq 5.0$	Uncommon	>10º	Variable
Lateral Spreads and	Soil Lateral Spreads	Translation on fluid basal zone	$M_L \geq 5.0$	Abundant	>0.3º	Variable
	Rapid Soil Flows	Flow	$M_L \geq 5.0$	Moderately Common	>2.3º	Shallow
	Subaqueous Landslides	Generally lateral spreading or flow; occasionally sliding	$M_L \geq 5.0$	Uncommon	>0.5º	Variable

Note: Shallow ≤3 m, Deep > 3m Very abundant: > 100,000 – Abundant: 10,000 to 100,000 – Moderately Common: 1,000 to 10,000 – Uncommon: 100 to 1,000 in the 40 historical earthquakes.

This classification divides failures into disrupted landslides, coherent landslides, and lateral spreads and flows. Accordingly, failures are classified considering their abundance, slope angle and depth. To visualize each type of landslides, Figure 2-1 presents a schematic view for each landslide type [28]. It is significantly useful to know the mechanism, material type and schematic view of the landslide type as each will be cited frequently in this chapter.

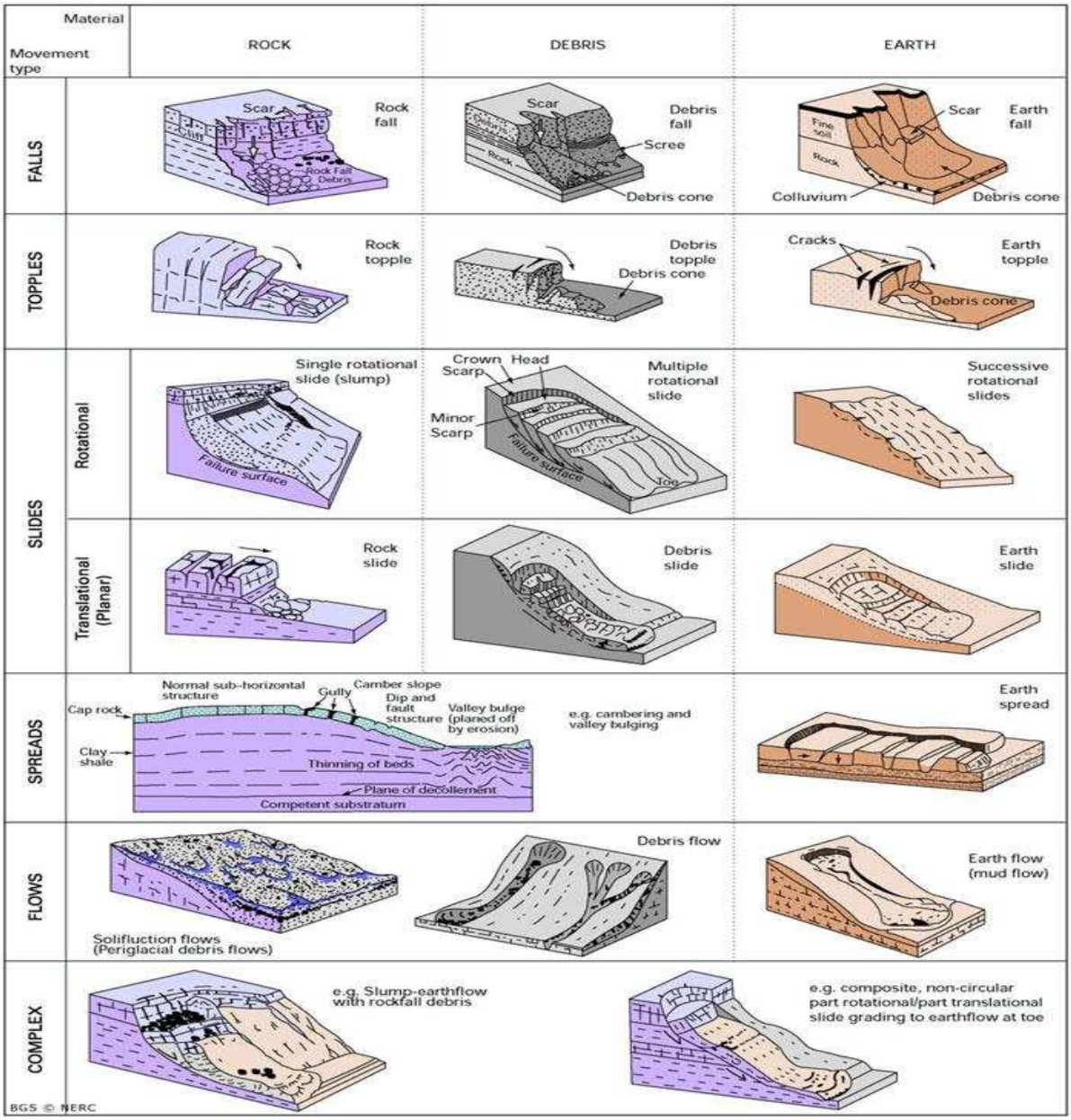

Figure 2-1 Schematic view of failure modes in natural slopes [28].

According to Keefer and Boomer [3,5], the most common failure types in earthquake-triggered natural slopes are rock falls, soil falls, rock and soil slides, rock and soil avalanches, rock and soil slumps, toppling, and soil flows [3, 5]. The main geological characteristics of earthquake-triggered failure types presented in Table 2-1 are as follows:

- **Rock Falls**

Rock falls were the most abundant failure type in 76 historical cases between 1811 and 1997 [3, 5]. The evidence collected on these 76 cases show that this failure type is primarily triggered in tuff, shale, siltstone, sandstone and conglomerate rock types. In well cemented rock masses, the rock falls are produced by closely fractured rock masses. Most of these joints are opened, weathered or filled with weak chemical-weathering material. Generally, the rock falls are triggered on steep to very steep slopes and mostly on crests, ledges and man-made cuts [3].

- **Rock Slides**

Rock slides are generally defined as disorder movements within a rock mass on planar or gently curved surfaces, like joints and bedding planes. These types of failures mostly occurred on steep to very steep slopes with the same materials as rock falls [26].

- **Rock Avalanches**

Rock avalanches are landslides that are disintegrated into streams of rock fragments that may travel on low-angle slopes. The speed of a rock avalanche often exceeds 100 km/h, and its volume is commonly greater than 1×10^6 m^3. One of the best examples of this failure type took place during the 1970 Peru earthquake. This type of failure occurs in intensely fractured slopes in which the rock is fractured by several sets of joints spaced from a few centimetres to a few

decimetres. They are less common than the other types of failures. However, if the failure occurs, it is generally deep. This failure type may occur on shallow as well as steep slopes [3].

- **Rock Slumps**

Rock slump is a coherent failure type that can be triggered by earthquakes in all types of rocks and on very shallow to very steep slopes [26]. Specifically, the rocks involved in slump failures are usually basalt with interbedded ash and breccia, pumice, andesite, granite, greenstone, slate, schist, amphibolite, shale, siltstone, and sandstone. These rocks are generally poorly cemented, closely jointed, weathered, or sheared [3].

- **Rock Block Slides**

In this failures type, relatively large blocks of rock detach and slide or fall down the slope. Rock types involved in this failure type are commonly tuff, andesite, poorly cemented pumice, weakly cemented or intensely jointed mudstone, siltstone, sandstone and shale, and can be initiated on very shallow slopes [26].

- **Soil Falls**

Soil falls were typically originated in coastal cliffs, canyon walls, terrace faces, stream and river banks, and cut slopes. Rock types involved in soil falls are generally weakly cemented sand or gravel and some occur in poorly cemented or unconsolidated clay [3]. Soil falls are often observed on steep slopes.

- **Disrupted Soil Slides**

Disrupted soil slides were reported as the most common failure types after rock falls that take place on very shallow to steep slopes [3, 26]. This type of failure is mostly common in loose, unsaturated, residual or colluvial sand with little to no clay or saturated volcanic soil consisting of alternating layers of scoriaceous gravel and sensitive clay produced by weathering of fine-grained ash [3].

- **Soil avalanches**

Soil avalanches can be initiated on moderate to steep slope angles in unsaturated sand, previous soil-avalanche deposits, and are similar to saturated volcanic soil, involved in disrupted soil slides [3, 26].

- **Soil Slumps**

Sandy flood-plain alluvium and man-made fills are dominant slope materials involved in soil slump failures in historic earthquake-triggered landslides and are usually triggered on very shallow basins [3].

- **Soil Block Slides**

The majority of material involved in soil block slides was silty or sandy flood-plain alluvium or man-made fill located on flood plains. Minor amounts of till, volcanic ash, colluvium, clayey playa sediment, lacustrine sediment, terrace gravel, sandy eolian sediment, sandy alluvial-fan sediment, and periglacial sediment, where also present in these soil block slides. Most block slides had a saturated basal shear surface due to the fact that the slides were in high water table areas. Many of the shear surfaces were nearly horizontal and almost flat [3].

- **Slow Earth Flows**

The slopes involved in slow earth flows had saturated basal shear surfaces. The slope material were mostly clayey residual soil, clayey loam, till, volcanic ash, colluvium, and older earth-flow deposits triggered mostly on very shallow slopes [3, 26].

- **Soil Lateral Spreads**

Most soil lateral spreads occurred in granular man-made fill and flood-plain alluvium along river valleys. The materials in these slopes were mostly silt, silty sand, or fine-grained sand that may fail on almost flat surfaces [3, 26].

- **Rapid Soil Flows**

Rapid soil flows typically initiate in saturated slopes, due to the combination effect of earthquakes and heavy rain falls, high water tables and/or river valleys on gentle to very steep basins [3, 26].

2.2.2 Tailing Dam Slopes

Tailing dams are built to contain waste materials from the mining process and are often designed to stand in perpetuity. A catastrophic failure of a large tailing dam usually results in significant financial liability associated with cleanup regularity consequences, social issues, and in some cases with fatalities. Earthquakes are known to have been one of the causes of tailing dam failures. The main failure mode associated with earthquakes is liquefaction due to the excess pore pressure which highly depends on the construction mode of these slopes. There are different methods of tailing dam construction which the main three types are upstream, downstream, and centerline. Figure 2-2 illustrates the schematic cross section of these three construction methods and Figure 2-3 shows the distribution of tailing dam failures from 1928 to 2000 for different dam

types [28, 29]. According to Figure 2-3, earthquakes were the second most common failure reason for tailing dams, and upstream construction method were the most failed tailing dam type. This method was basically designed for arid areas because of high susceptivity to liquefaction. Additionally, upstream embankments are not designed for active seismic areas as the risk of liquefaction increases as a result of the excess pore pressure built by dynamic loading and the insufficient compaction and improper drainage [27]. In some countries, as an example Chile, upstream construction is not permitted for this reason. Moreover, investigating tailing dams could be more important in this study because they are usually built close to the open pit mines as such would be subjected to the same seismic events.

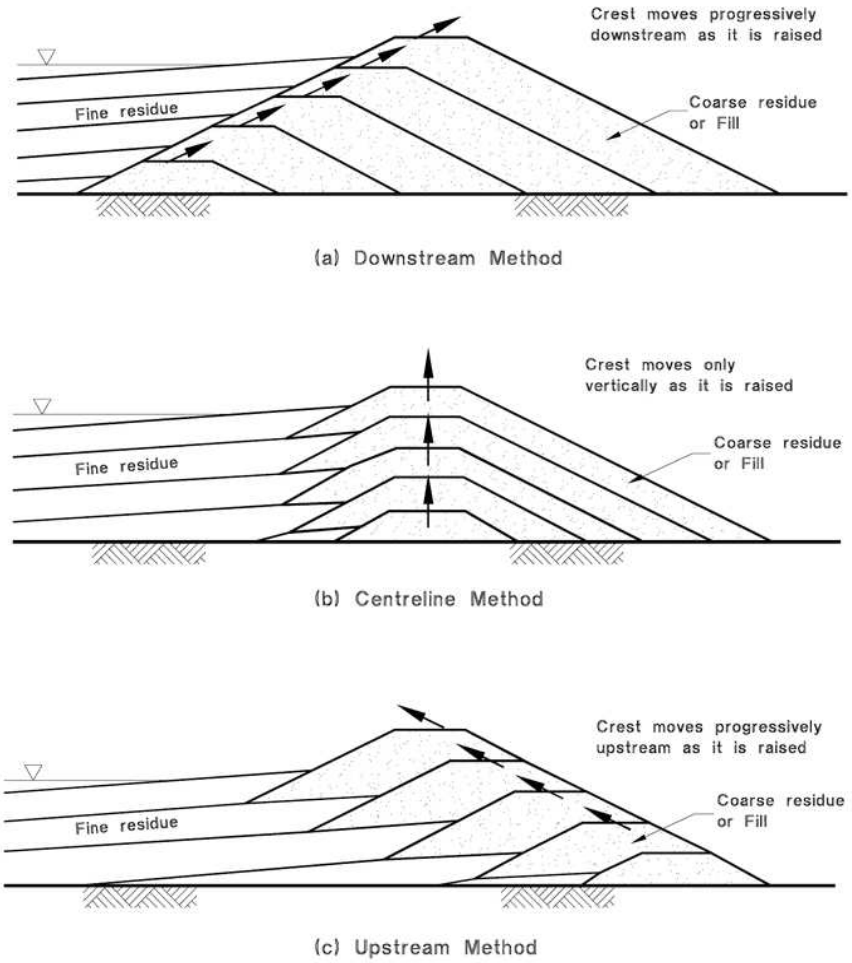

Figure 2-2 Schematic cross sections of upstream, centreline and downstream construction methods [29].

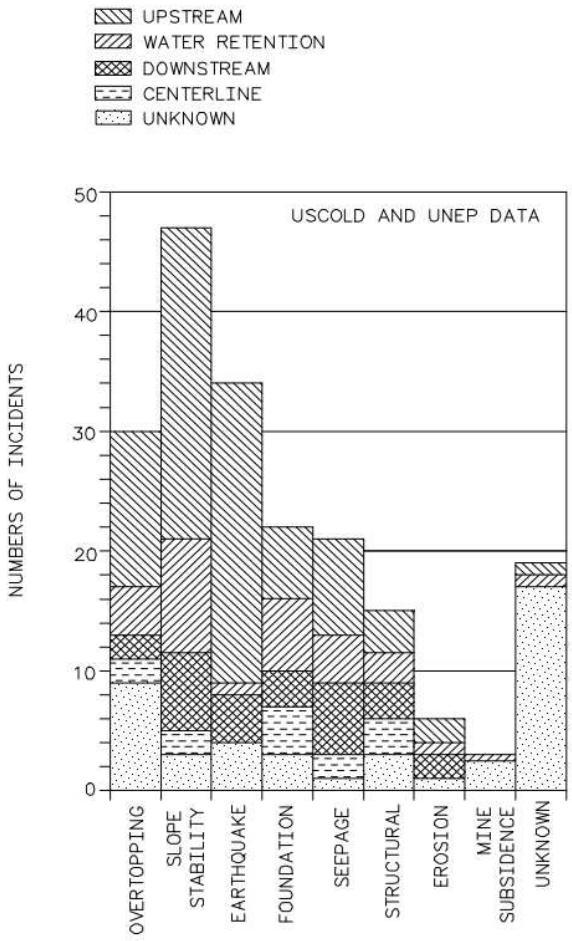

Figure 2-3 The distribution of failures for tailing dam failures from 1928 to 2000 for different dam types [28].

2.2.3 Open Pit Mine Slopes

The definition of failure in open pit mine slopes and natural slopes can be different. Not all failures in natural and civil slopes are considered as failures in open pit mines. For instance, shallow failures such as rock falls are not usually considered as "reportable" failure in open pit mines unless they fall into the "reportable" category. Generally, reportable failures are those that cause injury or interrupt the mining process and production. However, the failures triggered by earthquakes on open pit mines were mostly small scale rock falls rolling down the slope.

2.3 Earthquake Parameters Associated with Slope Failures

The earthquake parameters investigated in this study that control the effect of earthquakes on slope sites are magnitude, intensity, epi-central distance and focal depth. Figure 2-4 illustrates the schematic view of these four parameters. The influence of these parameters on slope stability is briefly discussed below.

- **Magnitude and Intensity**

Magnitude is a scale of the released energy at the earthquake source, i.e. fault or subduction plate, whereas the effect of earthquake on the slope site is defined by the earthquake intensity at the region. Earthquake Intensity depends on the location of the slope site in regards to the earthquake origin (epi-central distance) and the other two earthquake parameters, magnitude and focal depth.

- **Epi-central Distance**

Studies show that the epi-central distance has a direct effect on the shaking intensity at the slope site [30, 31]. Increase in the epi-central distance and the distance from the fault rupture decrease the shaking intensity significantly. Ghosh and Mahajan studied the intensity-epicentral relation for 14 strong earthquakes where a logarithmic relation was detected between earthquake epi-central distance and intensity (Figure 2-5) [30]. This relation shows that generally the shaking intensity decreases 50% in the epi-central distance of 100 km.

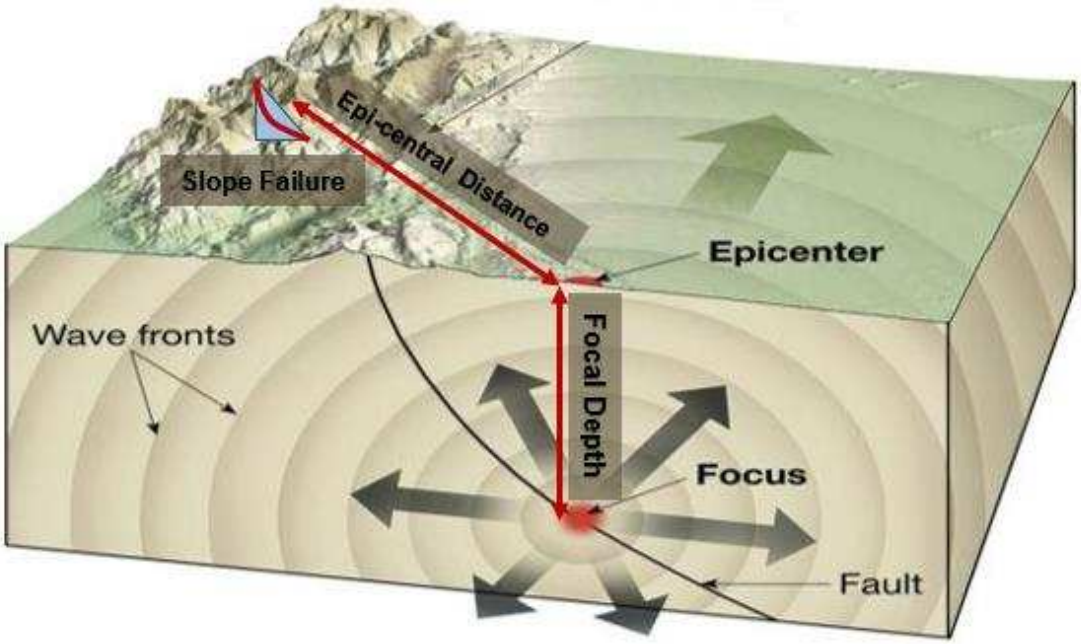

Figure 2-4 Schematic view of the earthquake parameters.

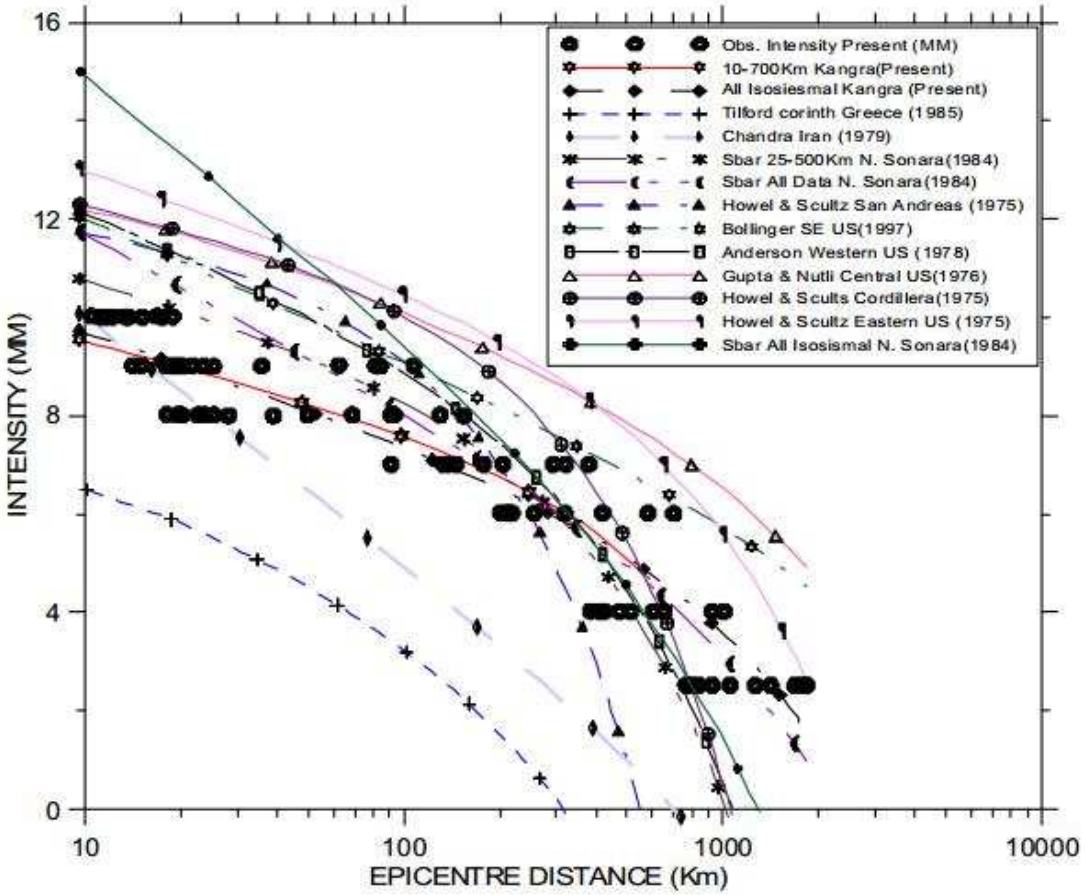

Figure 2-5 Relation between the epi-central distance and intensity (MM) for 14 strong earthquakes in different regions of the world [30].

- **Focal Depth**

Earthquakes are known to occur up to 700 km below the surface. The earthquake depth range is divided into three zones: shallow (<70 km), intermediate (70-300 km), and deep (300-700 km). Studies show that, similar to epi-central distance, focal depth has also a reverse relationship with the shaking intensity meaning that the intensity decreases by increasing in focal depth [31-33].

- **Occurrence Frequency**

One of the differences between natural slopes and open pit mines is their life time period. Table 2-2 presents typical values for the frequency of earthquake occurrence [34]. According to this table, a number of large earthquakes that may occur during natural slope life is significantly greater than the ones subjected to open pit slopes. Natural slopes are hit by numerous strong earthquakes in their life time which results in damage accumulation and gradual reduction in stability and safety factor.

Table 2-2 Frequency of earthquake occurrence in different magnitude ranges and their effects.

Magnitude	< 2.0	2.0-2.9	3.0-3.9	4.0-4.9	5.0-5.9	6.0-6.9	7.0-7.9	8.0-8.9	9.0-9.9	> 10
Frequency of Occurrence	Continual	**1,300,000** Per year	**130,000** Per year	**13,000** Per year	**1,319** Per year	**134** Per year	**15** Per year	**1** Per year	**1** per 10 years	Extremely rare (unknown/ may not be possible)

2.4 Water Condition

The presence of water has a considerable effect on the stability of slopes. Water could affect the slope stability in different ways:

- Water from rainfalls or snow melting increases the weight of the material because water is heavier than air pores of slope voids. This additional weight increases the driving force and can cause slope instability.

- Water surrounding the grain material in soil material decreases the friction contact between the grains. In this condition, the material tend to act like a fluid and can easily become a flow and make the slope unstable.

- Water affects the mechanical performance of rock structures. Water filling the fractures and joints in rock mass produces a pressure acting upward to open the discontinuity. This effect is called the effective stress law. Water, under pressure of the discontinuity, decreases the normal effective stress between the discontinuity surfaces and therefore reduces the shear strength of the discontinuity.

- Soil minerals may absorb or adsorb water. Minerals which absorb water take the water molecules into their structure. This absorbance causes an increase in the weight and, in addition to the absorption on the surface in which the friction of the grains could be lost and lead to losing the cohesion. Clay is a good example of this type of material. Figure 2-6 shows that the water absorbance of clay increases the clay weight and decreases the friction between grains.

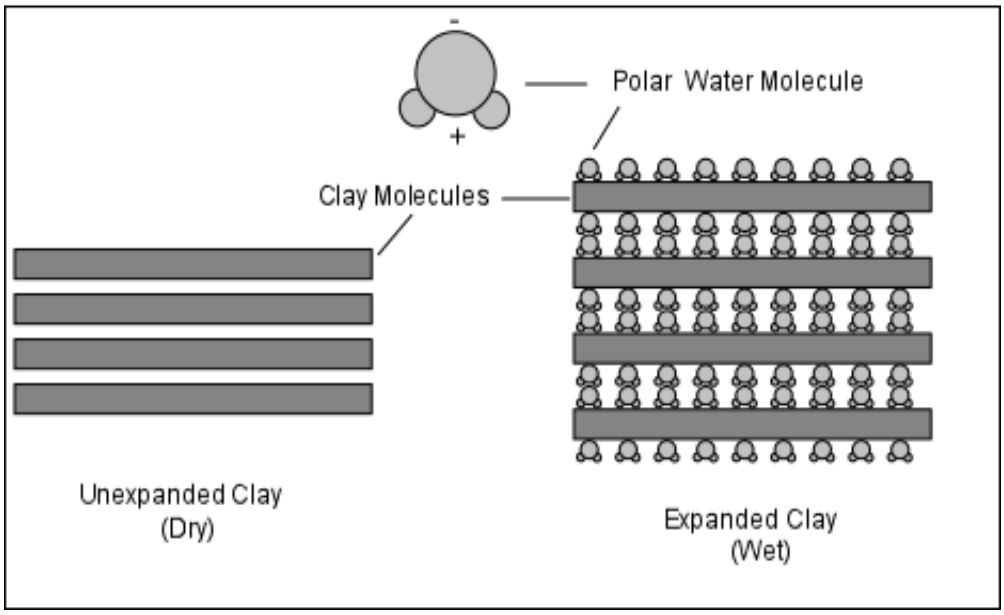

Figure 2-6 Schematic view of water absorbance in clay structure [35].

- Dissolving the mineral cement holding the material is another effect of water. Highly dissolvable materials like calcite, gypsum or halite are common cement materials. Water dissolving these material leads to cohesion reduction between material grains and makes the slope instable.

- External forces will affect the behaviour of water condition on the stability of the slopes. One of the main external forces stem from earthquakes. During an earthquake, the water pressure in the soil and rock structure will increase and this excess water pressure may cause liquefaction in the soil or decrease the effective stress on the discontinuity surfaces in the rockmass. Liquefaction is a phenomenon in which a saturated, or partially saturated, soil loses its strength and stiffness because of an external applied stress which is usually caused by an earthquake. Tailing dams commonly failed structures due to the liquefaction in response to large earthquakes. Figure 2-7 shows the difference between saturated sediment before and after an external force like earthquake that produced by a result in liquefaction [36].

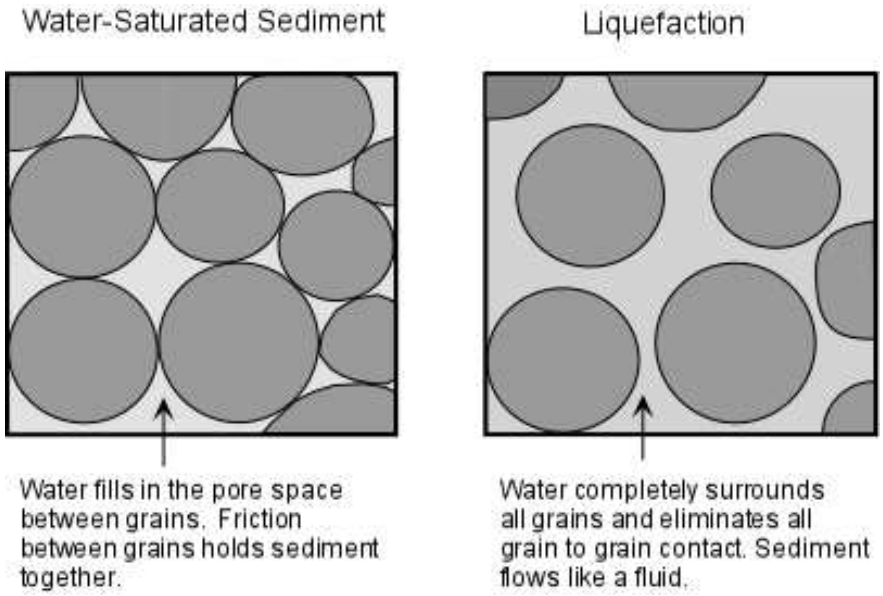

Figure 2-7 Saturated sediment before (left) and after (right) earthquake force [35].

Water plays a significant role in the instability of both natural slopes and tailing dams. Open pit mines are subjected to natural or mechanical drainage to decrease the water table level and pore pressure, and improve the pit slope stability.

2.5 Site Effects

Slope failures triggered by earthquakes, are not only dependent on the characteristics of the earthquake source such as magnitude, depth and epi-central distance, but also on the characteristics of the slope site. It has been commonly experienced that for a unique earthquake event, the shaking intensity at sites located in the same epi-central distance varies as a result of different local conditions. These local conditions are called site effects.

Topographic conditions and the stiffness contrast of the material are the two main site effects involved in the seismic stability of slopes. The field measurements show that the topography of a structure that the wave is traveling through has a significant effect on ground shaking amplification [8, 9, 11, 13]. Furthermore, the contrast in the material stiffness changes the wave characteristics traveling through the material that may amplify or reduce the shaking amplitude [9, 11, 14, 15].

2.5.1 Topographical Conditions

The surface topography is one of the important influential types of site effects. It has been observed that the power of ground shaking during earthquakes is amplified on the slope crests and steep slopes. There are three phenomena involved in the topographical site effect, including refracting and reflecting, focusing and defocusing, and seismic wave inclination.

- **Refracting and Reflecting**

When the wave travels through a material with different layers, it will be reflected or refracted [37]. Once the wave angle of the input wave is altered in the same arrival angle after it arrives at different material layer to the direction of the arrival wave it is called reflection. Whereas, if the wave passes through the next layer it is called refraction. Figure 2-8 shows a schematic view of these two phenomena.

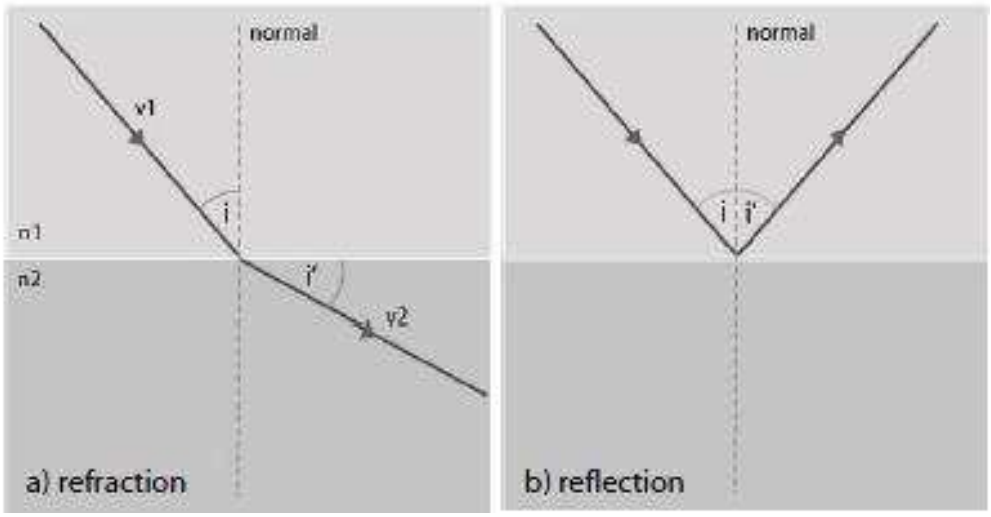

Figure 2-8 Refraction and Reflection of the seismic waves. (i is the angle between the initial wave (V1) and the normal of the intersection of two layers and i' is the refracted or reflected wave (V2) angle) [37, 38].

If the wave velocity in layer 2 is greater than the wave velocity in layer 1, the angle of refraction is greater than the initial wave angle, which is called critical refraction. A wave travelling from bedrock to top soil will cause this phenomenon; therefore, most abundant failures occur in soils (Table 2-5).

This phenomenon widely occurs on natural slopes because of the top soil layer. Tailing dams are also subjected to this phenomenon due to the different material used in their construction considering hard core material and rock fill on the top. In contrast, open pit mines are less likely

to get affected by this phenomenon because of the top soil layer is usually excavated at the first mining stages.

- **Focusing and Defocusing (effect of hill and valley topographies)**

Focusing and defocusing is defined by the direction of the wave. Wave merging to a point is called focusing and scattering from a point is called defocusing. Focusing and defocusing phenomena can cause ground shake amplification, which depends on the topography curvature. Generally, the seismic waves will be trapped in hill shape topographies and scattered in valley topography features [39]. Figure 2-9 illustrates these two phenomena.

The focusing phenomenon may also occur in tailing dams because of their geometry. It is observed that ground acceleration can amplify three times at the crest level of the dam tailing. In contrast to natural slopes and tailing dams which their topography causes focusing, open pit mines are subjected to defocusing phenomenon because of the valley-shape or one-face slopes.

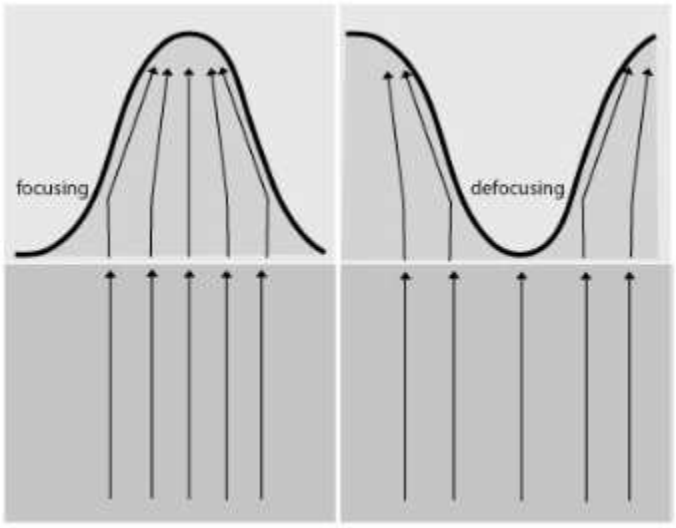

Figure 2-9 Focusing and defocusing effects of seismic waves interacted with topography [37].

- **Slope angle and seismic wave inclination**

Different slope angles create a variety of propagation patterns for the seismic waves, which is another aspect of topographical amplification or reduction [37]. Figure 2-10 shows the effect of different slope angles subjected to a same seismic wave direction. The steep slope (Figure 2-10(a)) makes the input wave incline toward the hill which amplifies the ground shaking on the hill top. In contrast, the shallower slopes (Figure 2-10(b)) scatter the input wave and attenuate the ground shaking. The relationship between slope angle and the direction of the seismic wave can cause an amplification on one side and reduction on the other side of the slope (Figure 2-10(c)). The amplification of an inclined wave could reach two times greater than a vertical wave [39, 40]. In open pit mines, by reaching the final stage of mining, the slope angle gets steeper [2]. The steeper pit slopes will incline the wave toward the slope top and decrease the stability of pit slopes.

Figure 2-10 The effect of slope angle and seismic wave inclination on the wave propagation [37].

2.5.2 Stiffness Contrast

The elastic properties of ground materials range from high to low stiffness. The seismic wave velocity depends on the stiffness of the materials in which the wave is traveling through. Seismic waves travel faster in stiff material and slower in soft material.

The softness of the rock and the thickness of the sediment above the bedrock affect the earthquake wave. Softer and thicker sediments on top of the hard bed rock make greater wave

amplifications. As seismic waves travel though the ground, they travel faster through hard rock than soft soil. As a result, when the waves move from hard rock to soft soil, the amplitude of the waves needs to be increased in order to be able to carry the same amount of energy, creating stronger shaking. Moreover, the deeper sediment above the bedrock creates stronger amplifications [9, 11, 14, 27, 41].

This phenomenon is widely observed on tailing dams, river and lake basins that may cause liquefaction. Open pit mines are less prone to the stiffness contrast effect because the slope materials are more uniform on these excavated slopes and the top soil layer is usually mined in the first stage of mining. The topographical and stiffness contrast site effects are further studied in Chapter 5 using numerical methods.

2.6 Current Methods for Designing Slopes against Earthquakes

There are two commonly used approaches in designing rock slopes against earthquakes. The early efforts, based on simply adding an earthquake force to a static limit-equilibrium analysis, were formalized by Terzhagi, and it is called the Pseudo-Static approach [42]. After that, Newmark proposed a method for estimating the displacement of slopes during earthquakes that addressed some of the crude assumptions of the pseudo-static analysis but was still quite simple to apply in practice, and thus it gives a less reasonable answer for complex situations [20, 21, 43]. In recent years, by computational enhancements, numerical methods are becoming more prominent in projects where they include more characteristics of the field behavior in the analysis. Recently, there have been several studies performed, using numerical modeling for evaluating the rock slope behavior during earthquakes [44-48]. The following is a brief description of these three methods.

2.6.1 Pseudo-Static Method

Pseudo-static method is a simple quasi static approach typically performed to investigate the response of pit slope stability to earthquake loading, required by open pit mines regulations. This method models the seismic shaking as permanent body forces are added to the force-body diagram of a conventional static limit-equilibrium analysis; Figure 2-11 shows the horizontal (αW) and vertical body forces (βW) acting on a slope. Therefore, the safety factor will be calculated from Equation 2-1.

$$FS = \frac{resisting\ Forces}{driving\ Forces} = \frac{cA+\big((W-\beta W)\cos\psi-\alpha W\sin\psi-u\big)\tan\varphi}{(W-\beta W)\sin\psi+\alpha W\cos\psi+v\cos\psi}. \qquad \text{(Eq. 2-1)}$$

where, c is the cohesion, A is the sliding area, φ is the friction along discontinuity, W is the weight of block; u and v are the water forces in the discontinuities and α, β are earthquake horizontal and vertical accelerations respectively.

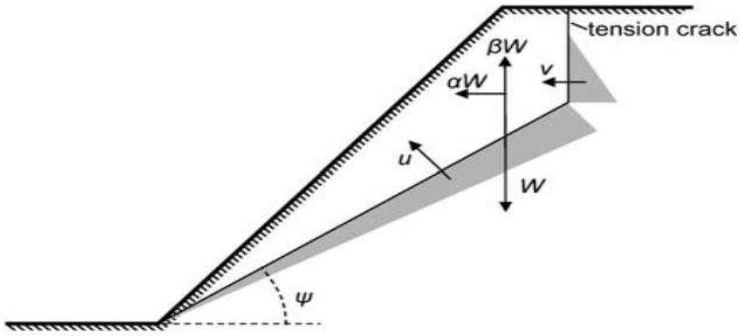

Figure 2-11 Pseudo-static slope stability analysis; stresses working on a block of rock with tension crack on a sliding plane and during an earthquake. The discontinuity is free draining at the toe of the slope [49].

Pseudo-static approach has some obvious limitations. Foremost among these limitations is that the approach considers the earthquake shaking as a permanent, unidirectional body force

which is extremely conservative. This assumption, considers the earthquake force constantly acting only in a direction that increases the slope instability, which is not realistic.

2.6.2 Newmark Method

Newmark method models a slope failure as a rigid block that slides on an inclined plane. The block has a known critical acceleration, which may overcome the resisting frictional force and initiate sliding (Figure 2-12). The desired earthquake strong-motion record is selected, and those parts of the record that exceed the critical acceleration are integrated to get the velocity-time history of the block, then the velocity-time history is integrated to obtain the cumulative displacement of the landslide block (Figure 2-13).

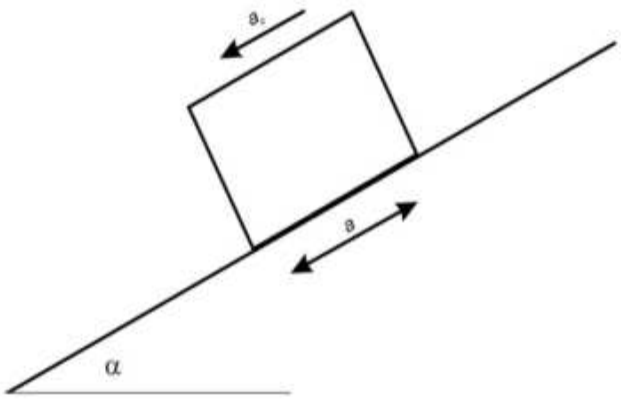

Figure 2-12 Acceleration (critical) required to overcome the resistance and initiate sliding

The critical acceleration (a_c), in its simplest form, can be estimated as Equation 2-2.

$$a_c = (FS - 1)gsin\alpha \qquad \text{(Eq. 2-2)}$$

where, a_c is the critical acceleration in terms of g, the acceleration of gravity, FS is the static factor of safety (the ratio of resisting to driving forces), and α is the angle from the horizontal for the sliding surface.

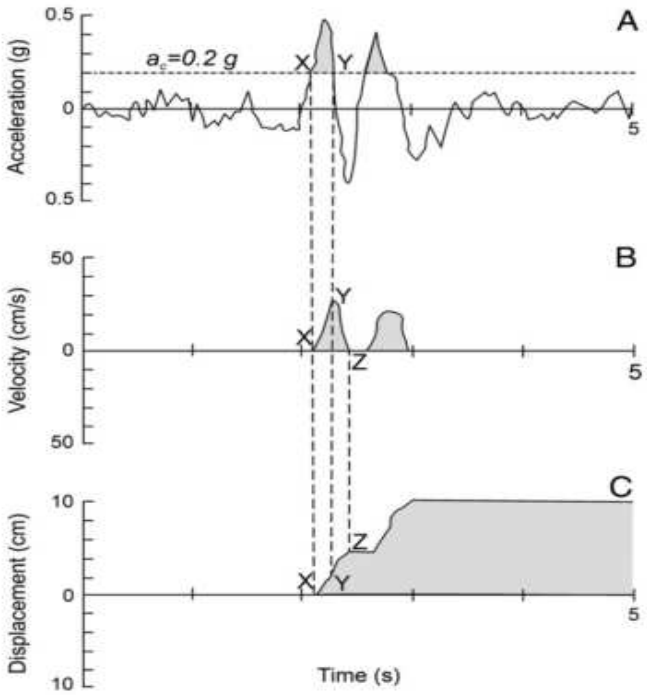

Figure 2-13 Illustration of the Newmark integrations algorithm. A, an earthquake acceleration-time history and a critical acceleration of 0.2g; B, the velocity-time of the shaded area from graph A; C, displacement of landslide versus time. Points X, Y, and Z are for reference between plots [49].

There are five main limitations to this approach which are [49]:

1. A key assumption of Newmark's method is that it treats a landslide as a rigid-plastic body: the mass does not deform internally, experiences no permanent displacement at the accelerations below the critical level, and deforms plastically at constant stress along a discrete basal shear surface when the critical acceleration is exceeded,
2. The critical acceleration is not strain-dependent and thus remains constant throughout the analysis,
3. The upslope resistance to sliding is taken to be infinitely large such that upslope displacement is prohibited,
4. Newmark assumes that the seismic force is applied parallel to the slope, and

5. The effects of dynamic pore pressure are neglected.

2.6.3 Numerical Modelling

The third approach, numerical analysis, has been recently used in the stability of slopes during earthquakes. Because the stability of the rock slopes is mostly controlled by the movement of joint-bounded blocks and/or intact rock deformation, discrete-element codes can be considered as a proper approach. Discrete element codes have been increasingly used in the analysis of rock slopes in recent years and are being used routinely in civil and mining engineering.

Distinct Element Method is a type of the discrete element method that considers a discontinuous rock mass as deformable blocks interacting through deformable joints of definable stiffness. Therefore, numerical model represents two types of mechanical behavior for discontinuities and the solid material.

Universal Distinct-Element Code (UDEC) is the method preferably used in previous studies [22]. This code has been used to investigate a wide variety of rock slope failure cases including those ranging from simple planar mechanisms to complex deep seated toppling instability and buckling [23]. These cases show the need for considering both intact rock and joint-controlled displacements in the analysis of complex rock slope instabilities. Therefore, the dual nature of distinct-element codes, such as UDEC, makes them particularly well suited to problems that involve jointed rock slopes. On one hand, they are highly applicable to the model discontinuity-controlled instabilities, and are capable of simulating large displacements due to slip. On the other hand, UDEC is also capable of dynamic analyses by applying seismic loads as a function of time. Due to these reasons, there have been several studies considering the effect of earthquake on the slope stability, using UDEC [44-47]. Later in this thesis (see Chapter 5), a

numerical method (UDEC) is used to study the effect of topographical conditions and stiffness contrast on the stability of slopes during earthquakes.

2.7 Conclusion

There has been a significant number of natural slope and tailing dam failures due to earthquakes. However, among some seismically induced failure instances in open pit slopes, none of those were significant by recorded as a cause for operational interruptions or injuries. Studies show that earthquake parameters, along with geological characteristics, govern the response of slopes to earthquakes. Studying the effect of these parameters on earthquake-triggered natural slope and tailing dam failures will increase the understanding about the effect of earthquake on open pit mine slopes. The following chapters investigate the status of earthquake parameters and slope characteristics for the three slope types; natural slopes, tailing dams and pit slopes. The effect of these parameters will be analyzed by creating a comprehensive database for the three slope types. Moreover, numerical analysis is later performed to investigate the effect of topography and stiffness contrast in more detail on different slope types.

CHAPTER 3

DATABASE

3.1 Introduction

A comprehensive database is built on open pit mine slopes, natural slopes, and tailing dams to study the effect of earthquake and geological parameters discussed in the second chapter. The database is developed on four main components, namely earthquake-triggered natural slopes and tailing dam failures, large open pit mines, and earthquakes. The developed database covers the location, earthquake parameters and geological characteristics of the three slope types. This information contains different aspects of slope failures, including failure location, failure type, depth of the failure, water condition, slope angle, material type; and corresponding earthquake parameters that include earthquake magnitude, depth, and epi-central distance. The data is imported into the world map to relate the earthquakes to slopes locations in order to study the effect of epi-central distance and intensity. These parameters are studied to find out if the earthquakes subjected to open pit mines were strong enough to trigger failure compared to those affected natural slopes and tailing dams. Moreover, the geological and geomechanical properties involved in natural slope and tailing dam failures are investigated and compared to those in open pit mines.

3.2 Earthquakes Location, Magnitude and Depth

The first step of creating the database is to include the earthquakes which are related to natural slope and tailing dam failures since 1800. In addition, earthquakes subjected to open pit mines during their life time period that is assumed 25 years are included in the database. This data

is derived from United States Geological Survey website database and added to the developed database. This section of database contains more than 4500 earthquakes along with their locations, magnitudes and focal depths.

3.3 Earthquake and Slope Failure Parameters

This section of the database contains the geological characteristics and earthquake parameters of earthquake-triggered natural slope and tailing dam failure cases. This information is collected from various sources, such as journal papers, conference papers, web sites, and news. Following sections present the procedure of creating the database and the utilized references for earthquake-triggered natural slope and tailing dam failures.

3.3.1 Earthquake-triggered Natural Slope Failures

There were a significant number of natural slope failures caused by earthquakes and many of these were reported with varying degree of details. Most of the reported failures come from those that caused loss of life, injuries or construction damages. There are two studies complemented each other which list the reported historical failure events from 1811 until 1997 [3, 5]. The list of natural slope failure cases provided by these two studies is updated in this study until 2015 and each event is investigated in detail using the available information. A comprehensive database is developed based on these detailed information including landslides characteristics and earthquake parameters involved in each event. The geological characteristics in the database consist of the name and date of failure, failure cause and mode, water condition, slope angle and material involved in the failure. And the earthquake parameters included in the database are the magnitude, depth and epi-central distance of the earthquake for each failure (Table 3-1). Figure 3-1 shows the location of these natural slope failures on the world map.

3.3.2 Earthquake-triggered Tailing Dam Failures

Tailing dams are significantly important in this study because they are normally built close to the open pit mines and are subjected to the same earthquake as the open pit mines. In this study, 37 reported tailing dam failures during earthquakes have been studied [124-126]. The earthquakes induced tailing dam failures are mostly located in California, Chile, and Peru. This is because of the high number of tailing dams in the vicinity of active seismic zones. Figure 3-2 shows the location of earthquake triggered tailing dam failures in the world and particularly in these three areas. Similar to the natural slopes a database was created for tailing dams, including the name, location and date of failure, slope angle, construction method and failure type, and the magnitude, focal depth, epi-central distance and intensity of the corresponding earthquake. Table 3-2 presents the characteristics of the reported tailing dam failures triggered by the earthquakes since 1928.

Table 3-1 The characteristics of the historical natural slope failures triggered by the earthquakes since 1811.

No.	Name	Country	Year	M	Slope Angle (deg)	Epi. Dis. (km)	Depth (km)	Int.	Water (Y/N)	Failure Cause & Mode	Material	Water Type	Ref.
1	New Madrid	SC, USA	1811	7.8	>60	40	NA	9.1	Y	RF, SSl		HWT, RV	[3,50]
2	Marlborough	New Zealand	1848	7.5		15-30	10	9.0	Y	Topo	Al	RB, Co, Sat	[3,51]
3	Wairarapa	New Zealand	1855	8.2	35-45	10-15	20	10.4	Y	RAV, Topo, Cr, Lq			[3,51,52]
4	Charleston	SC, USA	1886	6.8	>60	21	NA	8.6	Y	Sl, Lq	WR, CL, Cl	RV	[3,53]
5	North Canterbury	New Zealand	1888	7.3			10	10.0	Y	RAV, SAV, RF		RV	[3]
6	Cheviot	New Zealand	1901	6.9	>30	85-90	10	6.5	Y	RF, SF	SiS, SS, LS	Sat, RV	[3]
7	Costa Rica	Costa Rica	1904	6.8			NA		Y			Rf	[3,54]
8	Cape Turnagain	New Zealand	1904	6.8	~ 90 (RF)	130-250	NA	4.8	Y	Lq, RF, Topo		RV	[3,55]
9	Panama	Panama	1913	6.7	>60		NA		Y	Lq	S	RV, SM	[3,54]
10	Haiyuan	China	1920	7.8		56	25	8.4	Y	SFl		RV	[3,56]
11	Izu-Oshima	Japan	1923	6.8	8-34	6	5	10.0	Y	RAV		Rf	[3,57]
12	Arthur's Pass, South Island	New Zealand	1929	7.1	35-45	24	12	8.6	Y	RAV	GrWa, SS, Fr, Qu		[3,58]
13	Murchison	New Zealand	1929	7.8	15-50	4-120	10	7.4	Y	Lq, RAV, RF	W,Fr, SS, MS,Gr	Co	[3,51,58]
14	Hawke's Bay	New Zealand	1931	7.8	11-20(Lq) 30->50 (CoCl)	17- 64	17	8.3	Y	Lq, Sh, RF, Topo	LS, MS, SS	RB	[3,51]
15	Wairoa	New Zealand	1932	6.9		10- 20	20	8.8	Y	Sh, RS	WR, MS, LS	RV, Lq	[3,51]
16	Nepal–Bihar	Nepal	1934	8.1		144	35	7.6	Y	Lq	Al	RV	[3]
17	Pahiatua	New Zealand	1934	7.6			15	10.0	Y	SSl, RS, Lq		RB	[3,59]
18	Vancouver Island	Canada	1946	7.3	45	30	35	8.1	Y	SF, Sl		LV	[3,60]
19	Lake Coleridge	New Zealand	1946	6.4			10	9.1	Y	RF	Fr	LV	[3,61]
20	Khait	Tajikistan	1949	7.6		8	35	9.0	Y	SFl	Lo	RV	[3,62]
21	Puget Sound	WA, USA	1949	7		43	30	7.5	Y	RF	Fr, WR	RV	[3,63]
22	Assam - Tibet	India, China	1950	8.6	24-33	40	35	9.9	Y	RF, SSl, RSl		RV	[3,64]
23	Daly City	CA, USA	1957	5.3		2	15	6.8	Y			LV	[3,65]
24	Alaska	Alaska	1958	7.7	70-90(RF) 15 (RSl)	70	15	8.1	Y	RS, RAV, RSl, Sl		RV, Sn	[3,66]
25	Hebgen Lake	MT, USA	1959	7.1		54	15	7.5	Y	RF, RAV, SAV		RV	[3,67]
26	Valdivia	Chile	1960	9.5	>60	64	33	9.6	Y	SAV, Sl	Gl	Ice	[3,68]
27	Valdivia	Chile	1960	7.4	>60	128	24	6.7	Y	SAV, RAV	Gl	Ice, RV	[3]
28	Peria	New Zealand	1963	3.2			10	4.3	NA				[3,69]
29	Seward Alaska	AL, USA	1964	9.2		142	6	9.3	Y			SM	[3,70]
30	Hope Slide BC.	Canada	1965	3.2	45- 80	10	10	4.3	Y	Topo, RS	Fr, WR, W	Rf, Sn	[3,71]
31	Inangahua	New Zealand	1968	7.1	25- >65	4-17	46	7.7	Y	RF, DFl	Gr, GrWa, LS, W	RB	[3,51]
32	Ancash	Peru	1970	7.9		134	73	7.2	Y	RAV, RF, RS, Sl, SSl	Gl	Ice	[3,72]
33	San Fernando Valley	CA, USA	1971	6.5	>60	8	5	9.3	Y	Topo, Cr	Fr	Sat	[3,73]

Table 3-1 Continued.

No.	Name	Country	Year	M	Slope Angle (deg)	Epi. Dis. (km)	Depth (km)	Int.	Water (Y/N)	Failure Cause & Mode	Material	Water Type	Ref.
34	Hawaii	Hawaii, USA	1973	6.2		NA	41-50	6.4	NA	LatDis, Sub	Fr		[3,74]
35	Hawaii	Hawaii, USA	1975	7.1		24	2	8.8	Y	DFl	WR	SM	[3,75]
36	Guatemala	Guatemala	1976	7.5	20 -30	160	12	6.5	Y	RF, RAV, RSl,	Lo, Tu	RV	[3,76]
37	Panama	Panama	1976	7		18	17	8.6	Y	Topo, Cr, Lq	S, WR	RV	[3,54]
38	Friuli	Italy	1976	6.5	1- >30	60	8-26	6.4	Y		Cl	SM	[3,77]
39	Khulm	Afghanistan	1976	5.5		10	33	5.9	NA				[3]
40	Khurgu	Iran	1977	7	>60	48	31	7.4	Y		WR	Sat	[3,78]
41	Miyagi-ken-oki	Japan	1978	7.4	>45	85	52	7.1	Y	RF, RS, Sl	Sl, Fr	RV	[3,79]
42	Mexico	Mexico	1978	7.8	35-80	18	24	9.5	Y	Sh,RS		Rf	[3,54]
43	Imperial Valley	CA, USA	1979	7.1		75	8	7.1	NA				[3,80]
44	Coyote Lake	CA, USA	1979	5.4		2	10	7.6	Y			LV	[3,81,82]
45	Mt Diablo	CA, USA	1980	5.8		15-40	8	6.1	NA	RF, Sl, SSl			[56]
46	Mammoth Lakes	CA, USA	1980	3.1		21	7	2.9	Y	Lq	Lo, SS	HWT	[3,83]
47	Irpinia	Italy	1980	6.9	5-40	0-15	12	8.9	Y		Carb, WR	RV, HWT	[5,84]
48	Coalinga	CA, USA	1983	6.2	>60	15-34	10	6.9	Y	RF, RS, Lq	SS, SiS, Sh	Sat	[5,85]
49	Borah Peak	ID, USA	1983	6.9		70	16	6.9	Y		WR, Lo	HWT	[5,86]
50	Waiotapu	New Zealand	1983	5.1			3	9.0	Y	SF		LV	[51]
51	Valparaíso	Chile	1985	7.8			33	9.4	Y	Lq, Sub	SS, Fr	Sat	[5,87]
52	San Selvador	El Salvador	1986	5.7		16	7	7.2	NA				[5,88]
53	El Napo	Ecuador	1987	7.1		70	10	7.2	NA				[5]
54	Whittier Narrows	CA, USA	1987	6.1		3 -10	14	7.8	NA	Sh, Cr			[5,89,90]
55	Superstition Hills	CA, USA	1987	6.2		27	1	7.3	Y	Lq	SiS, SS,	RV	[5,90]
56	Edgecumbe	New Zealand	1987	6.6	>40	25-30	6	7.7	Y	Lq, RF, RS	WR, SS	RB	[5]
57	Nepal	Nepal	1988	6.8		40	61	6.7	Y	Lq, Rf		RV, Rf	[5,91]
58	Seguenay	Canada	1988	5.8		180	26	3.8	Y	Sh		Sat, Rf	[5,92]
59	Spitak	Armenia	1988	6.8		85	6	6.4	NA				[5]
60	Loma Prieta	CA, USA	1989	6.9		120	11	6.1	Y	Lq, RF		RV, Co	[5]
61	Soviet Tajik	Tajikistan	1989	5.5			NA		NA				[5,93]
62	Manjil	Iran	1990	7.3	47-81	90	18	7.1	Y	RF,Lq	Cl	RV, Dam	[5,94]
63	Luzon	Philipines	1990	7.8		200	23	6.6	Y	RF		Rf	[5,95]
64	Weber	New Zealand	1990	6.4	~60	10-15	11	8.2	Y	Lq, RF	MS, LS	RB	[51]
65	Valle de la Estrella	Costa Rica	1991	7.6		75	13	7.8	NA				[5,96]
66	Erzincan	Turkey	1992	6.8		60	25	6.9	Y	RF, Lq	S	HWT	[5,97]
67	Cape Mendocino	CA, USA	1992	7.1		25	18	8.4	Y	RF, Lq Topo	S	RV	[5,98]
68	Suusamyr	Kyrgutzstan	1992	7.3	55	45	13	8.1	Y	Topo, RF	Gl, W Gr	Ice, RV	[5,99,100]

Table 3-1 Continued.

No.	Name	Country	Year	M	Slope Angle (deg)	Epi. Dis. (km)	Depth (km)	Int.	Water (Y/N)	Failure Cause & Mode	Material	Water Type	Ref.
69	Murindo	Colombia	1992	6.7		< 100	10	6.0	Y	Lq	Fr, Tu	SM, Rf	[5,101]
70	Kalamata	Greece	1993	5.8			NA		NA				[5,102]
71	Hokkaido–Nansei	Japan	1993	7.6		<160	12	6.7	Y	Lq	S, WR	Sat	[5,103]
72	Fiordland	New Zealand	1993	7	>45	100	28	6.4	Y	Sh, Topo, SSl, RS		LV	[5,104]
73	Klamath Falls	OR, USA	1993	5.8		30	9	6.5	Y			LV	[5,105]
74	Ormondville	New Zealand	1993	6.2		5-10	5	8.6	Y	RF, SF, Lq, Cr, Topo		RV	[5,51]
75	Northridge	CA, USA	1994	6.7			11	9.4	Y		CL	RV	[5,106]
76	Paez	Colombia	1994	6.8		50	6	7.2	Y	Topo	Ash, S	Rf	[5,107]
77	Arthur's Pass	New Zealand	1994	6.8	22-51	2-12	10	9.0	Y		GrWa, SS, Fr, Qu. Cl	RV	[5,108]
78	Hyogu-ken Nanbu	Japan	1995	6.9		25	15	8.2	Y			HWT	[5,109]
79	East Cape	New Zealand	1995	6.7		0-15	12	8.6	Y	Lq		RB	[51]
80	Umbria–Marche	Italy	1997	5.5		20	9	6.6	NA				[5,110]
81	chi chi	Taiwan	1999	7.3	12-14	23	31	8.4	Y			Rf	[111]
82	Planica	Slovenia	2001	5.6		16	NA	7.2	Y	RF, Sh		Rf, RB	[112]
83	El Salvador	El Salvador	2001	7.6	>60		60	8.2	Y	RS	Tu, Ash	RV	[113]
84	Denali	Alaska	2002	7.9	>32	<10	19	10.0	Y	RAV	Gl	Ice	[114]
85	Tecomán	Mexico	2003	7.6	60-80	34	24	8.7	Y	RF, Sh	W, Fr	Co	[115]
86	Veliki Lemež Mt	Slovenia	2004	5.6		12	8	7.3	Y	RF, Sh, SSl, DFl	S, WR	Rf, RB	[112]
87	Niigata	Japan	2004	7.3	>50	5-10	16	9.5	Y	RF, DFl	SS, Congl, SiS, WR	HWT	[116]
88	Kashmir	Pakistan	2005	7.6		38	19	8.7	Y	DFl	SS, SiS, LS, MS. Dp	RV	[117]
89	Wenchuan	China	2008	8	30-50	80	19	8.3	Y	Sh, Cr	Carb, WJnt	Rf	[95]
90	Sichuan	China	2008	8		120	19	7.7	Y			RV	[118]
91	Papua New Guinea	New Guinea	2012	5			10	7.0	NA				[119]
92	Afghanistan	Afghanistan	2012	5.5		43	15	5.4	NA				[120]
93	Sichuan, Lushan	China	2013	8	45-55	5-10	13	10.0	Y	RF, Sh, DR	W, Clvm	Rf	[121]
94	Minxian–Zhangxian	China	2013	5.9	5- 40	13	20	7.0	Y	RF, TPL	Congl, SS, W	Rf	[122]
95	Kumamoto	Japan	2016	7.0	40-50	2	10	8.9	Y	DFl	SS	RV	[123]

Note: Cells left blank in case of no available data; 'Y' is involvement and 'N' is the absence of water; other abbreviation are:
RF: Rock Fall, SH: Shallow Failure < 3m, SSL: Soil Slide, DFl: Debris Flow, Tpl: Toppling, RAV: Rock Avalanche, SAV: Soil Avalanche, Lq: Liquefaction, Sl: Soil Slumps, RS: Rock Slide, SFl: Soil Flow, RSl: Rock Slump, SF: Soil Fall, Cr: Crest Failure, Topo: Topographical Effect, Dp: Deep Failure, Sub: Subsidence, Lat Dip: Lateral Displacement; WJnt: Weakly Jointed, WR: Weak Rock, W: Weathered Rocks, S: Soil, Carb: Carbonate, Congl: Conglomerate, SS: Sand Stone, Fr: Heavy Fractured Rock, Gl: Glacier, Al: Aluvial, Lo: Loose Material, Sl: Slate, Tu: Tuff, SiS: Silt Stone, Gr: Granite, GrWa: Greywake, LS: Loose Soil, CL: Cohesionless Material, Cl: Clay, MS: Mudstone, Qu: Quarts, Sh: Shale, Ash: Ash; Rf: Heavy Rainfall, RB: River Basin, Ice: Ice, RV: River Valley, HWT: High Water Table, LV: Lake Valley, SM: Submarine, Sat: Saturated, Sn: Snow, Dam: Dam, Co: Coast Cliff.

Figure 3-1 Location of the failed natural slopes triggered by earthquakes (Landslides are labelled as the numbers in Table 3-1)

Table 3-2 Characteristics of the reported tailing dam failures triggered by the earthquakes since 1928.

No.	Name	Year	Construction Method	M	H:V	Epi. Dist.(km)	Depth (km)	Int.	Type
1	Barahona 1	1928	US	8.3	2.0:1	95	20	8.5	LQ+FF
2	El Cobre	1965	US	7.1					LQ
3	Los Maquis 1	1965	US	7.4	1.7:1	15	70	7.1	SI+SID
4	Los Maquis 3	1965	US	7.4	1.4:1	15	70	7.1	LQ+FF
5	La Patagua	1965	US	7.4	1.4:1	25	70	7.1	LQ+FF
6	Cerro Negro No. 3	1965	US	7.4	1.2:1	38	70	7.1	LQ+FF
7	Bellavista	1965	US	7.4	1.7:1	55	70	7.1	LQ+FF
8	Hierro Viejo	1965	US	7.4	1:01	63	70	7.1	LQ+FF
9	El Sauce 1	1965	US	7.4	1.7:1	66	70	7.4	LQ+FF
10	El Sauce 2	1965	US	7.4		66	70	7.2	SI+SID
11	El Sauce 3	1965	US	7.4		66	70	7.6	SI+SID
12	El Sauce 4	1965	US	7.4		66	70	7.6	SI+SID
13	El Cerrado	1965	US	7.4	1.4:1	68	70	7.6	SI+SID
14	El Cobre Viejo	1965	US	7.4	1.4:1	68	70	7.3	LQ+FF
15	El Cobre Chico	1965	US	7.4	1.4:1	68	70	7.2	SI+SID
16	El Cobre Nuevo	1965	US	7.4	3.7:1	68	70	7.2	LQ+FF
17	Cerro Negro No. 1	1965	US	7.4	1.2:1	68	70	7.2	SI+SID
18	Cerro Negro No. 2	1965	US	7.4	1.2:1	68	70	7.2	SI+SID
19	San Fernando	1971		6.6		24	5	8.0	LQ
20	Mochikoshi No.1	1978				45	12		LQ
21	Veta del Agua No. 2	1981	US	6.5	1.2:1	85	65	5.6	LQ+FF
22	Veta del Agua No. 1	1985	US/CL	7.8	1.5:1	80	50	7.8	LQ+FF
23	Cerro Negro No. 4	1985	US/CL	7.8	1.7:1	105	50	7.5	LQ+FF
24	Cobre No. 4	1985	US	7.8	4.6:1		50	8.8	SI+SID
25	Soda Lake	1989		5.4		47	11	5.2	LQ
26	Amatista	1996				70	33		LQ
27	Algarrobo	1997	US	7	1.5:1	80	68	6.2	LQ+FF
28	Tranque AntiguoPlanta LaCocinera	1997	US/CL	7	1.7:1	80	68	6.4	LQ+FF
29	Almendro	1997	US	7	1.5:1	100	68	6.0	LQ+FF
30	Maitén	1997		7	1.5:1	120	68	6.4	LQ+FF
31	cuajone mine heap	2001		8.3		300	32	6.8	LQ
32	quebrada honda	2001		8.4		313	32	6.9	LQ
33	Las Palma	2010	-	8.8		96	35	7.8	LQ+FF
34	Tranque Adosado	2010	DS	8.8	4.5:1	252	35	9.2	LQ+SI
35	Tranque PlantaChacón	2010	-	8.8	1.8:1	290	35	7.6	SI+SID
36	Veta del AguaTranque No. 5	2010	US	8.8	1.4:1		35		SI+SID
37	Tranque No. 1	2010	US	8.8	1.2:1		35		SI+SID

Note: H, horizontal; V, vertical; LQ+FF, liquefaction with flow failure; SI+SID, slope instability with seismically induced deformations; US: Upstream, DS: Downstream, CL: Centreline.

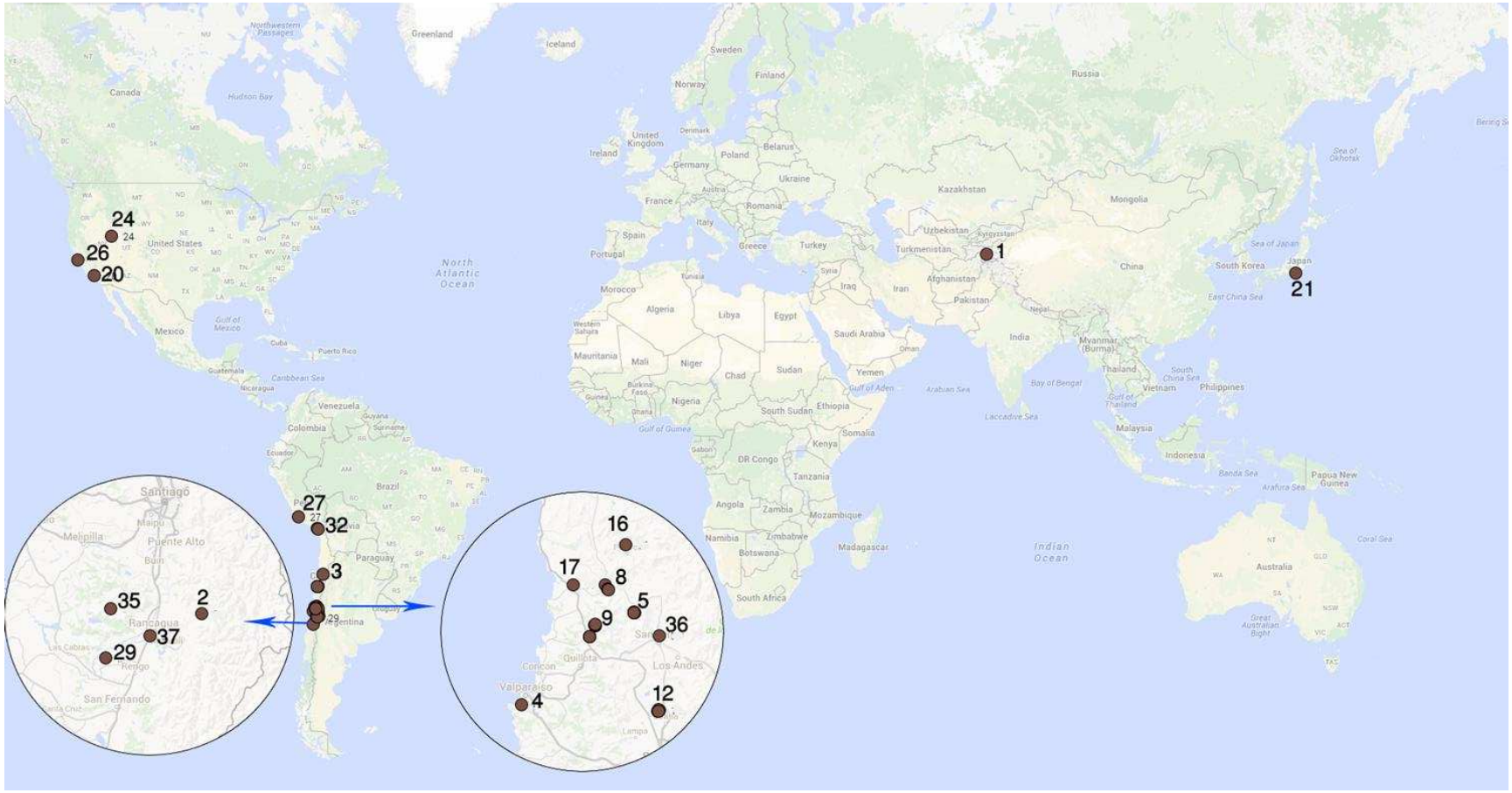

Figure 3-2 Location of the failed tailing dams triggered by earthquakes (Landslides are labelled as the numbers in Table 3-2)

3.4 Open Pit Mine Locations and Earthquake Parameters

The open pit mine section of the database includes the large open pit mines (LOP) over the world and the earthquake parameters which endured each open pit mine during its life time. In order to create a comprehensive database containing all major open pit mines, different resources of data have been used. The main sources of data were the *infomine.com* and *micla.ca* websites listing the world major large open pit mines. The mining websites for mining countries were also considered to complete this list [127-132]. According to this list there are 177 major open pit mines all over the world (Table 3-3). Because the relative location of open pit mines to earthquakes is essential to study the effect of earthquake parameters the exact location of each open pit mines is recorded on the world map. Figure 3-3 shows the world map of the open pit mines locations. In addition to open pit mine locations the parameters of earthquakes occurred in the vicinity of these open pit mines during their lifetime is considered in the database including their magnitude, focal depth, epi-central distance and intensity. It should be noted that there are open pit mines not located in active seismic zones, therefore there are no earthquakes associated with these mines in the database.

Table 3-3 Large open pit mines and the endured earthquake parameters.

No.	Name	Commodity	Country	$Year_1$	M_1	Epi_1	$Depth_1$	$Year_2$	M_2	Epi_2	$Depth_2$	$Year_3$	M_3	Epi_3	$Depth_3$	Int_1	Int_2	Int_3	Max. Int
1	Alumbrera	Copper	Argentina	1993	6.6	41.6	30	-	-	-	-	-	-	-	-	6.9	-	-	6.9
2	Cerro Vanguardia	Gold	Argentina					-	-	-	-	-	-	-	-		-	-	-
3	Pirquitas		Argentina	1993	7.0	48.0	218.0	2005	6.8	148.8	154.0	2015	6.7	49.60	223	5.3	5.0	4.8	5.3
4	Bengalla	Coal	Australia	-	-	-	-	-	-	-	-	-	-	-	-	-	-	-	-
5	Blair Athol	Coal	Australia	-	-	-	-	-	-	-	-	-	-	-	-	-	-	-	-
6	BMA Queensland (Peak Downs Mine)	Coal	Australia	-	-	-	-	-	-	-	-	-	-	-	-	-	-	-	-
7	Clermont	Coal	Australia	-	-	-	-	-	-	-	-	-	-	-	-	-	-	-	-
8	Hail Creek	Coal	Australia	-	-	-	-	-	-	-	-	-	-	-	-	-	-	-	-
9	Hunter Valley	Coal	Australia	-	-	-	-	-	-	-	-	-	-	-	-	-	-	-	-
10	Integra	Coal	Australia	-	-	-	-	-	-	-	-	-	-	-	-	-	-	-	-
11	Isaac Plains	Coal	Australia	-	-	-	-	-	-	-	-	-	-	-	-	-	-	-	-
12	Mt. Arthur	Coal	Australia	-	-	-	-	-	-	-	-	-	-	-	-	-	-	-	-
13	Ulan	Coal	Australia	-	-	-	-	-	-	-	-	-	-	-	-	-	-	-	-
14	Mount Thorley Warkworth	Coal	Australia	-	-	-	-	-	-	-	-	-	-	-	-	-	-	-	-
15	Mt. Owen	Coal	Australia	-	-	-	-	-	-	-	-	-	-	-	-	-	-	-	-
16	Telfer Mine	Copper	Australia	-	-	-	-	-	-	-	-	-	-	-	-	-	-	-	-
17	Cadia-Ridgeway	Copper/Gold	Australia	-	-	-	-	-	-	-	-	-	-	-	-	-	-	-	-
18	Argyle	Diamond	Australia	-	-	-	-	-	-	-	-	-	-	-	-	-	-	-	-
19	Super Pit Gold	Gold	Australia	-	-	-	-	-	-	-	-	-	-	-	-	-	-	-	-
20	Boddington	Gold	Australia	-	-	-	-	-	-	-	-	-	-	-	-	-	-	-	-
21	Sunrise Dam Gold	Gold	Australia	-	-	-	-	-	-	-	-	-	-	-	-	-	-	-	-
22	Yilgarn South	Gold	Australia	-	-	-	-	-	-	-	-	-	-	-	-	-	-	-	-
23	Brockman 2	Iron	Australia	-	-	-	-	-	-	-	-	-	-	-	-	-	-	-	-
24	Channar	Iron	Australia	-	-	-	-	-	-	-	-	-	-	-	-	-	-	-	-
25	Eastern Range	Iron	Australia	-	-	-	-	-	-	-	-	-	-	-	-	-	-	-	-
26	Hamersley (Mt. Tom Price)	Iron	Australia	-	-	-	-	-	-	-	-	-	-	-	-	-	-	-	-
27	Hope Downs	Iron	Australia	-	-	-	-	-	-	-	-	-	-	-	-	-	-	-	-
28	Marandoo	Iron	Australia	-	-	-	-	-	-	-	-	-	-	-	-	-	-	-	-
29	Mesa A	Iron	Australia	-	-	-	-	-	-	-	-	-	-	-	-	-	-	-	-
30	Mesa J	Iron	Australia	-	-	-	-	-	-	-	-	-	-	-	-	-	-	-	-
31	Nammuldi	Iron	Australia	-	-	-	-	-	-	-	-	-	-	-	-	-	-	-	-
32	Paraburdoo	Iron	Australia	-	-	-	-	-	-	-	-	-	-	-	-	-	-	-	-

Table 3-3 Continued.

No.	Name	Commodity	Country	$Year_1$	M_1	Epi_1	$Depth_1$	$Year_2$	M_2	Epi_2	$Depth_2$	$Year_3$	M_3	Epi_3	$Depth_3$	Int_1	Int_2	Int_3	Max. Int
33	West Angelas	Iron	Australia	-	-	-	-	-	-	-	-	-	-	-	-	-	-	-	-
34	Yandicoogina	Iron	Australia	-	-	-	-	-	-	-	-	-	-	-	-	-	-	-	-
35	Ranger	Uranium	Australia	-	-	-	-	-	-	-	-	-	-	-	-	-	-	-	-
36	Don Mario	Gold/Copper	Bolivia	-	-	-	-	-	-	-	-	-	-	-	-	-	-	-	-
37	Sossego	Copper	Brazil	-	-	-	-	-	-	-	-	-	-	-	-	-	-	-	-
38	Paracatu	Gold	Brazil	-	-	-	-	-	-	-	-	-	-	-	-	-	-	-	-
39	Alegria Mine	Iron	Brazil	-	-	-	-	-	-	-	-	-	-	-	-	-	-	-	-
40	Azul	Manganese	Brazil	-	-	-	-	-	-	-	-	-	-	-	-	-	-	-	-
41	Morro da Mina	Mangenes	Brazil	-	-	-	-	-	-	-	-	-	-	-	-	-	-	-	-
42	Onca puma	Nickel	Brazil	-	-	-	-	-	-	-	-	-	-	-	-	-	-	-	-
43	Elkview	Coal	Canada	-	-	-	-	-	-	-	-	-	-	-	-	-	-	-	-
44	Fording River	Coal	Canada	-	-	-	-	-	-	-	-	-	-	-	-	-	-	-	-
45	Greenhills	Coal	Canada	-	-	-	-	-	-	-	-	-	-	-	-	-	-	-	-
46	Line Creek	Coal	Canada	-	-	-	-	-	-	-	-	-	-	-	-	-	-	-	-
47	Coal Mountain	Coal	Canada	-	-	-	-	-	-	-	-	-	-	-	-	-	-	-	-
48	New Afton Mine	Copper	Canada	2014	6.6	499	11.4	2011	6.5	464	22	-	-	-	-	3.5	3.4	-	3.5
49	Highland Valley Copper	Copper	Canada	2014	6.6	499	11.4	2011	6.5	432	22	-	-	-	-	3.5	3.5	-	3.5
50	Copper Mountain	Copper	Canada	2011	6.5	452	22	2001	6.7	288	54	2014	6.6	496	11.4	3.5	4.4	3.5	4.4
51	Huckleberry	Copper	Canada	2012	6.2	341	9	2012	7.8	341	14	2012	6.3	374	9	3.4	5.8	3.4	5.8
52	Gibraltar	Copper	Canada	-	-	-	-	-	-	-	-	-	-	-	-	-	-	-	-
53	Ekati	Diamond	Canada	-	-	-	-	-	-	-	-	-	-	-	-	-	-	-	-
54	Victor	Diamond	Canada	-	-	-	-	-	-	-	-	-	-	-	-	-	-	-	-
55	Porcupine	Gold	Canada	-	-	-	-	-	-	-	-	-	-	-	-	-	-	-	-
56	Carol Lake	Iron	Canada	-	-	-	-	-	-	-	-	-	-	-	-	-	-	-	-
57	Endako	Molybdenum	Canada	2012	7.8	480	14	2012	6.2	486	9					5.3	2.9		5.3
58	Voisey Bay	Nickel	Canada	-	-	-	-	-	-	-	-	-	-	-	-	-	-	-	-
59	Horizon Oil Sands	Oil Sand	Canada	-	-	-	-	-	-	-	-	-	-	-	-	-	-	-	-
60	Athabasca	Oil Sands	Canada	-	-	-	-	-	-	-	-	-	-	-	-	-	-	-	-
61	Millennium	Oil Sands	Canada	-	-	-	-	-	-	-	-	-	-	-	-	-	-	-	-
62	Lac des Iles	PGM	Canada	-	-	-	-	-	-	-	-	-	-	-	-	-	-	-	-
63	McClean Lake	Uranium	Canada	-	-	-	-	-	-	-	-	-	-	-	-	-	-	-	-
64	El Salvador	Copper	Chile	1993	6.5	146	23	2006	6.6	187	12	2011	6.1	318	20	5.2	4.9	3.4	5.2
65	Collahuasi	Copper	Chile	2010	6.3	144	108	2007	7.7	184	40	2011	6.4	91.2	128	4.6	6.6	4.9	6.6

Table 3-3 Continued.

No.	Name	Commodity	Country	$Year_1$	M_1	Epi_1	$Depth_1$	$Year_2$	M_2	Epi_2	$Depth_2$	$Year_3$	M_3	Epi_3	$Depth_3$	Int_1	Int_2	Int_3	Max. Int
66	Candelaria	Copper	Chile	2011	6.7	75.2	20	2002	6.5	16.00	53	2006	6.6	107	12	6.4	6.6	5.8	6.6
67	Quebrada Blanca	Copper	Chile	2010	6.3	144	108.4	2007	7.7	176	40	2011	6.4	96	128	4.6	6.7	4.9	6.7
68	Carmen de Andacollo	Copper	Chile	2013	6.6	60.8	10.7	97	7.1	68.80	62	2003	6.7	60.8	32	6.6	6.8	6.6	6.8
69	Escondida	Copper	Chile	1996	6.6	100	47	1998	7.1	118	41		8	160	40	5.7	6.3	7.2	7.2
70	El Abra	Copper	Chile	2005	6.8	107	154	2010	6.3	52.8	108	2007	7.7	113	40	5.2	5.2	7.3	7.3
71	Radomiro Tomic	Copper	Chile	2007	7.7	102	40.00	2010	6.2	43.2	109	2010	6.3	56.00	108	7.4	5.1	5.1	7.4
72	Chuquicamata	Copper	Chile	2007	7.7	100	40	2010	6.2	44.8	109.4	2010	6.3	57.60	108	7.4	5.0	5.1	7.4
73	Maricunga	Gold	Chile	2002	6.5	112	53	2011	6.1	163	20	2010	6.1	166	41.4	5.4	4.4	4.3	5.4
74	Pascua Lama	Gold	Chile	2012	6.1	120	63	1995	6.7	148	15.00	1998	6.5	165	41	4.7	5.4	4.9	5.4
75	Los Pelambres	Copper	Chile	2015	8.3	72.0	22.4	-	-	-	-	-	-	-	-	8.9	-	-	8.9
76	Yimin	Coal	China	2011	6.1	658	12	-	-	-	-	-	-	-	-	2.3	-	-	2.3
77	Huolinhe	Coal	China	2010	6.9	944	573.7	-	-	-	-	-	-	-	-	2.7	-	-	2.7
78	Zhungeer Heidaigou	Coal	China	-	-	-	-	-	-	-	-	-	-	-	-	-	-	-	-
79	Yuanbaoshan	Coal	China	-	-	-	-	-	-	-	-	-	-	-	-	-	-	-	-
80	Tanjianshan	Gold	China	2001	7.8	448	15	-	-	-	-	-	-	-	-	5.4	-	-	5.4
81	Cerrejon	Coal	Colombia	1997	7	988	9	-	-	-	-	-	-	-	-	3.0	-	-	3.0
82	Angostura	Gold	Colombia	2015	6.2		157	-	-	-	-	-	-	-	-	4.6	-	-	4.6
83	Moa Bay	Nickel/ Cobalt	Cuba	-	-	-	-	-	-	-	-	-	-	-	-	-	-	-	-
84	Pueblo Viejo		Duminican	2010	7.0	256	15.0	2010	6.0	280	6.0	-	-	-	-	5.1	3.4	-	-
85	Sukari Mine	Gold	Egypt	1995	7.2	432	12	-	-	-	-	-	-	-	-	4.6	-	-	4.6
86	Iduapriem	Gold	Ghana	-	-	-	-	-	-	-	-	-	-	-	-	-	-	-	-
87	Marlin	Gold/Silver	Guatemala	1993	7.2	118	34.0	2013	6.6	76.8	67.0	2014	6.9	94.4	60.0	6.5	5.9	6.2	6.5
88	Fenix Project		Guatemala	2013	6.2	163	189	-	-	-	-	-	-	-	-	3.9			3.9
89	Omai	Gold	Guyana					-	-	-	-	-	-	-	-		-	-	-
90	San Andres		Honduras	2013	6.2	163	189	-	-	-	-	-	-	-	-	3.9	-	-	-
91	Hutti Mine	Gold	India					-	-	-	-	-	-	-	-		-	-	-
92	J Resources North Lanut	Gold	Indonasia	2010	6.1	109	28	2014	6.2	125	30	-	-	-	-	5.0	4.9	-	5.0
93	Vale INCO Nickel	Nickel	Indonasia	2011	6.1	12.8	16	2012	6.3	200	10	-	-	-	-	7.6	4.4		7.6
94	Nickel Mine	Nickel	Indonasia	2014	6.5	112	38	2014	7.1	149	35	-	-	-	-	5.5	6.0		6.0
95	Batu Hijau	Copper	Indonesia	2007	6.5	176	20	2011	6.2	246	39	-	-	-	-	4.9	3.9		4.9
96	Grasberg	Copper	Indonesia	2013	7	160	66	2004	7.3	229	20	-	-	-	-	5.7	5.7		5.7
97	Sarcheshmeh	Copper	Iran	1998	6.6	165	17	2003	6.5	250	14	-	-	-	-	5.1	4.4		5.1
98	Gol Gohar	Iron	Iran	1990	6.6	104	10	2013	6.4	370	12	2011	6.2	360	10	5.8	3.6	3.4	5.8

Table 3-3 Continued.

No.	Name	Commodity	Country	$Year_1$	M_1	Epi_1	$Depth_1$	$Year_2$	M_2	Epi_2	$Depth_2$	$Year_3$	M_3	Epi_3	$Depth_3$	Int_1	Int_2	Int_3	Max. Int
99	Choghart	Iron	Iran			0.0		-	-	-	-	-	-	-	-	-	-	-	
100	Bama	Zinc/Lead	Iran	2014	6.2	365	10	-	-	-	-	-	-	-	-	3.3	-	-	3.3
101	Kumtor	Gold	Kyrgyzstan	2013	6.1	150	15	-	-	-	-	-	-	-	-	4.5	-	-	4.5
102	Morila	Gold	Mali	-	-	-	-	-	-	-	-	-	-	-	-	-	-	-	-
103	Sadiola	Gold	Mali	-	-	-	-	-	-	-	-	-	-	-	-	-	-	-	-
104	Yatela	Gold	Mali	-	-	-	-	-	-	-	-	-	-	-	-	-	-	-	-
105	La Herradura	Gold	Mexico	2010	7.2	256	5.2	-	-	-	-	-	-	-	-	5.4	-	-	5.4
106	Cerro San Pedro	Gold	Mexico	1995	8.0	496	25	2012	6.1	432	53	-	-	-	-	5.6	2.9	-	5.6
107	Oro Dolores	Gold	Mexico	1995	6.5	368	6.0	2013	6.4	346	1.0	-	-	-	-	3.8	3.7	-	3.8
108	Palmarejo	Gold	Mexico	1995	6.5	245	6.0	2013	6.4	213	1.00	-	-	-	-	4.4	4.5	-	4.5
109	Ocampo Project	Gold/Silver	Mexico	1995	6.5	309	6.0	2013	6.4	277	1.00	-	-	-	-	4.0	4.1	-	4.1
110	Los Filos and Bermejal	Gold/Silver	Mexico	2011	6.5	32.0	54.2	2012	6.1	89.6	53.0	2014	7.2	128	24.0	6.5	5.1	6.4	6.5
111	The Penasquito	Gold/Silver	Mexico	-	-	-	-	-	-	-	-	-	-	-	-	-	-	-	-
112	Boroo Gold	Gold	Mongolia	-	-	-	-	-	-	-	-	-	-	-	-	-	-	-	-
113	Navachab	Gold	Namibia	-	-	-	-	-	-	-	-	-	-	-	-	-	-	-	-
114	Rossing	Uranium	Namibia	-	-	-	-	-	-	-	-	-	-	-	-	-	-	-	-
115	Goro	Nickel	New Caledonia	2014	7.1	291	19	2003	6.7	258	10	-	-	-	-	5.0	4.6	-	5.0
116	Martha	Gold	New Zealand	2012	6.3	118	163	2014	6.7	339	22	-	-	-	-	4.4	4.2	-	4.4
117	Macraes	Gold	New Zealand	2003	7.2	258	28	2007	6.8	232	18	-	-	-	-	5.4	4.9	-	5.4
118	la Libertad	Gold	Nicaragua	2011	6.0	104	177	2014	6.6	118	135	2014	6.1	133	13.0	3.9	5.0	4.7	5.0
119	Porgera	Gold	Papua New	2000	6.5	173	17	2010	6	211	33.6	-	-	-	-	4.9	3.8	-	4.9
120	Lihir	Gold	Papua New	2000	8.0	104	27	2013	6.5	102	10	2010	6.5	122	28	7.9	5.7	5.4	7.9
121	Cerro Corona	Copper	Peru	1990	6.5	178	17	2014	6.3	387	9.8	-	-	-	-	4.9	3.4	-	4.9
122	Tintaya	Copper	Peru	2013	6	94.4	7	-	-	-	-	-	-	-	-	5.1	-	-	5.1
123	Antamina	Copper	Peru	2012	6	226	129	1996	7.5	302	15	-	-	-	-	3.5	5.6	-	5.6
124	Toquepala mine	Copper	Peru	2001	6.7	118	24	2001	7.6	144	14	2010	6.2	92.8	46	5.8	6.8	5.2	6.8
125	Cuajone mine	Copper	Peru	2001	6.7	123	24	2001	7.6	141	14	2010	6.2	115	46	5.7	6.9	5.0	6.9
126	Cerro Verde Mine	Copper	Peru	2001	7.6	117	14	2013	6.0	101	7	1999	6.8	97.6	88	7.2	5.0	5.8	7.2
127	Toromocho Mine	Copper	Peru	-	-	-	-	-	-	-	-	-	-	-	-	-	-	-	-
128	Lagunas Norte	Gold	Peru	2014	6.3	387	9.8	-	-	-	-	-	-	-	-	3.4	-	-	3.4
129	Yanacocha	Gold	Peru	1990	6.5	178	17	2014	6.3	294	9.8	-	-	-	-	4.9	3.8	-	4.9
130	Pierina	Gold	Peru	2012	6	283	129	1996	7.5	248	15	-	-	-	-	3.3	5.9	-	5.9

Table 3-3 Continued.

No.	Name	Commodity	Country	$Year_1$	M_1	Epi_1	$Depth_1$	$Year_2$	M_2	Epi_2	$Depth_2$	$Year_3$	M_3	Epi_3	$Depth_3$	Int_1	Int_2	Int_3	Max. Int
131	Constancia	Copper	Peru	1991	6.8	138	100	2013	6.0	128	6.6	2014	6.9	195	101	5.4	4.6	5.2	5.4
132	Didipio	Gold	Philippines	1990	6.5	46.4	25		7.7	70.4	23	-	-	-	-	6.7	8.0	-	8.0
133	Sao Domingos	Gold	Portugal	2010	6.3	352	620	-	-	-	-	-	-	-	-	2.5	-	-	2.5
134	Rovinari	Coal	Romania	1990	7	294	89	-	-	-	-	-	-	-	-	4.8	-	-	4.8
135	Berbești	Coal	Romania	1990	7	238	89	-	-	-	-	-	-	-	-	5.1	-	-	5.1
136	Roșia Poieni	Copper	Romania	1990	7	272	89	-	-	-	-	-	-	-	-	4.9	-	-	4.9
137	Mirny	Diamond	Russia	-	-	-	-	-	-	-	-	-	-	-	-	-	-	-	-
138	Udachnaya pipe	Diamond	Russia	-	-	-	-	-	-	-	-	-	-	-	-	-	-	-	-
139	Venetia	Diamond	South Africa	2006	7	453	11	-	-	-	-	-	-	-	-	4.2			4.2
140	Big Hole	Diamond	South Africa	-	-	-	-	-	-	-	-	-	-	-	-	-	-	-	-
141	Jagersfontein	Diamond	South Africa	-	-	-	-	-	-	-	-	-	-	-	-	-	-	-	-
142	Marikana Platinum	PGM	South Africa	-	-	-	-	-	-	-	-	-	-	-	-	-	-	-	-
143	Letseng	Diamond	South Africa	-	-	-	-	-	-	-	-	-	-	-	-	-	-	-	-
144	Corta Atalaya	Copper	Spain	2010	6.3	285	620	-	-	-	-	-	-	-	-	2.5	-	-	2.5
145	Sierra Menera	Iron	Spain	2010	6.3	440	619	-	-	-	-	-	-	-	-	2.4	-	-	2.4
146	Rosebel	Gold	Suriname					-	-	-	-	-	-	-	-		-	-	
147	Geita	Gold	Tanzania	2005	6.7	488	16	-	-	-	-	-	-	-	-	3.6	-	-	3.6
148	Buzwagi	Gold	Tanzania	2005	6.7	406	16	-	-	-	-	-	-	-	-	3.9	-	-	3.9
149	North Mara	Gold	Tanzania					-	-	-	-	-	-	-	-	-	-	-	-
150	Kisladag	Gold	Turkey	2012	6	232	35	2014	6.9	376	10					3.7	4.3	-	4.3
151	Ffos-y-fran Land Reclamation Scheme	Coal	UK	-	-	-	-	-	-	-	-	-	-	-	-	-	-	-	-
152	Penrhyn Quarry	Slate	UK	-	-	-	-	-	-	-	-	-	-	-	-	-	-	-	-
153	Spring Creek	Coal	USA	1992	7.2	138	18	2010	6.5	162	20.6	2014	6.8	221	16.6	6.3	5.0	5.0	6.3
154	Minorca Coal	Coal	USA	-	-	-	-	-	-	-	-	-	-	-	-	-	-	-	-
155	Colowyo Mine	Coal	USA	-	-	-	-	-	-	-	-	-	-	-	-	-	-	-	-
156	Cordero Rojo	Coal	USA	-	-	-	-	-	-	-	-	-	-	-	-	-	-	-	-
157	North Antelope	Coal	USA	-	-	-	-	-	-	-	-	-	-	-	-	-	-	-	-
158	Sierrita	Copper	USA	2010	7.2	392	5.2					-	-	-	-	4.7			4.7
159	Bagdad	Copper	USA	1999	7.2	293	5	1992	7.3	306	11	-	-	-	-	5.2	5.3		5.3
160	Bingham Canyon	Copper	USA	-	-	-	-	-	-	-	-	-	-	-	-	-	-	-	-

Table 3-3 Continued.

No.	Name	Commodity	Country	$Year_1$	M_1	Epi_1	$Depth_1$	$Year_2$	M_2	Epi_2	$Depth_2$	$Year_3$	M_3	Epi_3	$Depth_3$	Int_1	Int_2	Int_3	Max. Int
161	Chino	Copper	USA	-	-	-	-	-	-	-	-	-	-	-	-	-	-	-	-
162	Morenci	Copper	USA	-	-	-	-	-	-	-	-	-	-	-	-	-	-	-	-
163	Safford	Copper	USA	-	-	-	-	-	-	-	-	-	-	-	-	-	-	-	-
164	Tyrone	Copper	USA	-	-	-	-	-	-	-	-	-	-	-	-	-	-	-	-
165	Ruby Hill	Gold	USA	2014	6	563	7.8	-	-	-	-	-	-	-	-	2.4	-	-	2.4
166	Cortez	Gold	USA	2014	6	533	7.8	-	-	-	-	-	-	-	-	2.5	-	-	2.5
167	Round Mountain	Gold	USA	2014	6	461	7.8	-	-	-	-	-	-	-	-	2.7	-	-	2.7
168	Goldstrike	Gold	USA	1992	7.2	650	18	-	-	-	-	-	-	-	-	4.0	-	-	4.0
169	Fort Knox	Gold	USA	2002	6.6	160	19	-	-	-	-	-	-	-	-	5.2	-	-	5.2
170	Bald Mountain	Gold	USA	-	-	-	-	-	-	-	-	-	-	-	-	-	-	-	-
171	Cripple Creek & Victor	Gold	USA	-	-	-	-	-	-	-	-	-	-	-	-	-	-	-	-
172	Golden Sunlight	Gold	USA	-	-	-	-	-	-	-	-	-	-	-	-	-	-	-	-
173	Climax	Molybdenum	USA	-	-	-	-	-	-	-	-	-	-	-	-	-	-	-	-
174	Red Dog	Zinc	USA	-	-	-	-	-	-	-	-	-	-	-	-	-	-	-	-
175	Nchanga Mines	Copper	Zambia	-	-	-	-	-	-	-	-	-	-	-	-	-	-	-	-
176	Murowa	Diamond	Zimbabwe	2006	7.0	437	11		-	-	-	-	-	-	-	4.3	-	-	4.3
177	Zimplats	PGM	Zimbabwe	2006	7.0	453	11		-	-	-	-	-	-	-	4.2	-	-	4.2

Note: The blank cells are either for open pit mines not located in seismic areas or subjected to less than 3 earthquakes.

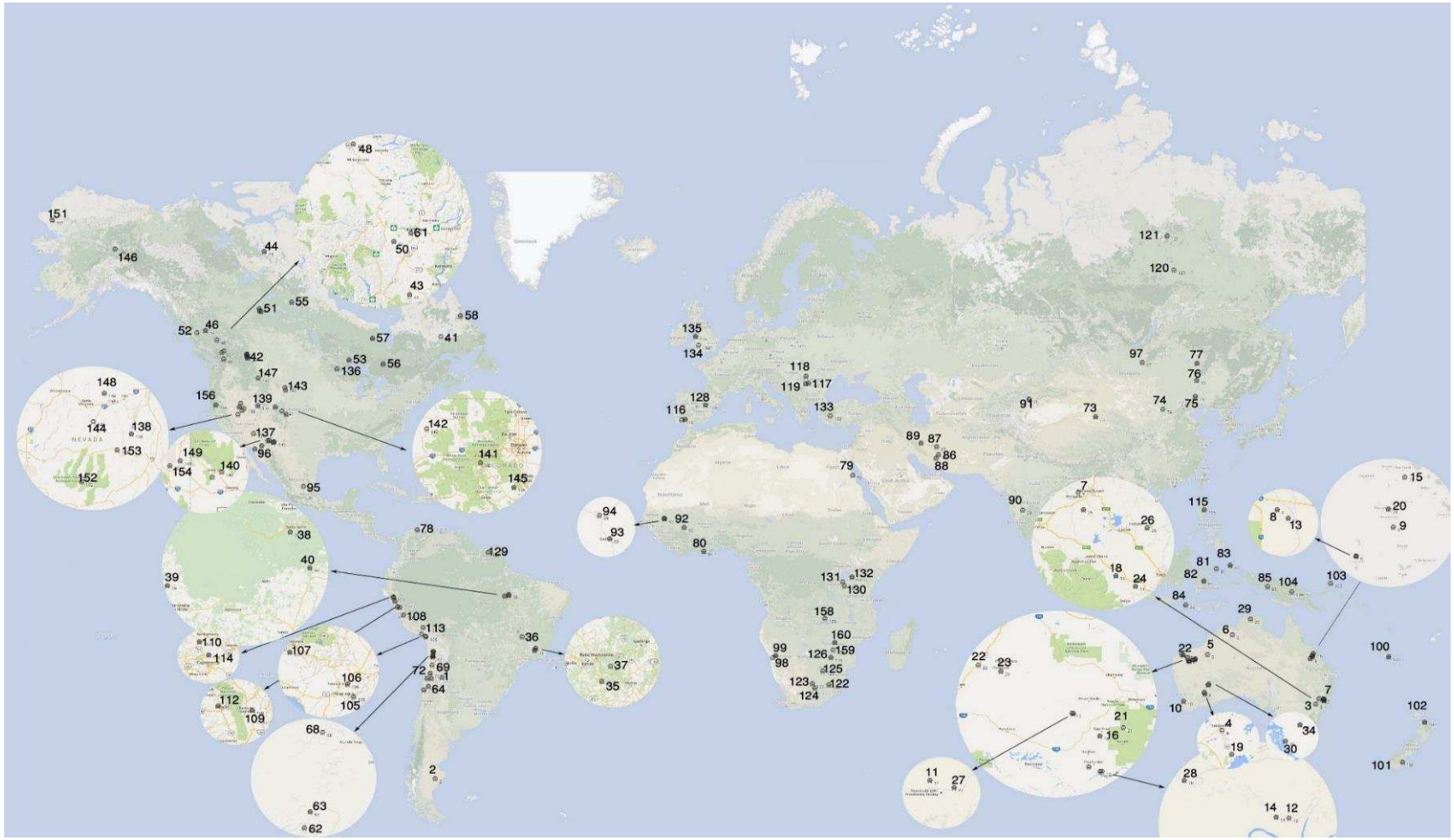

Figure 3-3 Location of major open pit mines (numbers refer to Table 3-3).

3.5 Conclusion

To investigate the earthquake and geological conditions of slope failures a detailed database is created. This database contains the earthquake parameters for three slope types, natural slopes, tailing dams and pit slopes and geological characteristics for natural and tailing dam slopes. Earthquake magnitude, epi-central distance, depth and intensity, are the earthquake parameters included in the database for each slope type. And the geological characteristics involved are water condition, failure mode, depth of the failure, slope angle and material type for natural slopes and slope angle, construction type and failure mode for tailing dam failures. The database is analysed in Chapter 4 considering each earthquake and geological aspect.

CHAPTER 4

CHARACTERISTIC RESPONSE OF NATURAL SLOPES, TAILING DAMS AND OPEN PIT SLOPES TO EARTHQUAKES USING THE DATABASE

4.1 Introduction

This chapter investigates the characteristic response of natural slopes, tailing dams and open pit mines to earthquakes in order to discover the seismic and geological instability conditions for each slope type. As discussed in Chapter 2, there are two groups of factors governing the response of slopes to earthquakes: internal and external. Internal factors include site effects, water condition and material type while external ones are earthquake magnitude, focal depth, epi-central distance and intensity. This chapter analyzes the comparison of each of the mentioned parameters among each of the three slope types using the database presented in Chapter 3.

4.2 Earthquake Parameters

This section studies the earthquake parameters involved in the instability of natural slopes and tailing dams and their relationship with earthquake parameters subjected to open pit mine slopes. This study shows whether the earthquakes occurred in the vicinity of open pit mines were sufficient to trigger pit slope failures, compared to those triggered natural slopes and tailing dam failures. According to the open pit mine database in Chapter 3, 85 of the 177 open pits mines are located in the active seismic zones while the rest are too far from the seismic regions to be affected by earthquakes. As discussed in Chapter 2, there are four earthquake parameters controlling the effect of shaking strength on the slope location: earthquake magnitude, epi-central distance, focal depth, and intensity.

4.2.1 Magnitude

Natural slope and tailing dam failures are triggered by a wide range of earthquake magnitudes from 3.1 to 9.5 on Richter scale. To study the magnitude parameter on open pit mines, earthquakes with an epi-central distance of a 200-km radius for each mine is considered. This is because the number of slope failures decreased when the epi-central distance increased in all the natural slope failures, and more than 80 percent of the tailing dam failures were triggered by earthquake epi-centers of less than 200 km (Figure 4-1). In addition to epi-central distance, earthquake magnitude is also limited to more than 5.0 on Richter scale in this analysis, because there are only three natural slope failures and one tailing dam failure triggered by earthquake magnitudes of less than 5.0. The earthquake magnitudes that triggered failure in natural slopes and tailing dams are shown in Figure 4-2.

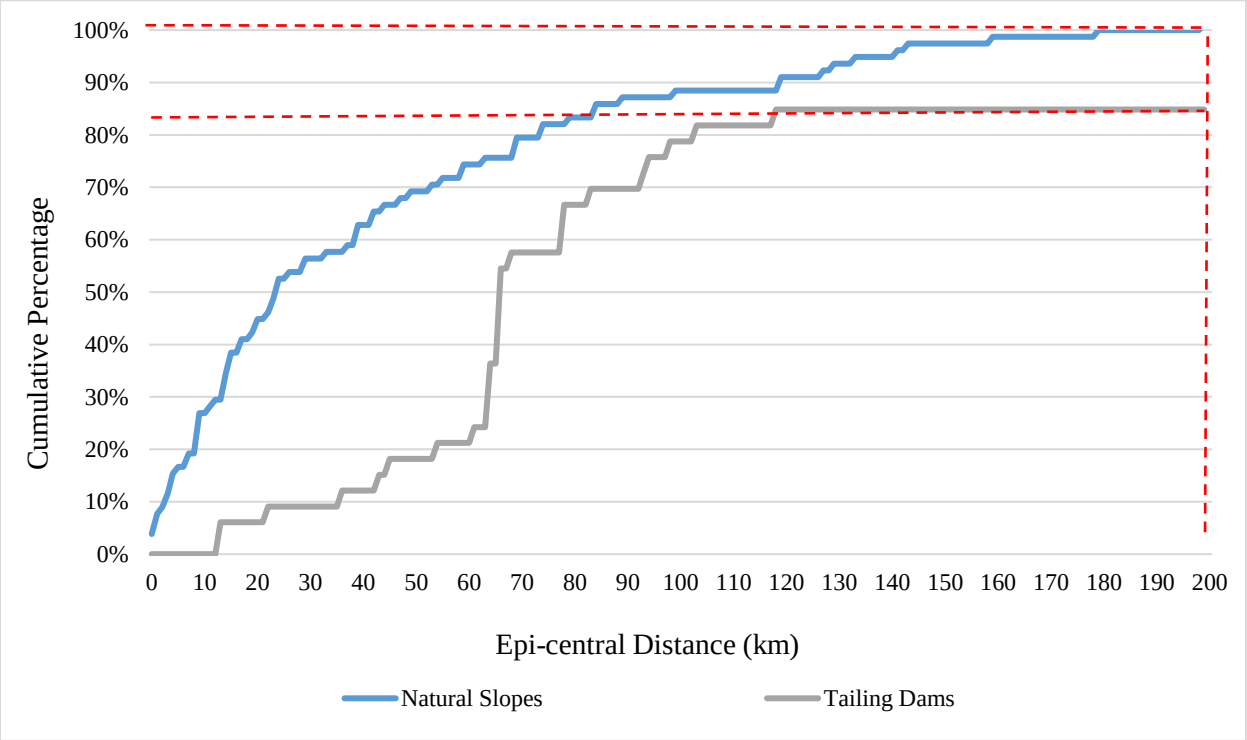

Figure 4-1 Relation between cumulative percentage of natural slope failures and earthquake epi-central distance.

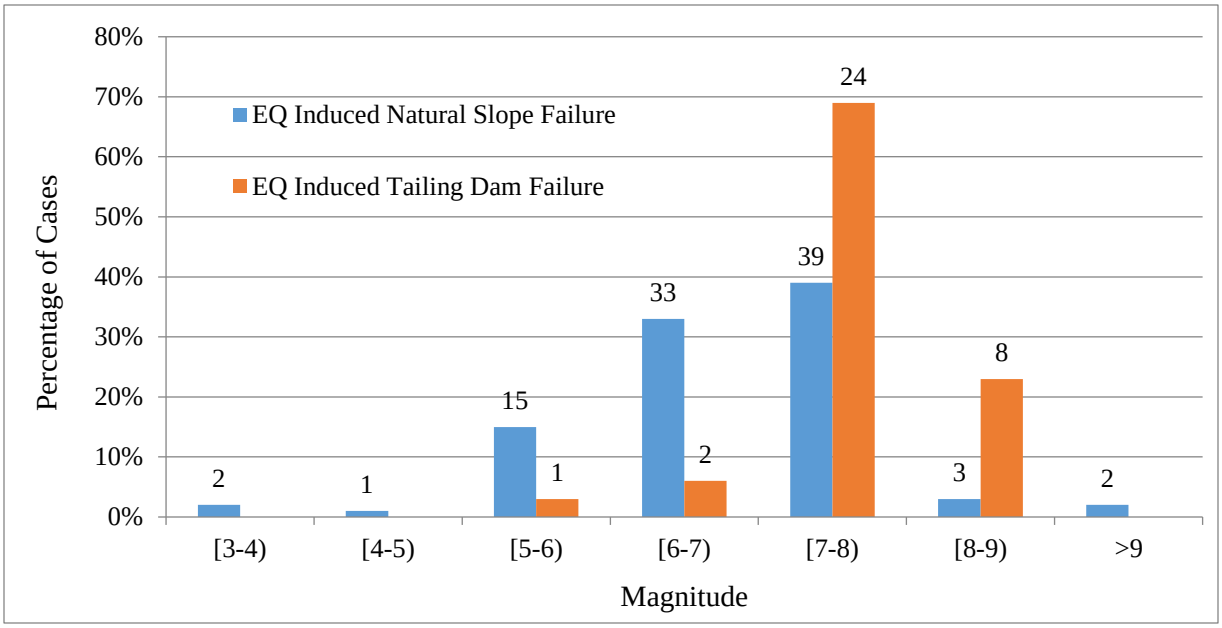

Figure 4-2 Distribution percentage of natural landslides and tailing dam failures in different earthquake magnitude ranges (values on the bars represent the number of cases).

According to Figure 4-2 natural slopes are mostly triggered by earthquakes with magnitudes of 5.0 to 8.0 with increase in the number of failures in higher magnitudes. There are only eight cases out of this range where three were in the range of 3.0 to 5.0 magnitude, and five were subjected to magnitudes of more than 8.0. Peria landslide in 1963 triggered by an earthquake magnitude of 3.2 (number 28 in Table 3-1) is an example of one of failures triggered by a relatively weak earthquake. The earthquake created a few rockfalls along the local road side slope which caused no injury. Figures 4-3 and 4-4 are pictures from this landslide showing the small scale failures. Another example of the landslides in this magnitude range is the Hope slide in 1965 triggered by 3.2 earthquake magnitude (number 30 in Table 3-1). In contrast to the Peria landslide this one is a catastrophic landslide in which 22 Mm^3 of material were relocated (Figure 4-5). This difference shows the involvement of other factors in addition to earthquake magnitude in the stability of slopes. The reason for this very large failure compared to the Peria earthquake was the different material properties. The material involved in Hope slide were very weak having a

Geological Strength Index of less than 40 with a low shear strength on a deep to very deep slope angle (45-80 degrees) [133]. Moreover, ongoing weathering and tectonic activity weakened the material to the point where it had reached the limit equilibrium. Observing only five cases for high earthquake magnitudes (M>8) is because of the significantly fewer number of earthquakes in this range, where only 92 events, compared to earthquake magnitudes of 5.0 to 8.0, which are more than 78,000 events since 1800. Figure 4-6 shows the number of slope failures per number of earthquakes in different magnitude ranges. The figure shows that, although the number of earthquakes decreases by increase in the magnitude, the number of failures per number of earthquakes is increasing. For instance, there were four earthquakes with a magnitude of more than 9.0 since 1900, where two of them caused historical natural slope failure. One of these high magnitude earthquakes events was the Seward Alaska in 1964 with a magnitude of 9.2 (number 29 in Table 3-1). The earthquake triggered a 1500 meters long and 150 meters wide submarine landslide causing a tsunami that killed 131 people in the local coast towns. The other large magnitude earthquake is the Valdivia earthquake in 1960 with a magnitude of 9.6 (number 26 in Table 3-1), that was the largest ever recorded earthquake magnitude. The earthquake triggered abundant landslides mainly in the steep glacial valleys of the southern Andes. This event did not cause significant number of fatalities nor major economic losses as most areas were unpopulated.

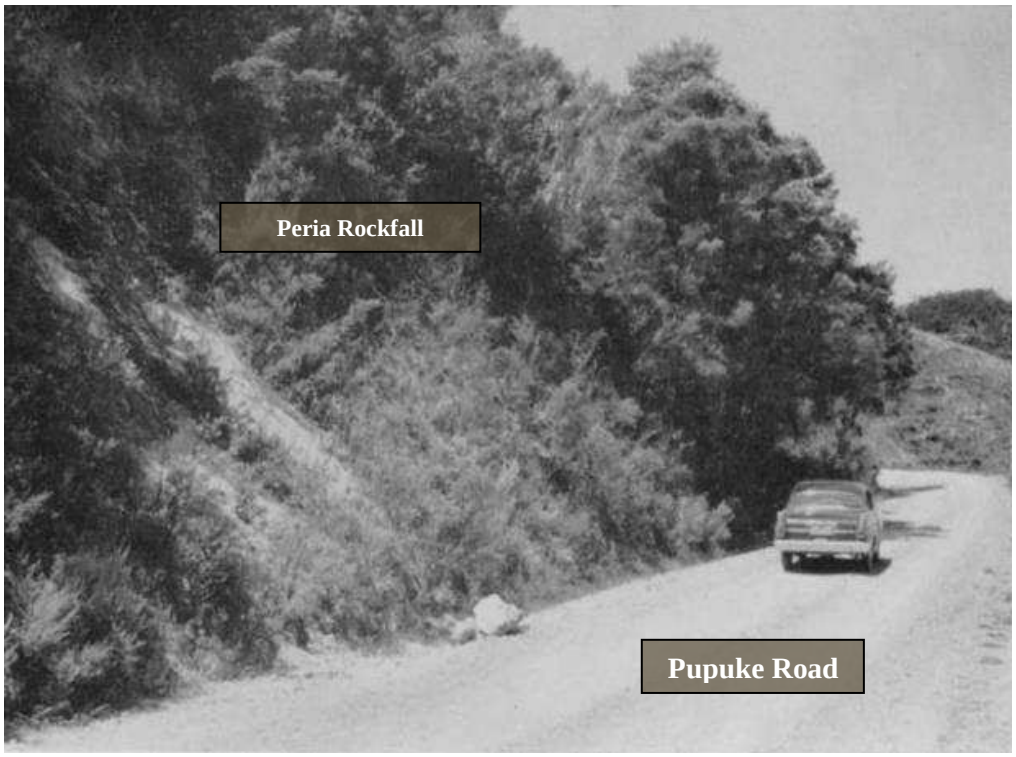

Figure 4-3 Material dislodged from an existing roadside slip at Kaingapipiwai, on the Pupuke Road [79].

Figure 4-4 Landslide on Akatere Trig. The scar of a landslide caused by the Peria earthquake is circled [79].

Figure 4-5 East view of Hope Slide occurred under earthquake magnitude of 3.2 in 1965, British Columbia, Canada.

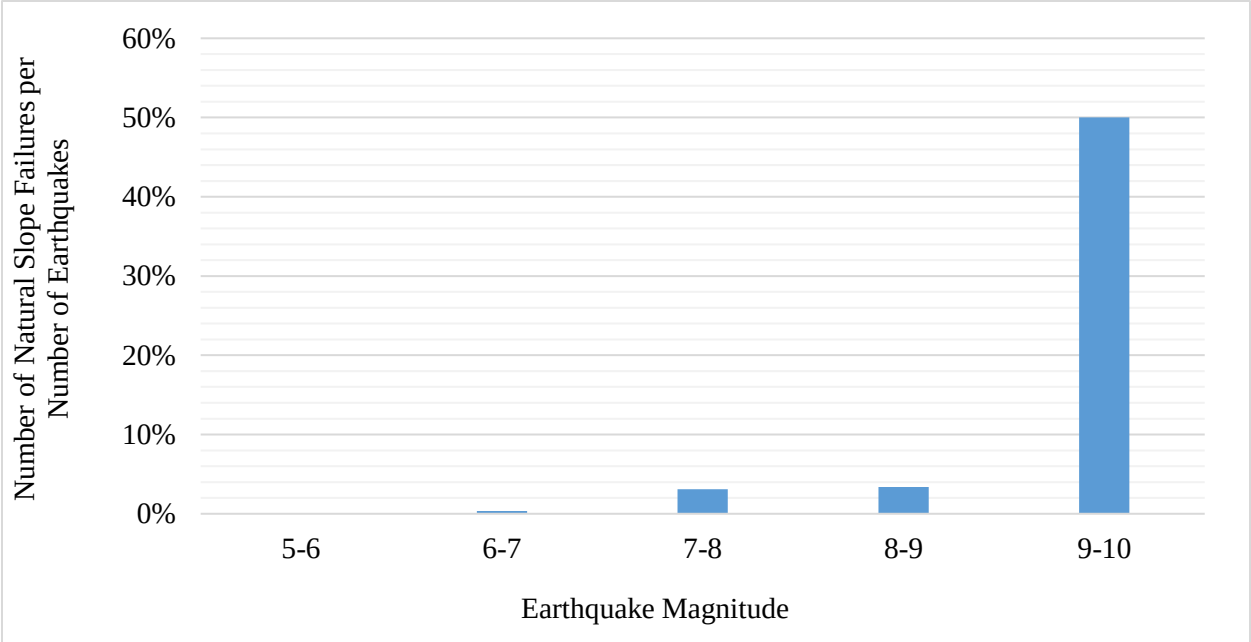

Figure 4-6 Percentage of number of natural slope failures per number of earthquakes in different magnitude ranges.

According to Figure 4-2, all tailing dam failures triggered by earthquake magnitudes of 5.0 to 9.0 were mostly located in Chile, Peru and western United States. Similar to the natural slope failures, the number of tailing dam failures increases by increase in the magnitude. Most tailing dam failures were in the magnitude range of 7.0 to 8.0 in which 19 (50% of events) were triggered by two specific earthquakes in 1965 and 1985. Eight failures (23% of events) were observed in tailing dams during earthquake magnitudes of more than 8.0 compared to the five events (5% of events) in natural slopes. However, it should be noted that only three earthquakes triggered eight tailing dam failures while there are five different earthquakes triggering the five natural slope failures in this magnitude range.

Figure 4-7 shows the percentage of open pit mines subjected to different earthquake magnitude ranges. The figure shows that during the last 25 years (since 1990) there were only 31 (18% of) open pit mines subjected to earthquake magnitudes of more than 5.0 and the increase in the earthquake magnitude is accompanied by decrease in the number of open pit mines. The figure shows that 137 (73% of) open pit mines are not located in seismic active regions.

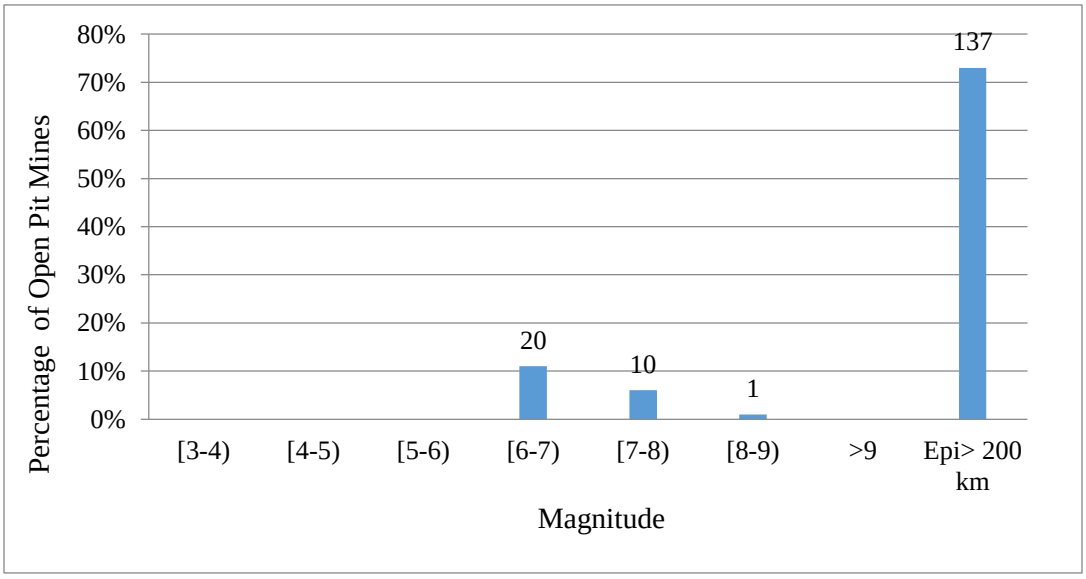

Figure 4-7 Percentage of open pit mines subjected to different earthquake magnitude ranges (values on the bars represent the number of cases).

This study also shows a significant difference in earthquake magnitudes triggered natural slope and tailing dam failures compared to those in the vicinity of the open pit mines. More than 95 percent of natural slope and tailing dam failures were triggered by magnitudes of more than 5.0 compared to the open pit mines that 18 percent were exposed to this magnitude range.

4.2.2 Epi-central Distance

As discussed in Chapter 2, epi-central distance has an inverse correlation with the shaking intensity that shows 50 percent decrease in shaking intensity reaching 100 km of epi-central distance. The analysis was performed to investigate the effect of epi-central distance on failed natural slopes and tailing dams, and endured open pit mines. Figures 4-8 to 4-10 show the cumulative frequency and number of cases, respectively, for the natural slope and tailing dam failures along with endured open pit mines in different earthquake epi-central distance ranges.

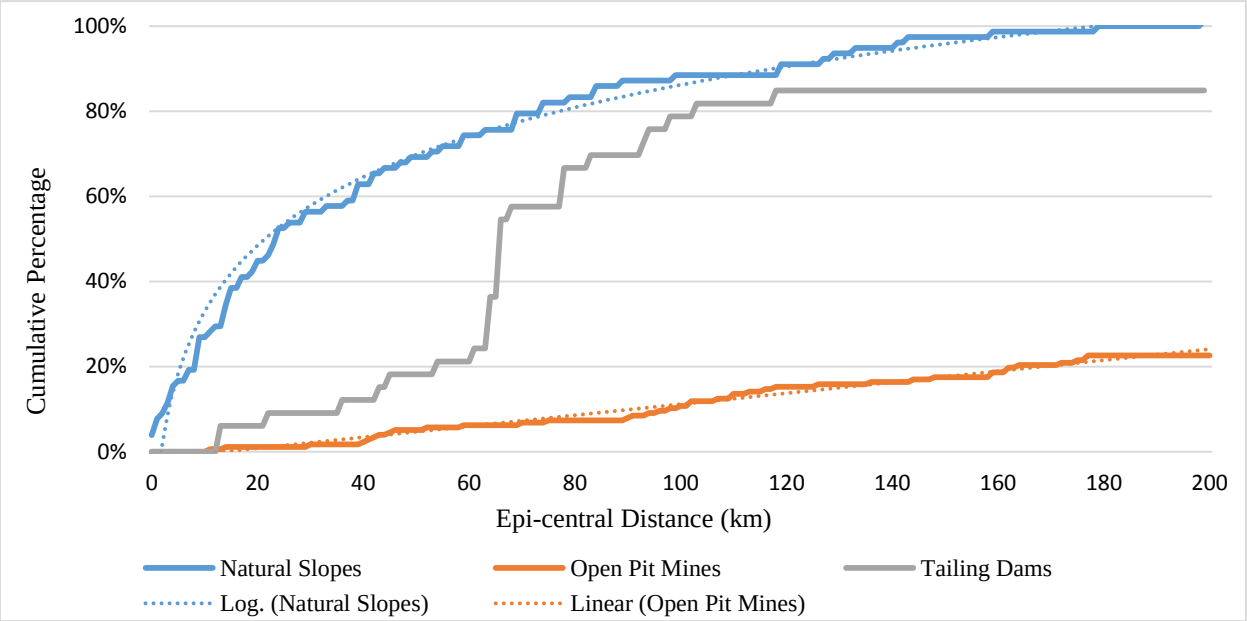

Figure 4-8 Cumulative percentage of natural slope and tailing dam failures and endured open pit mines in different epi-central distances.

According to Figure 4-8, 83 percent of natural slope failures were in 100km epi-central distance and all were in the range of 200 km. Figure 4-9 shows that the failure frequency in natural slopes decreases significantly while the epi-central distance increases. This reflects a similar logarithmic trend discussed in Chapter 2, Figure 2-5, between epi-central distance and shaking intensity. With increasing distance from the earthquake epi-center, landslide failures were more likely to take place in weak material or become shallow failures in stronger material. The Guatemala earthquake of 1976 (M=7.5, number 36 in Table 3-1) was one of the events in which landslides occurred relatively far from the earthquake epi-center up to 160 km. Dominant failure types in this event were rockfalls and shallow debris flows on steep and weak material slopes with a relatively small landslide volume of less than 15,000 m^3. The Luzan incident in 1990 (M=7.8, number 63 in Table 3-1) is another example where landslides were located in large epi-central distances (~200 km). The landslides that occurred in this event were in sand boils that where susceptible to liquefaction under seismic loads. In contrast, the landslides that occurred in short epi-central distances of about 20 km were mostly deep and in stronger material. A good example for these events is the Wairarapa landslide in 1885 (M=8.2, number 3 in Table 3-1) in which the earthquake triggered extensive landslides containing ~300,000 m^3 of material. Another example is the Irpinia landslide in 1980 (M=6.9, number 47 in Table 3-1), which had an epi-central distance between zero and 15 km. The failure types in this event, were earth flows that traveled up to 3 km and were relatively large in closer distances mostly rockfall in greater epi-central distances. The Wenchuan earthquake in 2008 (M=8.0, number 89 in Table 3-1) triggered thousands of natural and dam slope landslides. The occurrence of landslides in this event extended to more than 100 km, with a significant decrease in the number of events by distance.

Tailing dam failures are triggered with earthquake epi-central distance of up to 313 km, with most between 80 and 100 km. The expected trend for shaking intensity and epi-central distance observed for natural slope failures is not observed for this type of slopes. This is because the tailing dam locations are not scattered and are concentrated only in three locations that triggered by only 12 earthquakes which does not provide a decent distribution to see such a trend.

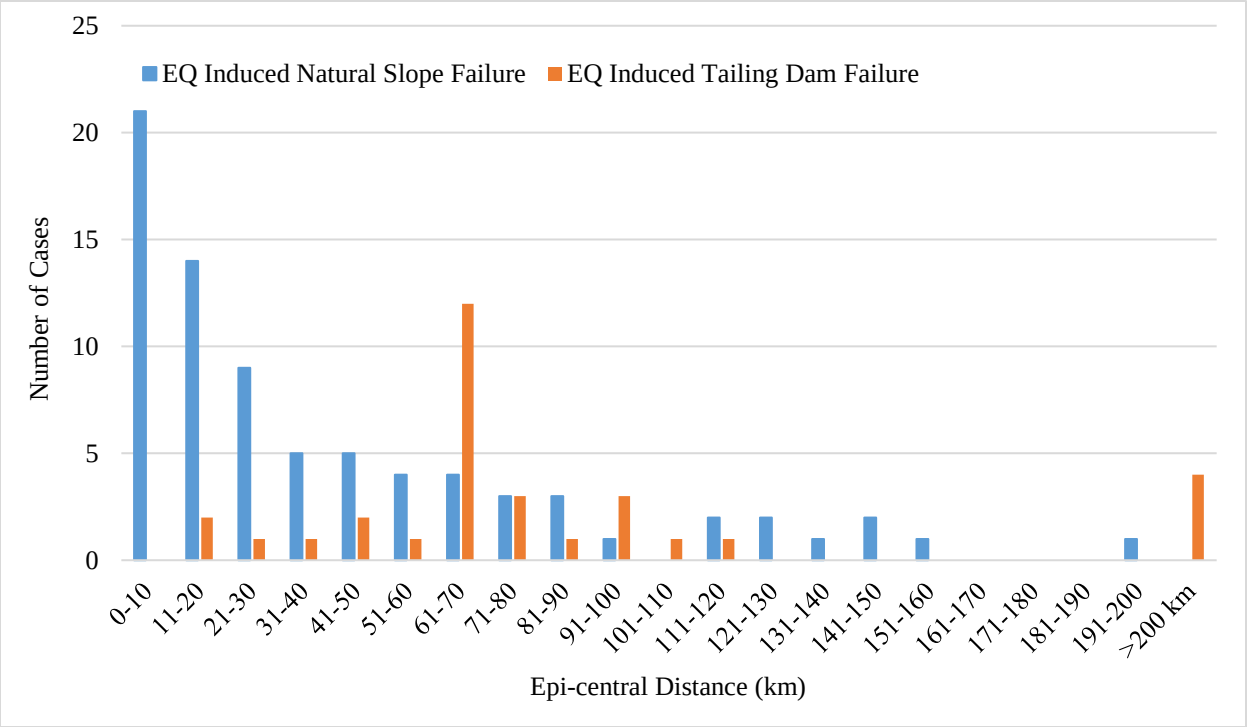

Figure 4-9 Distribution of natural landslides and tailing dam failures in different earthquake epi-central distance ranges.

Figure 4-10 shows the relationship between the number of open pit mines and epi-central distance in which there is no open pit mine located in the range of 10 km whereas 25 percent of natural slope failures occurred in this range of epi-central distance. The figure shows that 23% (40 cases) of open pit mines are subjected to earthquakes with epi-central distance of less than 200 km, where all natural slope failures and 85 percent of tailing dam failures were in this range. Furthermore, more than 85 percent of natural slope failures were in the range of 100 km of epi-

central distance, whereas only 11% (19 cases) of open pit mines were located in this range. This shows that considering the epi-central earthquake parameters, 89% of open pit mines are not subjected to strong enough shaking intensities to produce slope failure. Comparing tailing dam failures and open pit mines, 85% of tailing dam, which are significantly more susceptive to failure due to liquefaction, were located in the range of 200 km epi-central distance. This shows that open pit mines located beyond 200 km from earthquake epi-center are not expected to be impacted.

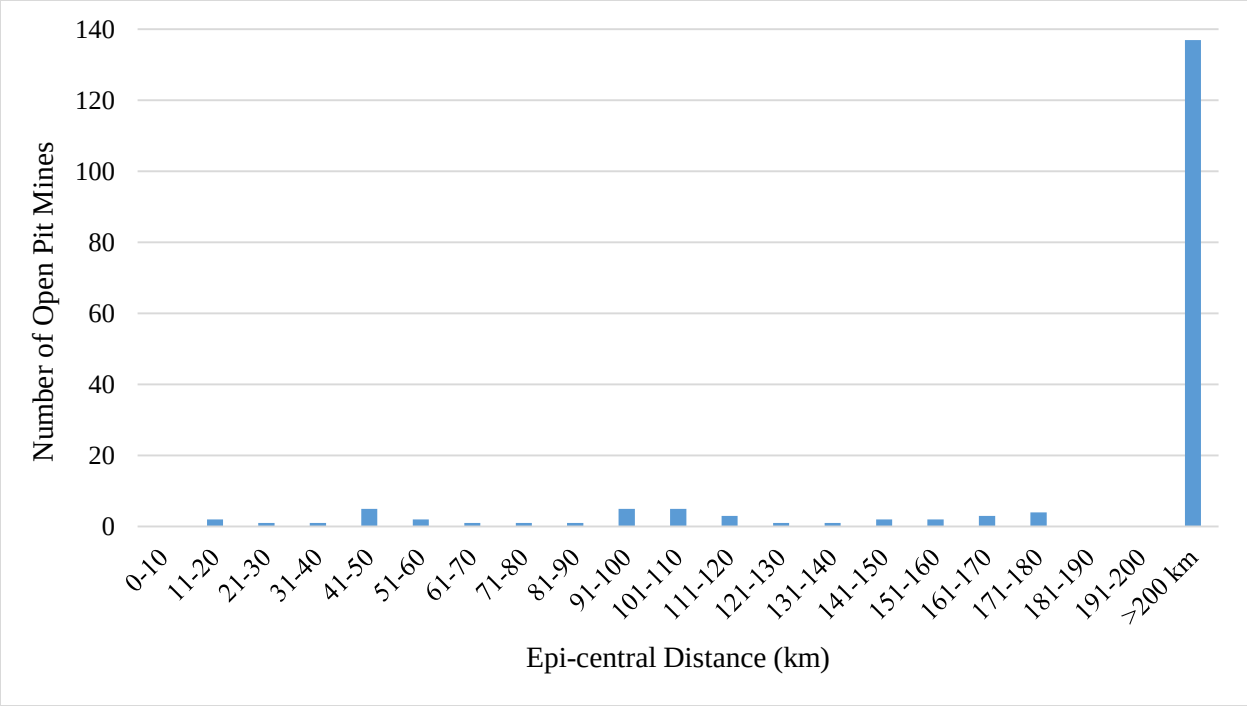

Figure 4-10 Distribution of open pit mines in different earthquake epi-central distance ranges.

4.2.3 Focal Depth

As discussed in Chapter 2, focal depth has a reverse correlation with shaking intensity. Shallower earthquakes with the same focal energy create more shaking intensity on surface compared to deep earthquakes. Figures 4-11 to 4-13 show the frequency and cumulative percentage of natural slope and tailing dam failures and enduring open pit mines in different earthquake focal depths, respectively.

Figure 4-11 shows that natural slope failures except one (number 83 in Table 3-1, depth= 73 km) are triggered by shallow earthquakes (<70 km). Figure 4-13 shows a similar logarithmic trend shown for epi-central distance relationship in which the number of failures decrease significantly with increase in the focal depth. More than 65 percent of the natural slope failures occurred at earthquake focal depths of less than 20 km, where 95 percent occur in less than 40 km. The depth of an earthquake is known to correlate with the earthquake source type in terms of fault or subduction and its location on these geological structures. Figure 4-14 shows the worldwide earthquake depth of magnitudes 7.0 and above from 1900 to 2013 [134]. The Nazca plate in South America is one of the subduction zones which generates shallow earthquakes on the west coast of Chile and Peru trench and progressively deeper earthquakes eastward as the subduction plate derives deeper. Figure 4-15 shows this subduction zone with the magnitude and depth of the generated earthquakes by the Nazca plate movements. The large natural slope failures occurred close to the coast edge are triggered by shallow earthquakes (numbers 26 and 51 in Table 3-1). New Zealand as a region with high seismicity is another example for the effect of shallow earthquakes. Figure 4-16 shows the Australia and Pacific subduction on the west and east borders of the New Zealand plate, respectively. The Pacific plate moves under the east side of the North Island generating shallower earthquakes around the east border of the North Island. The Australia plate moves under the west side of the South Island produce shallower earthquakes around the west border of the South Island. Figure 4-17 shows the natural slope failures and open pit mines in Central America subjected to the earthquakes generated by the subduction of Cocos plate beneath the Caribbean plate. Figures 4-18 and 4-19 show the natural slope and open pit mines in Iran and western Asia, respectively, which are in the vicinity of earthquakes generated by subduction zones and faults. It is observed from Figures 4-15 to 4-19 that the natural slope failures

are mostly triggered close to the large magnitude earthquakes with shallow depths and the larger failures occurred close to the coast edge triggered by shallower earthquakes (numbers 5, 26 and 51 in Table 3-1). In New Zealand, 17 out of 19 landslides were triggered by less than 20 km deep earthquakes. In contrast, the El Salvador (number 83 in Table 3-1) and Ancosh (number 32 in Table 3-1) events, with depths of 60 and 73 km, are examples for deep subduction zones that generated relatively small landslides. Figure 4-11 shows that all tailing dams are triggered by shallow earthquakes (<70 km). However, the trend observed for natural slope failures is not seen for tailing dams and the number of failures fluctuate by the earthquake depth. This is because of the same reason mentioned in the epi-central distance analysis, such as limited number and local concertation of earthquakes triggering tailing dam failures.

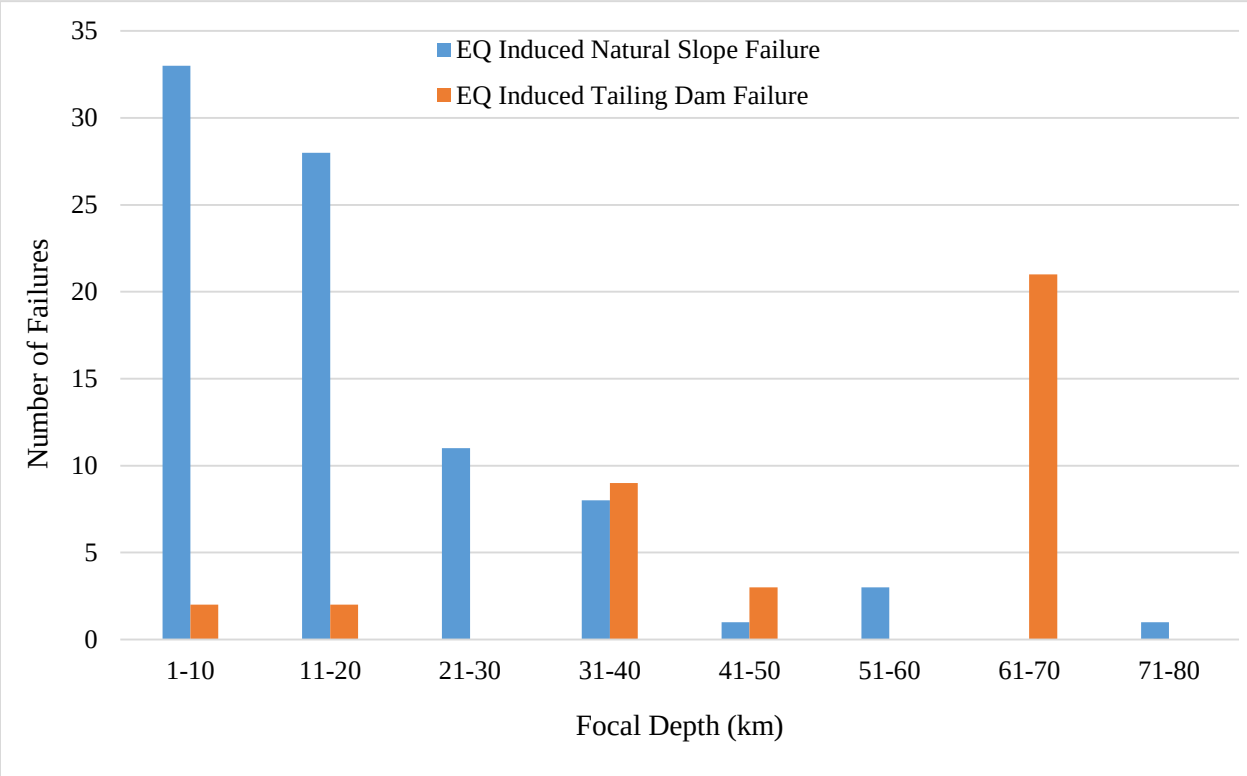

Figure 4-11 Frequency of natural landslides and tailing dam failures in different earthquake depth ranges.

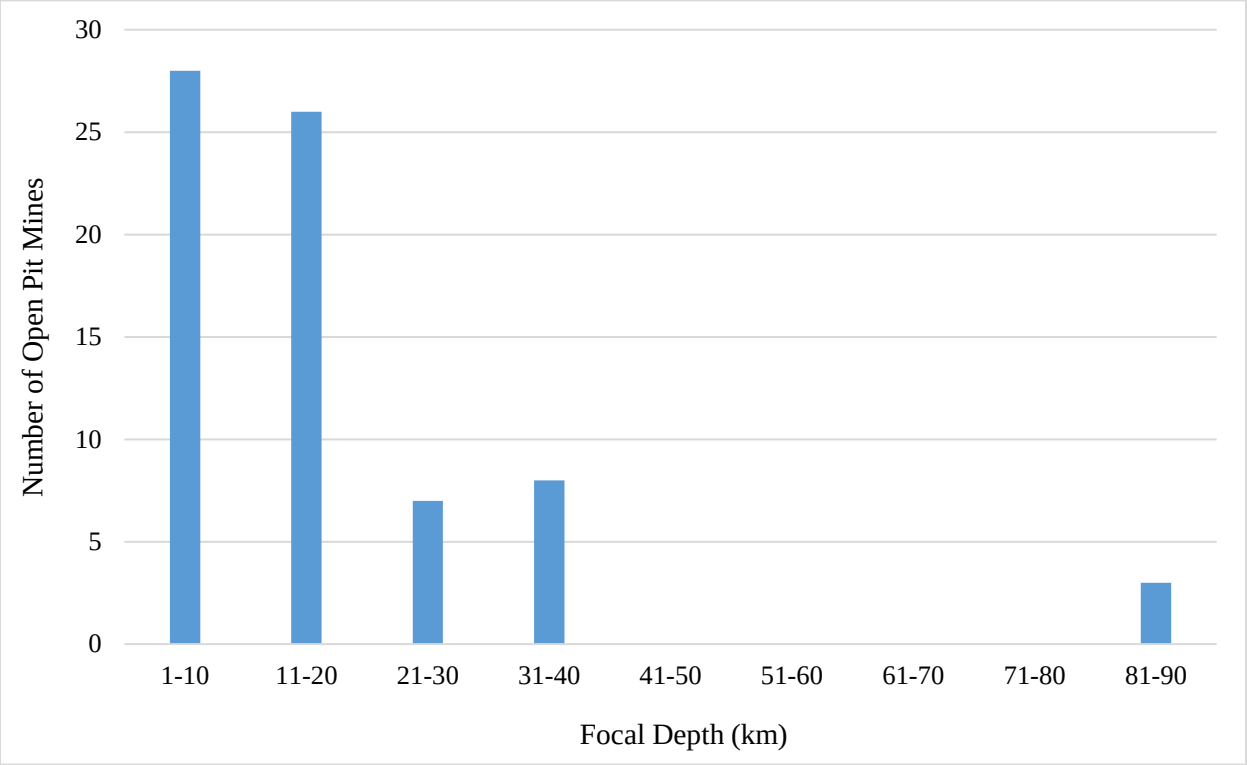

Figure 4-12 Frequency of open pit mines in the vicinity of different earthquake depth ranges.

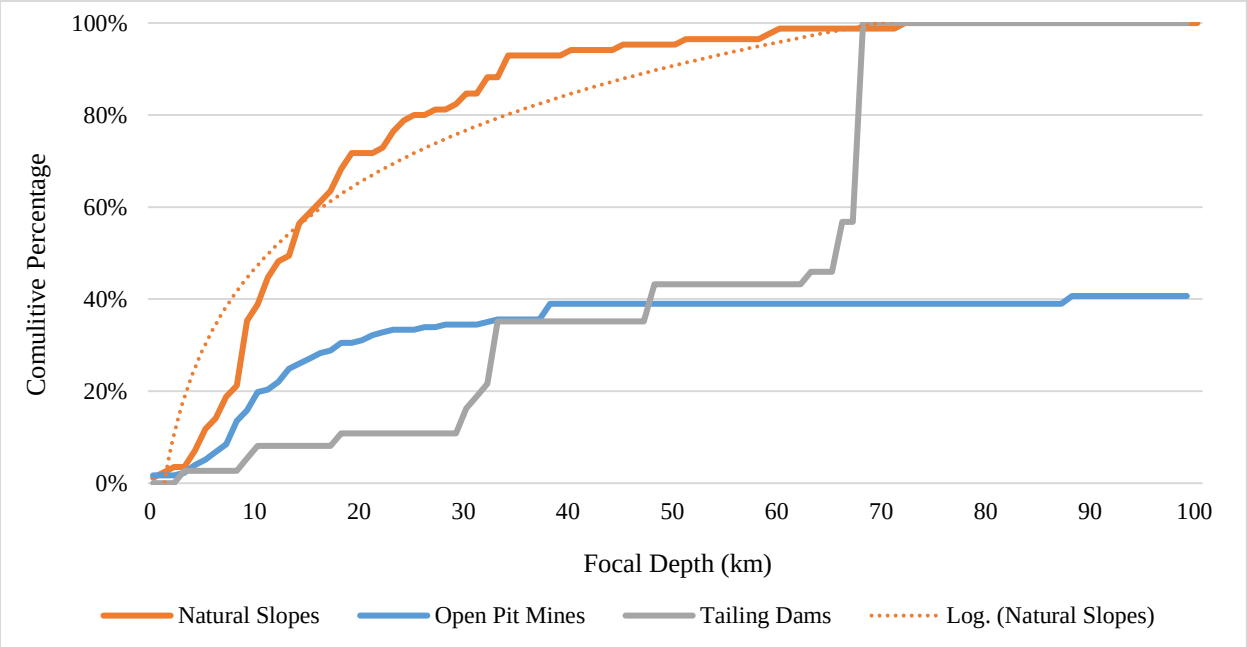

Figure 4-13 Cumulative percentage of natural slope and tailing dam failures and endured open pit mines in different focal depths.

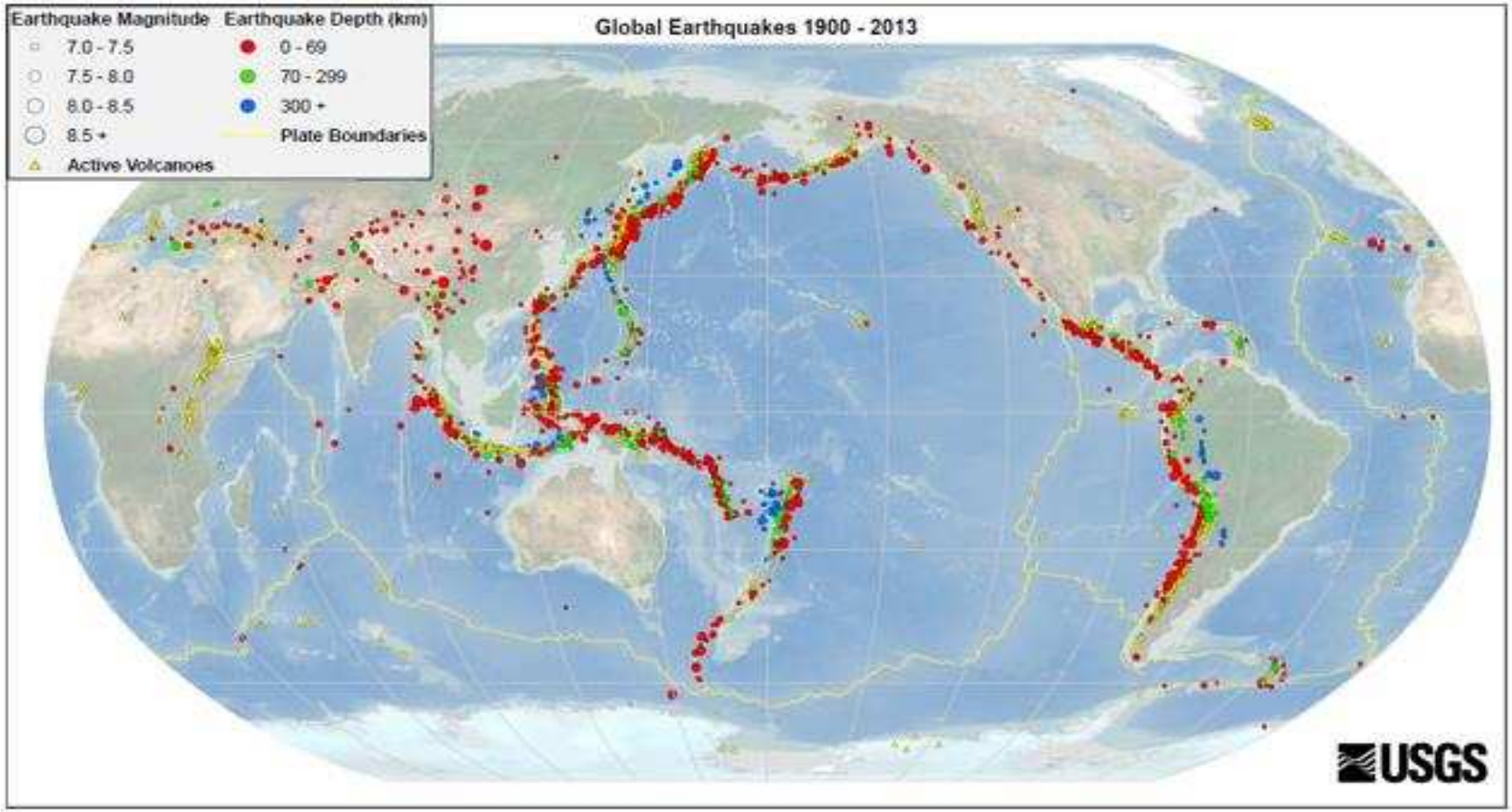

Figure 4-14 Earthquake focal depths of magnitude 7.0 and above from 1900 to 2013 [135].

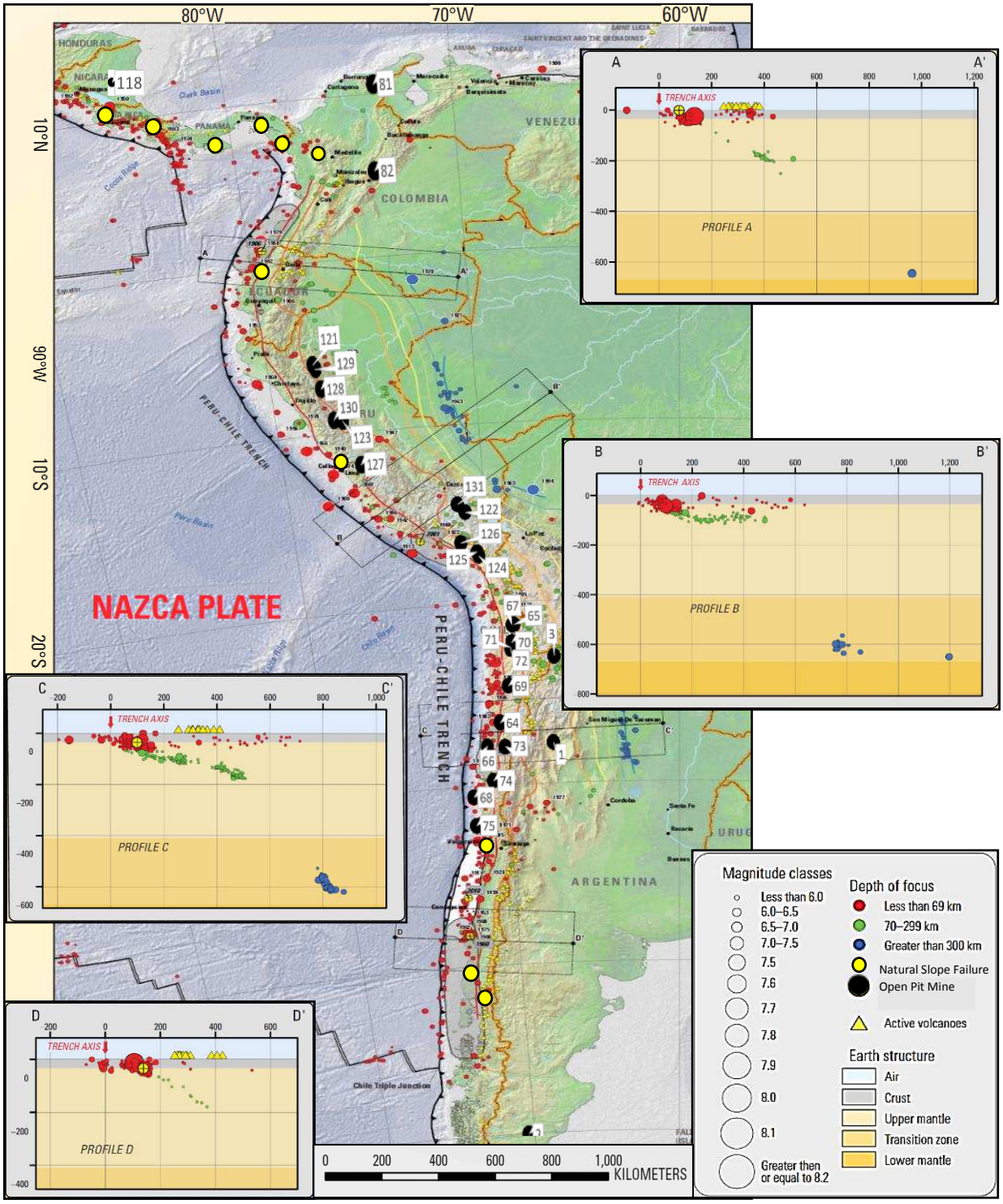

Figure 4-15 Natural slope failures and open pit mines subjected to earthquakes generated by the subduction of Nazca plate beneath the Peru-Chile trench with the produced earthquake magnitudes and focal depths from 1900 to 2013 (Modified USGS map [136]).

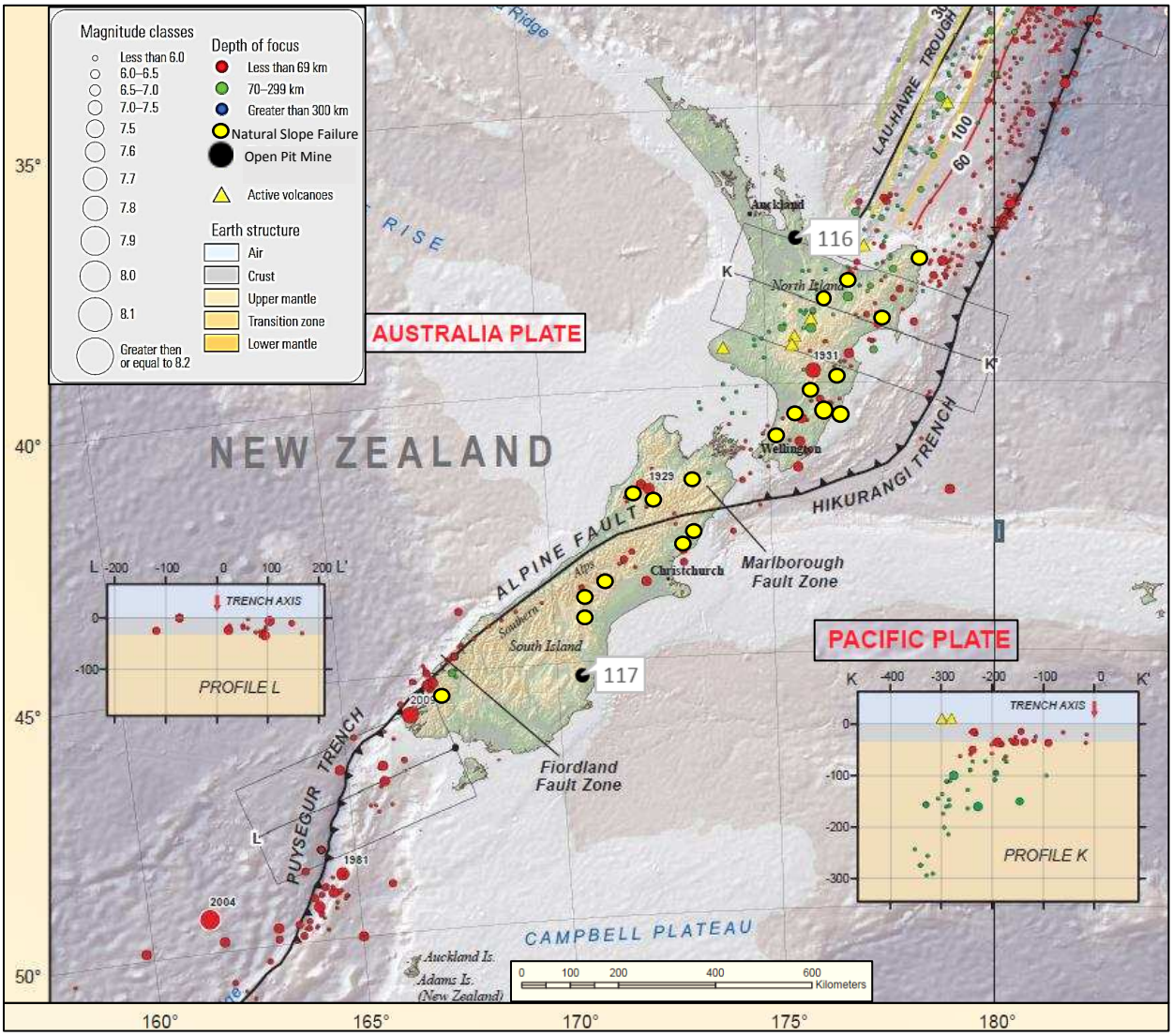

Figure 4-16 Natural slope failures and open pit mines subjected to earthquakes generated by the subduction of Australia and Pacific plate under New Zealand plate with the created earthquake magnitudes and focal depths from 1900 to 2010 (Modified USGS map [136]).

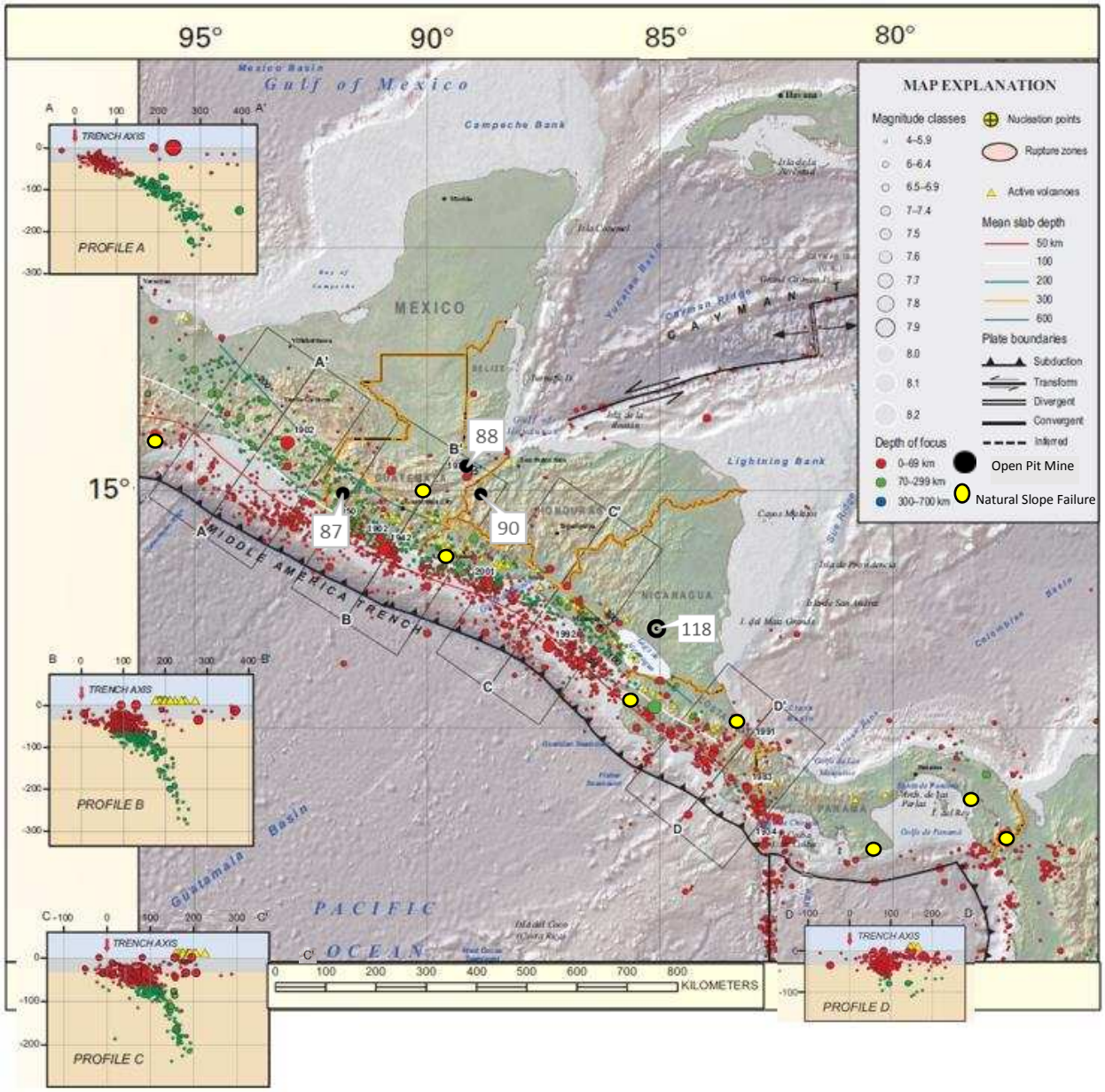

Figure 4-17 Natural slope failures and open pit mines subjected to earthquakes generated by the subduction of Cocos plate beneath the Caribbean plate along with the produced earthquake magnitudes and focal depths from 1900 to 2013 (Modified USGS map [137]).

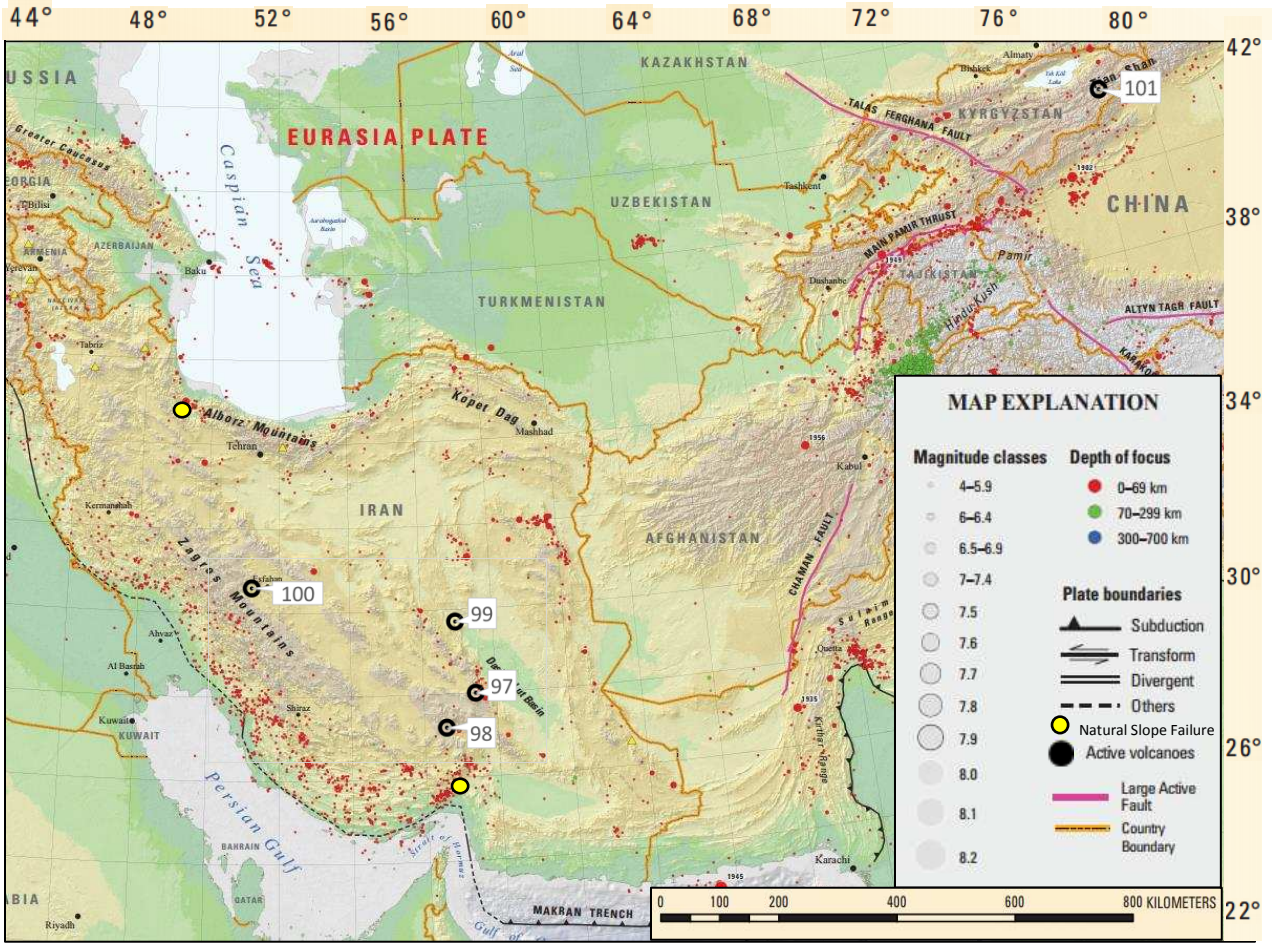

Figure 4-18 Natural slope failures and open pit mines subjected to earthquakes generated in the middle east region by the subduction of Arabia plate beneath the Iran plate and the Talas fault along with the produced earthquake magnitudes and focal depths from 1900 to 2010 (Modified USGS map [138]).

Analyzing the relation between open pit mines and focal depth shows that there are 69 open pit mines, exposed to shallow earthquakes (<70 km). However, among these 69 cases, 36 mines are located in 200 km epi-central distance in which the earthquakes would be effective based on the epi-central distance analysis. Figures 4-20 and 4-21 present the natural slope failure events and open pit mines that are located in high, medium and low risk zones, respectively. These risk zones are defined from the natural slopes analysis in which the high risk zone is the epi-central and focal depth ranges, where 90 percent of natural slope failures were triggered, and earthquake epi-center and depths of less than 40 and 100 km, respectively. The medium risk zone is the epi-central and

focal depth range where 10 percent of natural slope failures occurred, and epi-center and depths of less than 70 and 200 km, respectively. Finally, the low risk zone is the epi-central and focal depth range in which no natural slope failure was occurred, where depths of more than 70 km and epi-central distance of more than 200 km. Table 4-1 defines the risk zones based on the focal depth, epi-central distance and percentage of natural slope failures. According to Figures 4-20 and 4-21, only seven open pit mines are located in the high risk zone. Table 4-2 presents open pit mines in the vicinity of earthquakes with less than 200 km epi-central distance and 70 km deep along with their corresponding earthquakes and risk zones.

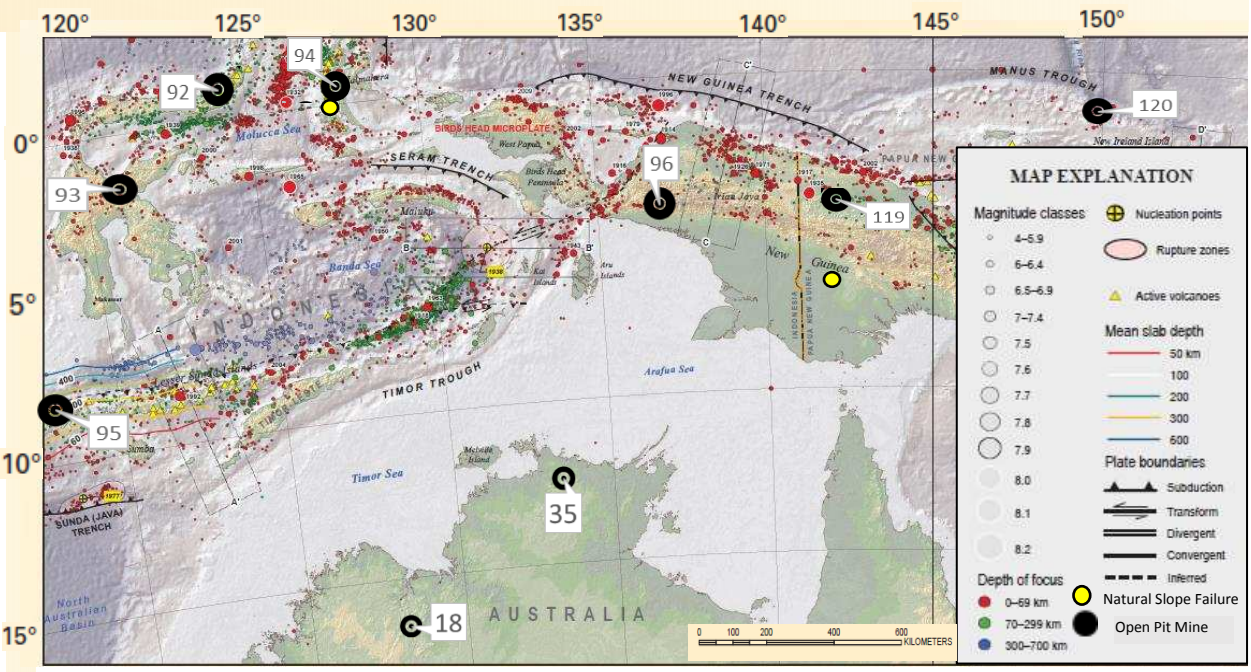

Figure 4-19 Natural slope failures and open pit mines subjected to the earthquakes generated by the subduction of Pacific Ocean plate beneath the Coral Sea plate along with the produced earthquake magnitudes and focal depths from 1900 to 2010 (Modified USGS map [139]).

Table 4-1 Definition of risk zones based on focal depth, epi-central distance and percentage of natural slope failures.

Risk Zone	Low	Medium	High
Epi-central Distance	>200 km	100 - 200 km	<100 km
Focal Depth	>40 km	40 – 70 km	<70 km
Natural Slope Failures	0%	10%	90%

According to Figure 4-16, the Martha and Macraes open pit mines in New Zealand are located far from the subduction zone (>200 km) which are subjected to deep (>70 km) earthquakes. However, Figures 4-15 and 4-17 show that among the open pit mines in Central and South America 24 are located in shallow seismic zones that could be a concern for the mining engineers. There are 10 other open pit mines located in shallow depths in Iran, Philippines, Papua New, Indonesia, and Kirghizstan.

Figure 4-20 Focal depth vs. epi-central distance of earthquakes triggered natural slope failures and defining high, medium and low risk zones considering the frequency of failures.

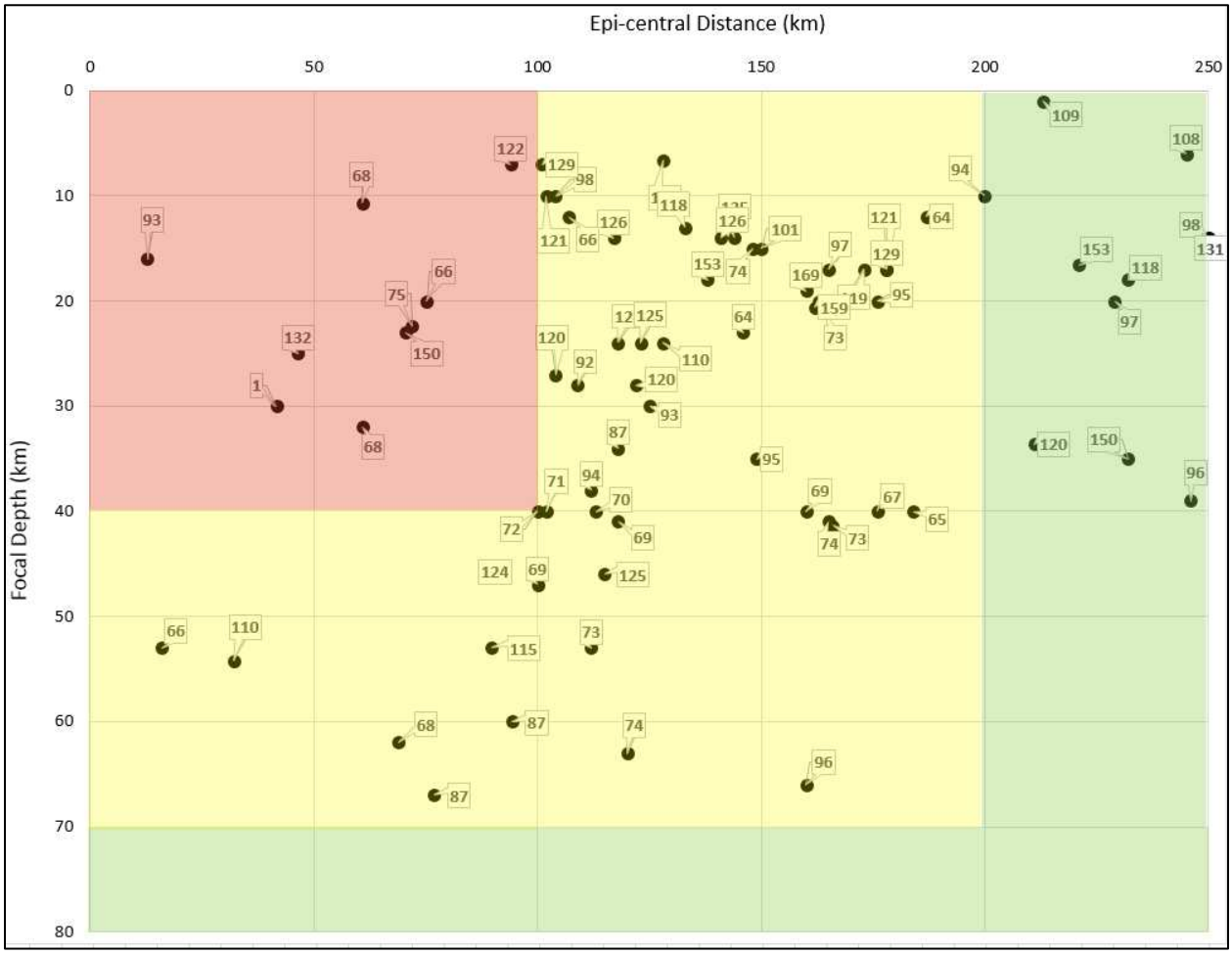

Figure 4-21 Focal depth vs. epi-central distance of earthquakes subjected to open pit mines and their risk zone according to natural slope failures (note: some open pit mines are defined by more than one point on the graph which shows that they were subjected to more than one earthquake).

Table 4-2 Open pit mines subjected to earthquake shallower than 70 km and epi-central distance of less than 200km and their risk zone distinguished by color (red: high risk; yellow: medium risk).

No.	Name	Country	$Year_1$	M_1	Epi_1	$Depth_1$	$Year_2$	M_2	Epi_2	$Depth_2$	$Year_3$	M_3	Epi_3	$Depth_3$
1	Alumbrera	Argentina	1993	6.6	41.6	30	-	-	-	-	-	-	-	-
64	El Salvador	Chile	1993	6.5	146	23	2006	6.6	187	12	-	-	-	-
65	Collahuasi	Chile	2007	7.7	184	40	-	-	-	-	-	-	-	-
66	Candelaria	Chile	2011	6.7	75.2	20	2006	6.6	107	12	-	-	-	-
67	Quebrada Blanca	Chile	2007	7.7	176	40	-	-	-	-	-	-	-	-
68	Carmen de Andacollo	Chile	2003	6.7	60.8	32	-	-	-	-	-	-	-	-
69	Escondida	Chile	1995	8	160	40	-	-	-	-	-	-	-	-
70	El Abra	Chile	2007	7.7	113	40	-	-	-	-	-	-	-	-
71	Radomiro Tomic	Chile	2007	7.7	102	40.00	-	-	-	-	-	-	-	-
72	Chuquicamata	Chile	2007	7.7	100	40	-	-	-	-	-	-	-	-
73	Maricunga	Chile	2011	6.1	163	20	-	-	-	-	-	-	-	-
74	Pascua Lama	Chile	1995	6.7	148	15.00	-	-	-	-	-	-	-	-
75	Los Pelambres	Chile		8.3	72	22.4	-	-	-	-	-	-	-	-
87	Marlin	Guatemala	1993	7.2	118	34.0	-	-	-	-	-	-	-	-
92	J Resources North Lanut	Indonesia	2010	6.1	109	28	2014	6.2	125	30	-	-	-	-
93	Vale INCO Nickel	Indonesia	2011	6.1	12.8	16	2012	6.3	200	10	-	-	-	-
94	Nickel Mine	Indonesia	2014	6.5	112	38	2014	7.1	149	35	-	-	-	-
95	Batu Hijau	Indonesia	2007	6.5	176	20	-	-	-	-	-	-	-	-
97	Sarcheshmeh	Iran	1998	6.6	165	17	-	-	-	-	-	-	-	-
98	Gol Gohar	Iran	1990	6.6	104	10	-	-	-	-	-	-	-	-
101	Kumtor	Kyrgyzstan	2013	6.1	150	15	-	-	-	-	-	-	-	-
110	Los Filos and Bermejal	Mexico	2011	6.5	32.0	54.2	2012	6.1	89.6	53.0	2014	7.2	128	24.0
118	la Libertad	Nicaragua	2011	6.0	104	177	2014	6.6	118	135	2014	6.1	133	13.0
119	Porgera	Papua New	2000	6.5	173	17	2010	6	211	33.6	-	-	-	-
120	Lihir	Papua New	2000	8.0	104	27	2013	6.5	102	10	2010	6.5	122	28
121	Cerro Corona	Peru	1990	6.5	178	17	2014	6.3	387	9.8	-	-	-	-
122	Tintaya	Peru	2013	6.0	94.4	7	-	-	-	-	-	-	-	-
123	Antamina	Peru	1996	7.5	302	15	-	-	-	-	-	-	-	-
124	Toquepala mine	Peru	2001	6.7	118	24	2001	7.6	144	14	2010	6.2	92.8	46
125	Cuajone mine	Peru	2001	6.7	123	24	2001	7.6	141	14	2010	6.2	115	46
126	Cerro Verde Mine	Peru	2001	7.6	117	14	2013	6.0	101	7	1999	6.8	97.6	88
129	Yanacocha	Peru	1990	6.5	178	17	-	-	-	-	-	-	-	-
131	Constancia	Peru	2013	6.0	128	6.6	-	-	-	-	-	-	-	-
132	Didipio	Philippines	1990	7.7	70.4	23	-	-	-	-	-	-	-	-
153	Spring Creek	USA	1992	7.2	138	18	-	-	-	-	-	-	-	-
169	Fort Knox	USA	2002	6.6	160	19	-	-	-	-	-	-	-	-

4.2.4 Intensity

Intensity of an earthquake is a scale of ground shaking considered at a specific region which is a function of magnitude, epi-central distance, and focal depth. Studying this parameter could be very valuable because it considers all the previously discussed earthquake parameters at the same time. Various relations are presented for different regions to estimate the intensity [138, 139]. The

selected relation for this study is from the research on Central and South Eastern Europe earthquakes from 342-BC to 1990-AD due to its relatively more comprehensive database [140]. According to this study, intensity is a function of earthquake magnitude, epi-central distance, and focal depth expressed in the form of Equation 4-1.

$$I_i = b\mathrm{M} - v\log\sqrt{\Delta^2 + h^2} + c \qquad \text{(Eq. 4-1)}$$

where, I_i is the earthquake intensity in MM (Modified Mercalli)[1], M is the magnitude, Δ is the epi-central distance in kilometers and h is the focal depth in kilometers. The symbols b, v, and c are statistical constants that can be determined for each region.

The intensity values of earthquake-triggered natural slopes, tailing dams and open pit mines since 1990 are calculated using the generic values for constants as, b =1.5, v =3.5 and c =3 [141]. The shaking intensity could be equal for two events with different earthquake magnitudes, focal depths and epi-central distances. Guatemala and Klamath Falls (numbers 36 and 73 in Table 3-1, respectively) events are examples of this circumstance (Table 4-3).

Table 4-3 Guatemala and Klamath Falls events with the same intensity and different magnitudes, epi-central distances and focal depths.

No.	Name	Country	Year	M	Epi-central Distance (km)	Depth (km)	Intensity (MM)
36	Guatemala	Guatemala	1976	7.5	160	12	6.5
73	Klamath Falls	OR, USA	1993	5.8	30	9	6.5

1- Modified Mercalli (The Modified Mercalli Scale is a qualitative measure of the strength of ground shaking at a particular site defined from 1 to 10, which the greater value shows a higher intensity).

Because there are no recorded failures for open pit mines, the intensity calculations consider all earthquakes in the vicinity of each open pit mine since 1990. To do this, a network was developed on the open pit mine and earthquake maps from the database that connects each open pit mine to all earthquakes around it up to 400 km distance since 1990. Figure 4-22 illustrates an example of the network created for three open pit mines in Chile, showing the parameters for each earthquake with respect to the mines. Figure 4-23 shows the intensity values for natural slope and tailing dam failures, and earthquakes in the vicinity of open pit mine sites, individually. The graph depicts the significant intensity range contrast between the natural slopes and tailing dams compared to enduring open pit mines. The open pit mines are mostly subjected to the intensities of range 2.0 to 6.0, while natural slope and tailing dam failures are triggered by earthquake intensities of more than 6.0. There are no open pit mines located in the vicinity of earthquake intensities of less than 2.0 in the graph is because they were not in the range of 400 km epi-central distance to be considered in this analysis. Figure 4-24 and 4-25 graphs the earthquake intensity range of failed natural slopes and tailing dams, and withstood open pit mines. This figure shows that 83 cases out of 95 natural slope failure events have an intensity of more than 6.0 and only eight landslide cases triggered by intensities of less than 6.0. Considering the cases triggered by intensities of 8.0 to 10.0, in most of them a large volume of material is moved and an extensive area is affected (numbers 1, 3, 23, 27, 30). The material involved in landslides triggered by low intensity earthquakes (<6) were relatively weaker, and more fractured and weathered (numbers, 8, 31, 59 and 93 in Table 3-1) with relatively less extended affected area.

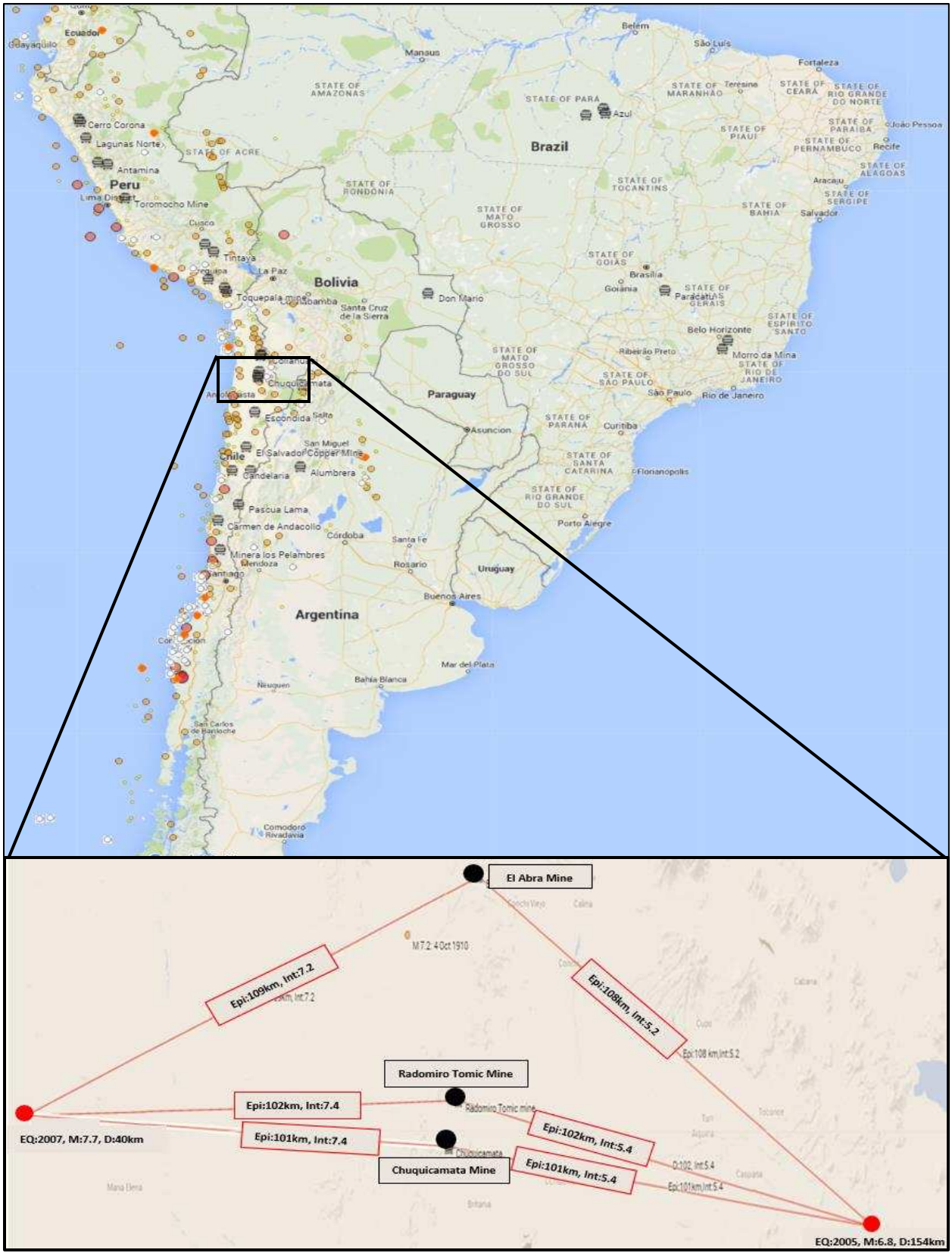

Figure 4-22 Example of extracting earthquake parameters from the database map to calculate the earthquake intensity of El Abra, Ramomiro Tomic and Chuquicamata open pit mines in Chile.

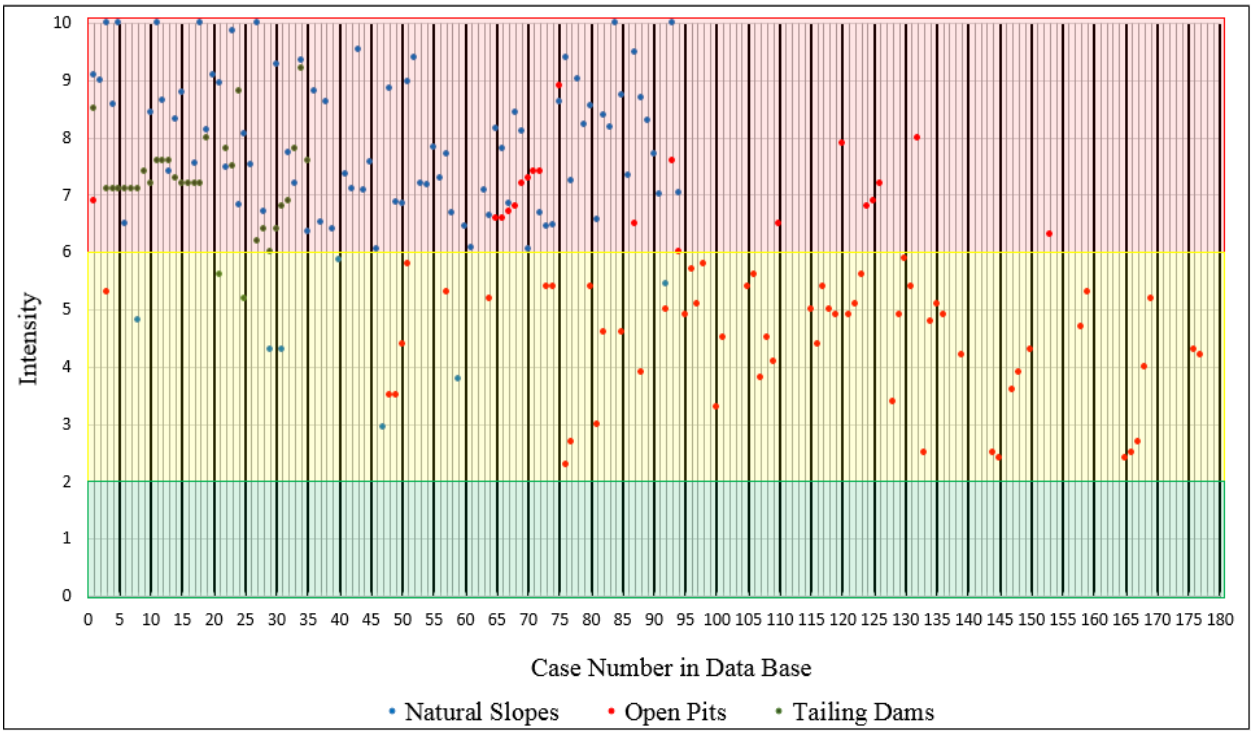

Figure 4-23 Intensity distribution of earthquakes triggered natural slope and tailing dam failures and subjected to open pit mines.

According to Figure 4-24, more than 90 percent of tailing dams failed during intensities of more than 6.0, and 75 percent were triggered by shaking intensities of more than 7.0. The reason that more than 60 percent (20 cases) failed between 6.0 and 7.0 intensities is because most of these tailing dam failures were triggered by the same earthquake and were located in the same region. More than 80 percent of failures were triggered in tailing dams constructed by the up-stream method which is the most susceptive to failure as described in Chapter 2.

In contrast to natural slope and tailing dam failures, the earthquake intensities exposed to open pit mine slopes are significantly lower and are mostly located between 2.0 and 6.0. There are 20 open pit mines (11%) located in seismic regions with intensities of more than 6.0, and only one open pit mine, Los Pelambres mine, has an intensity of more than 8.0 (see Table 4-4). This could be one of the reasons that even the open pit mines located in seismic regions are not mostly

subjected to strong enough earthquakes to observe failure. The effects of some of these earthquake events on open pit mines are reported in the news. Table 4-5 presents the reports for some of these mines by different news agencies. The reports state that there were no injury or operation interruption for these mines. This shows that other factors besides earthquake parameters are the reason why open pit mines have not failed during earthquakes. The following sections in this chapter discuss the effect of these other factors that may have been involved in natural slope and tailing dam failures compared to open pit mines.

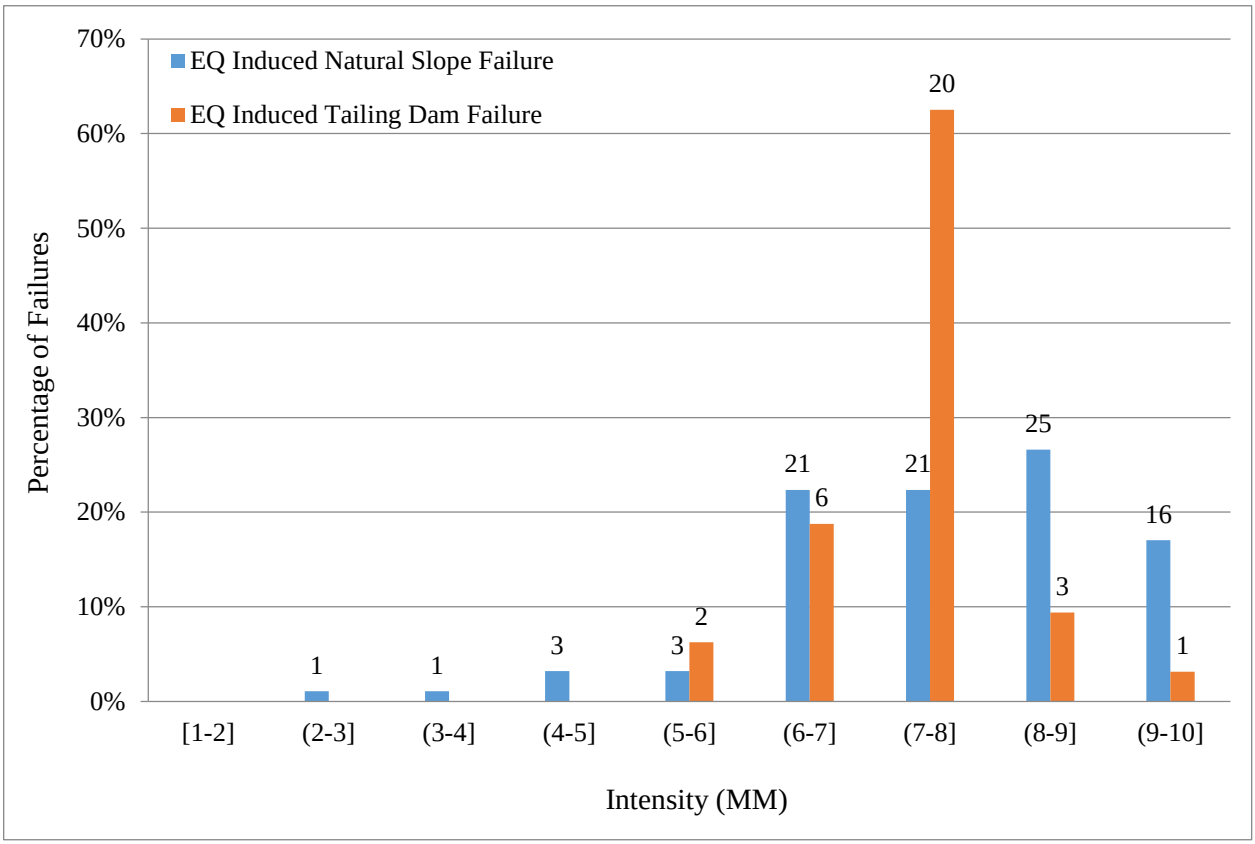

Figure 4-24 Frequency percentage of natural landslides and tailing dam failures in different intensity ranges (values on the bars represent the number of cases).

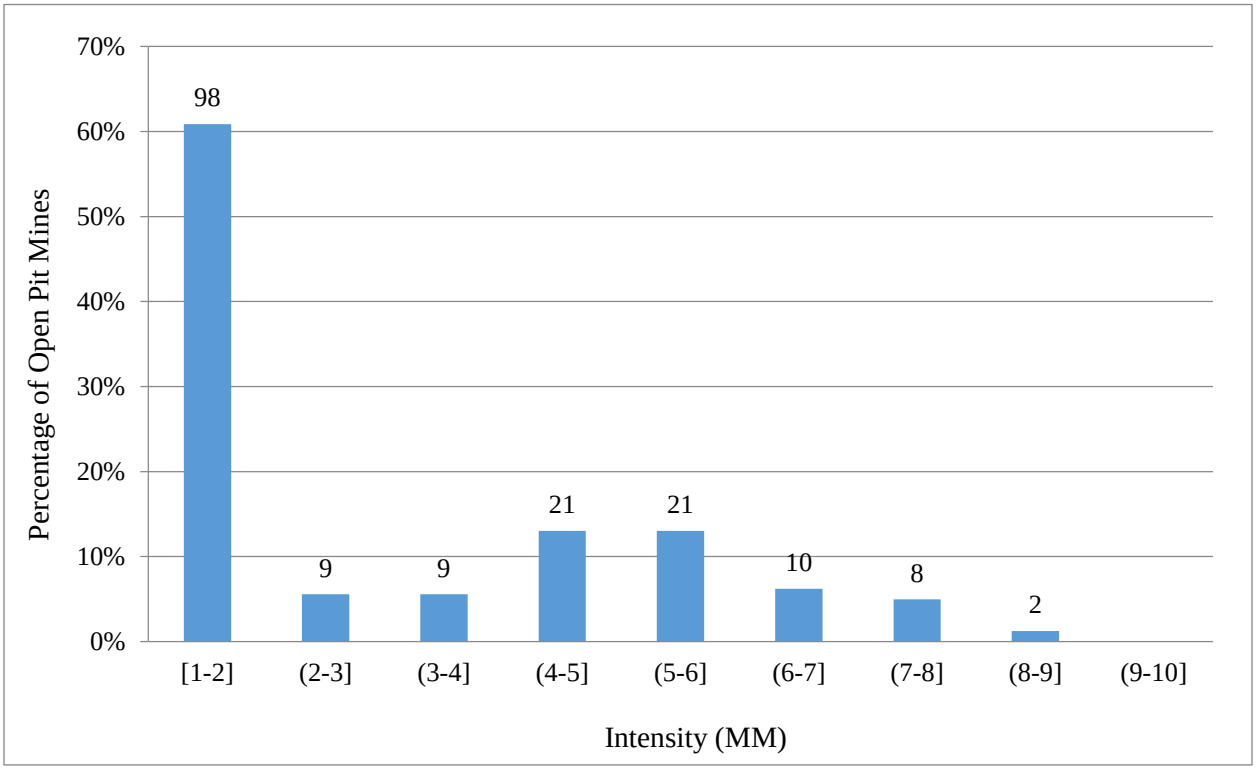

Figure 4-25 Frequency percentage open pit mines in the vicinity of different intensity ranges (values on the bars represent the number of cases).

Table 4-4 Open Pit mine examples subjected to earthquake intensity of more than 6.0.

No.	Name	Commodity	Country	Year	M	Epi-central Distance(km)	Focal Depth (km)	Intensity (MM)
1	Alumbrera	Copper	Argentina	1993	6.6	41.6	30.0	6.9
65	Collahuasi	Copper	Chile	2007	7.7	184.0	40.0	6.6
66	Candelaria	Copper	Chile	2002	6.5	16.0	53.0	6.6
67	Quebrada Blanca	Copper	Chile	2007	7.7	176.0	40.0	6.7
68	Carmen de Andacollo	Copper	Chile	1997	7.1	68.8	62.0	6.8
69	Escondida	Copper	Chile	1995	8.0	160.0	40.0	7.2
70	El Abra	Copper	Chile	2007	7.7	113.0	40.0	7.3
71	Radomiro Tomic	Copper	Chile	2007	7.7	102.0	40.0	7.4
72	Chuquicamata	Copper	Chile	2007	7.7	100.0	40.0	7.4
75	Los Pelambres	Copper	Chile	2015	8.3	72.0	22.4	8.9
87	Marlin	Gold/Silver	Guatemala	1993	7.2	118.0	34.0	6.5
93	Vale INCO Nickel	Nickel	Indonesia	2011	6.1	12.8	16.0	7.6
94	Nickel Mine	Nickel	Indonesia	2014	7.1	149.0	35.0	6.0
110	Los Filos and Bermejal	Gold/Silver	Mexico	2011	6.5	32.0	54.2	6.5
120	Lihir	Gold	Papua New	2000	8.0	104.0	27.0	7.9
124	Toquepala mine	Copper	Peru	2001	7.6	144.0	14.0	6.8
125	Cuajone mine	Copper	Peru	2001	7.6	141.0	14.0	6.9
126	Cerro Verde Mine	Copper	Peru	2001	7.6	117.0	14.0	7.2
132	Didipio	Gold	Philippines	1990	7.7	70.4	23.0	8.0
153	Spring Creek	Coal	USA	1992	7.2	138.0	18.0	6.3

Table 4-5 Reports on the effect of earthquakes on a few open pit mines.

Earthquake	Open Pit Mine	Consequence	Reference
July 30, 1995, M: 8.1	Escondida and Chuquicamata	no damage	New York Times [142]
June 23, 2001, M: 8.4	Toquepala and Cuajone	no damage, liquefaction on Cuajone Heap Leach Pads.	Peer Research Center, Berkeley [143]
November 14, 2007, M:7.7	Chuquicamata	no "relevant" damage, power outage, minor landslides	Southeast Missourian News [144]
	Escondida	power cut off	Reuters [145]
	Candelaria and El Abra	power outages	Reuters [145]
December 16, 2007, M: 6.7	Escondida	running at full capacity	Wordpress [146]
February 27, 2010, M: 8.8	Candelaria	no damage, temporary shutdown due to power outage	Freeport McMoRan Copper & Gold Inc. [147]
April 1, 2014 , M: 8.2	Quebrada Blanca	operating normally	Bloomberg [148]
	Collahuasi	didn't damage installations or cause injuries, operating normally	Buenos Aires Herald [149]
September 16, 2015, M: 8.3	Carmen de Andacollo	no obvious damage, full operation, no injuries	Reuters [150]

4.3 Water Condition

As discussed in Chapter 2, water is an important parameter affecting the slope stability during earthquakes. Analyzing the natural slope database shows the presence of water in all the failures where data is available. These slopes were either close to an existing water source such as rivers, lakes and oceans or subjected to intense precipitation. Figure 4-26 presents the types of water condition affecting earthquake-triggered natural slope failures and their frequency which reveals that river valleys are the most commonly failed slope type.

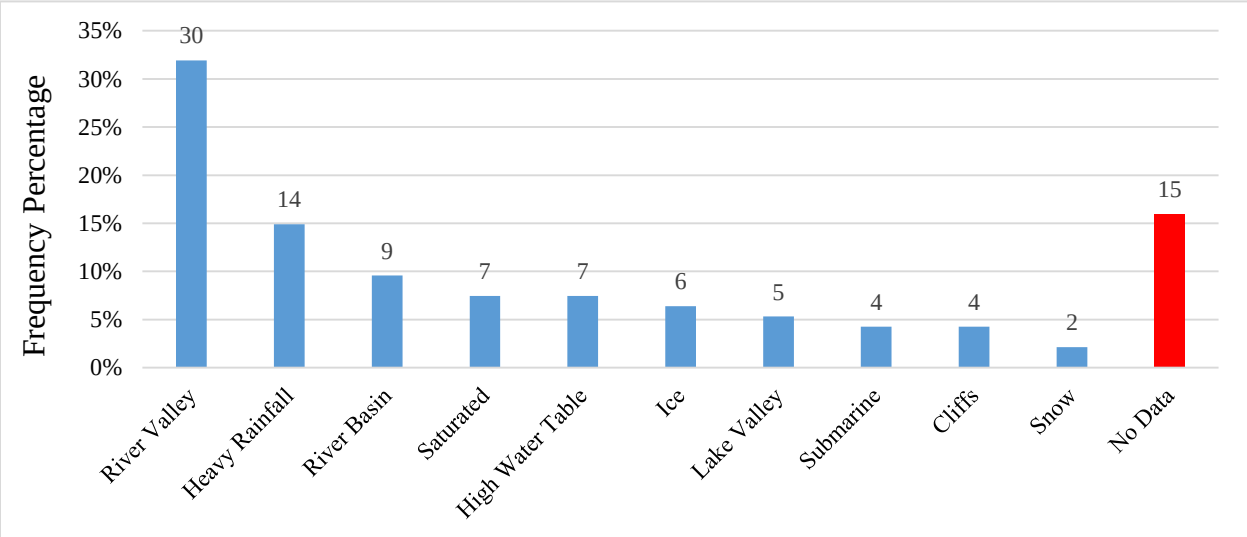

Figure 4-26 Water types distribution in earthquake-triggered natural slopes.

There is a typical mechanism for the impact of each water condition type on the stability of slopes under earthquake loads. The typical mechanism of failure in river, lake and ocean valleys is initiated when the water undercuts the valley slope by liquefaction and makes the slope unstable. Figure 4-27 gives a schematic view of this typical failure mechanism in river, lake and ocean valleys.

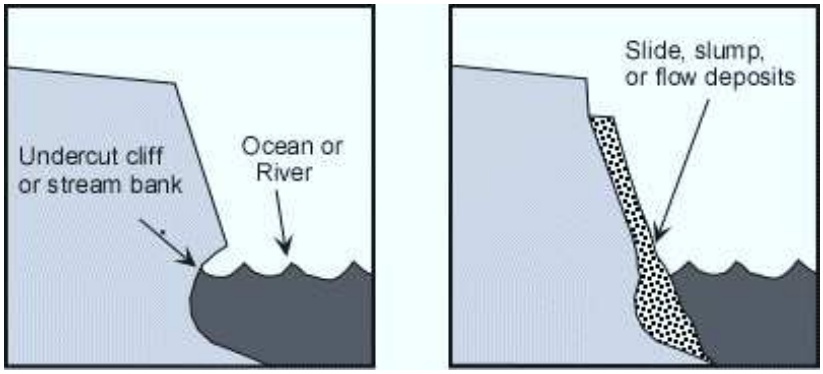

Figure 4-27 Typical mechanism of failure in river valleys initiated by water undercutting the slope [31].

An example of this failure mechanism is one of the largest landslides in the database that was a consequence of the earthquake on October 8, 2005 in Kashmir, Pakistan. This earthquake triggered several thousand landslides (number 88 in Table 3-1, M=7.6) located in a tributary valley of the Jhelum River at southeast of Muzafarrabad [151]. During this landslide, 80 Mm^3 of rock, mostly sandstone, mudstone, shale and limestone travelled approximately 1.5 km downslope as a debris avalanche. The landslide buried the village of Dandbeh and killed more than 1,000 residents. This landslide is called the Hattian Bala debris avalanche because the closest village to it was Hattian Bala. Figure 4-28 shows the debris which impounded the lake in the Karli stream drainage slope after the landslide.

Another type of failed slope close to the water sources are ocean valleys. Another example for this mechanism is an ocean valley failure on Turnagain Heights in Alaska during the Good

Friday earthquake on March 27, 1964 (number 29 in Table 3-1, M=9.2). As shown in Figure 4-29, the sand and gravel were overlaying marine clay layers in which the upper layers were stiff and the lower parts were sensitive clays. The slope broke into several slump blocks and slid about 610 m toward the ocean. After 1.5 minutes of earthquake shaking, liquefaction occurred in the lower clay layer. The liquefaction extruded the clay layer from the bottom of the slope, and caused failure on the ocean cliff. However, the failure was prevented from further extrusion because the rotated failed blocks sealed the liquefaction zone. This landslide destroyed 75 houses on the coast because of the separation and movement of the slump blocks toward the ocean.

The second contribution of water in the earthquake-triggered slope failures is the heavy rainfall prior to the earthquake. According to the database, this condition is observed in 14 events where the rain water decreases the strength of the loose material or saturates the slope, resulting in liquefaction. An example for the effect of heavy rainfall is Minxian–Zhangxian event (number 94 in Table 3-1), where the earthquake occurred during the rainy season. Prior to the main shock, a continual moderate to strong rainfall of about 13 hours weakened the slope strength. This shows that heavy rainfalls may trigger failures after the earthquake when the earthquake weakens the discontinuities. This phenomenon is observed in Wenchan and Chi-Chi events (numbers 81 and 86 in Table 3-1, respectively).

River basins collapsed in seven earthquake events. Most of these failures occurred on steep basins (>40 degrees). The main factor of failure in river basin is the erosion caused by the water which makes the slope susceptive to failure during earthquake. Planica event (number 82 in Table 3-1) is an example of an intense rockfall and debris failure in the Upper Soča River basin.

Figure 4-28 Debris impounds the lake in the Karli stream drainage slope after the Hattian Bala landslide [127].

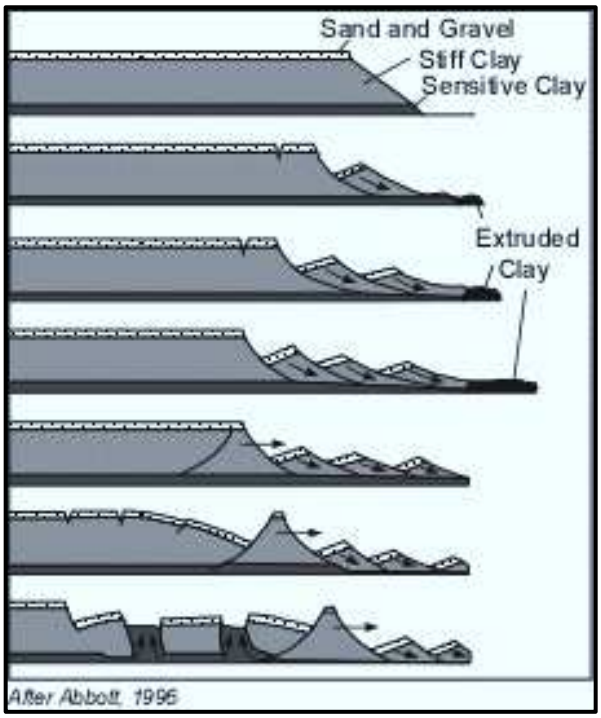

Figure 4-29 Failure procedure of the Turnagain Heights Alaska cliff failed during Good Friday earthquake [31].

Ice and snow are another type of water condition which were contributed in five natural slope failures triggered by earthquakes. Ice content reduces the shear strength of the material by creating layers between the material contacts that can be triggered by external forces such as earthquakes. Nevados de Huascarán peak failure, located in the Peruvian Andes Mountains, is a good example for the water involvement in the glacier failure mode (number 32 Table 3-1, M=7.9). Geologically, the peak is made by vertically fractured granite covered by glacier ice. The peak had two historic failures. The first one was a debris flow initiated by falling of a huge slab of rock and glacier [2]rock on January 10, 1962. There was no apparent triggering force involved in this failure. This shows that the peak was close to instability. The debris flow moved rapidly to the valley and killed 4,000 residents of Ranrahirca town. The second failure was triggered by an earthquake on May 31, 1970 with a magnitude of 7.7 on Richter scale with an epi-centeral distance of 135 km. The earthquake vibrated the area for more than 45 seconds. During this shaking another large rock and glacial block, located between 5,500 and 6,400 meters elevation, fell down (Figure 4-30). This block initiated a debris avalanche sliding down the slope at 335 km/hr velocity. The debris made blocks the size of a house fell on the Yungay town and buried 18,600 residents. Figure 4-31 shows the plan view of the area including the initiated origin of the slide and the Yungay town location.

As deliberated in Chapter 2, liquefaction is one of the main failure modes in tailing dams which is a result of water presence. Analyzing the database shows that liquefaction was the failure mode for 65 percent of the tailing dam failures and the reason for the rest of the failures was the seismic induce deformation (Figure 4-32).

2- A slowly moving mass or river of ice formed by the accumulation and compaction of snow on mountains or near the poles.

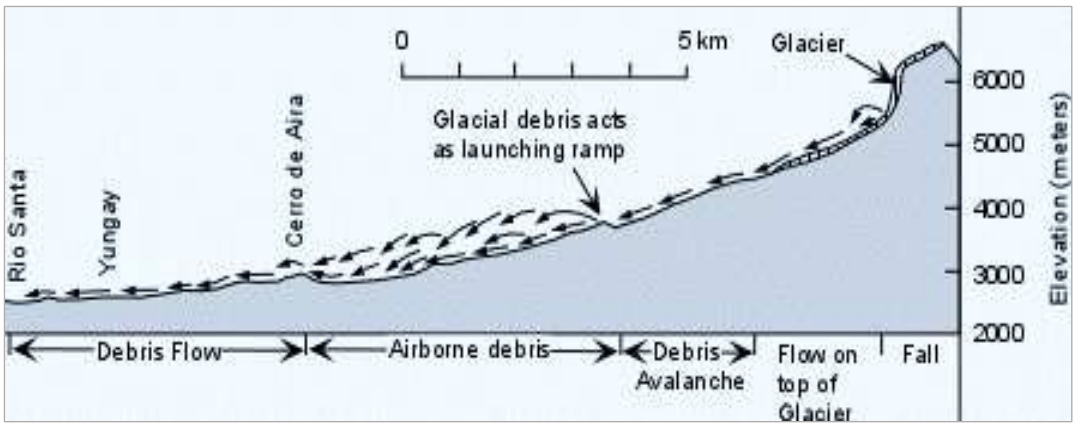

Figure 4-30 Cross section view of the debris and the glacier failure on Peruvian Andes Mountains [31].

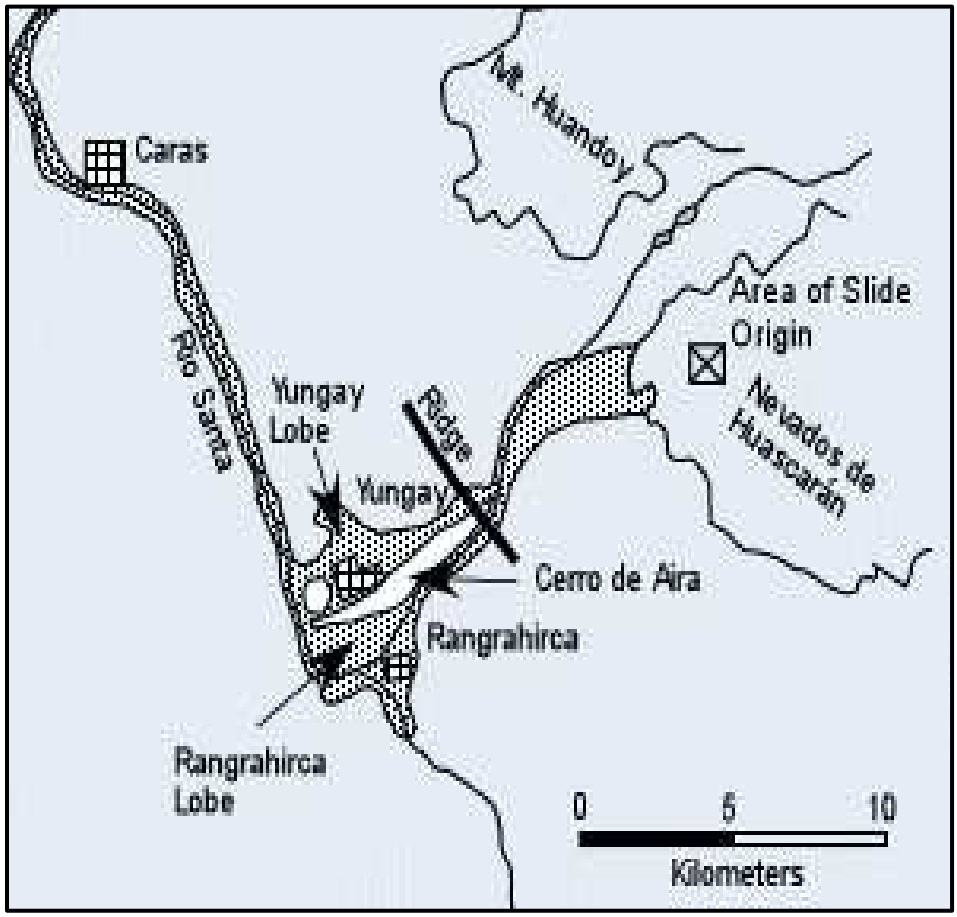

Figure 4-31 The plan view of the glacier failure origin on Peruvian Andes Mountains, and the Yungay Town [31].

One of the significant dam failures due to liquefaction was the lower San Fernando dam failure which was triggered by an earthquake on February 9, 1971 (number 19 in Table 3-2, M=6.6). The dam was constructed by hydraulic filling that includes fill soil with a large amount of water injected into the dam by pipelines and allowing the drainage of the excess water. The liquefaction is a result of earthquake shaking subjected to the loose filling.

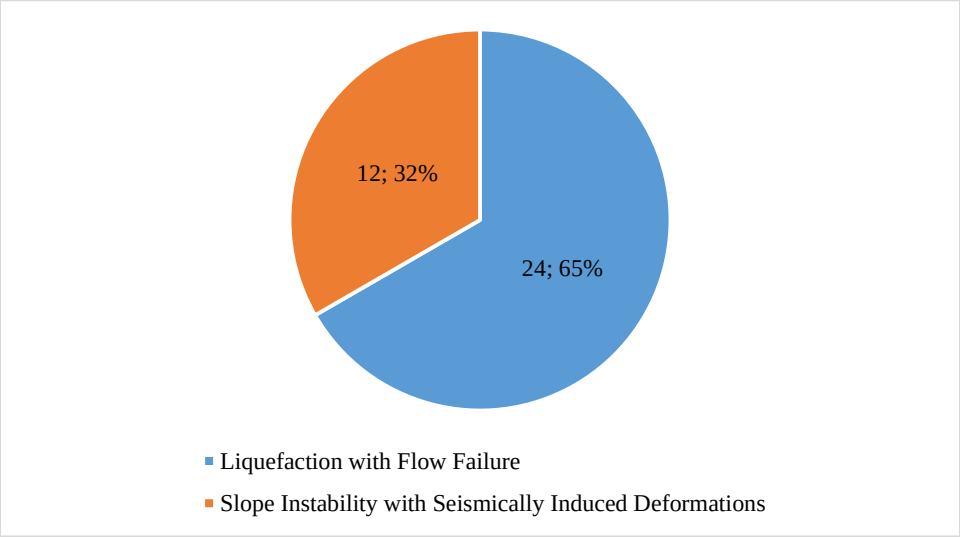

Figure 4-32 Number and percentage of tailing dam failure modes and their cause of failures.

Sixteen tailing dams failed as a result of a 7.4 magnitude earthquake on March 28, 1965 in Chile (numbers 3 to 18 in Table 3-2) in which eight failed due to liquefaction. These tailing dams failed primarily because of the excess pore water pressures generated under seismic load. The excess pore pressures cannot be dissipated quick enough to prevent undrained loading conditions from prevailing. Therefore, the effective stress is reduced to nearly zero and thus in the cohesionless material, the shear strength reduces to zero.

The first six water conditions in natural slopes and liquefaction in tailing dams occur less frequently in open pit mines. The reasons for this relationship include:

- The open pits developed in high water table areas are generally subjected to a form of natural or active pore pressure control. As soon as the pit slope is excavated below the water table, the natural dewatering starts to take place. If the natural drainage is not enough to provide stability, different pore pressure reduction methods would be implemented,

- Open pits are relatively less prone to seismicity induced liquefaction in saturated material because the pore pressure is maintained under a specific limit in these slopes, and

- The effect of heavy rainfall is less in mine slopes in comparison to natural slopes due to the lower water table and drainage system.

4.4 Failure Interpretations

The definition of failure in open pit mine slopes and natural slopes could be different. Not all failures in natural and civil slopes are considered failures in open pit mines. For example, shallow failures (≤3m thick), such as rock falls, are not deemed a failure in open pit mines unless they are reportable. For instance, according to Mine Safety and Health Administration requirements, a reportable failure is the one that causes injury or production interruption.

4.5 Failure Types

Considering the aforementioned failure interpretation, deep failures in rock structures are the major concern for open pit mine operations. Therefore, the natural slope failure database is analyzed considering their failure modes, depth and material. According to Keefer's study cited in Chapter 2, failure depths are classified as shallow (<3 m), deep (>3 m), and variable and each failure mode falls in one of these categories. Figure 4-33 shows the failure modes for natural slope failures regarding their failure depth and material type. To investigate the frequency of failure modes in natural slopes during earthquakes, Figure 4-34 presents the number of failures for

different failure depths and materials. Studying these failures shows more than 70 percent classified as shallow. These shallow failures mostly occur within top soil or weathered, weak and highly fractured rock layers, however the open pit mine slope surface is frequently shaved off during the life of the mine which does not allow an intense weathering on the slope surface. Moreover, specifically in the rock section of Figure 4-34, the number of failures decreases from shallow to deep and there is the same trend for the soil section in which the frequency of failures decreases from shallow failures to variable depth failures with the exception of soil slump failure type. However, because of the absence of these top layers in pit slopes, such failures usually do not take place. In contrast to shallow failures, a large volume of material is involved in deep failures (>3m thick) and among 57 failures in rock structures, only 15 events were recorded to be deep (Figure 4-35). Deep failures in rock structures, which are the major concern for open pit mine slopes include rock avalanches, rock slumps, and rock block slides.

Rock avalanches are generally uncommon. From the 11 recorded rock avalanche events in this study, seven were triggered on icy and river valley slopes and all were in rock; highly fractured rocks by several sets of joints spaced from a few centimeters to a few decimeters.

There were three rock slump events (numbers 22, 24 and 36 in Table 3-1), where all were triggered on river valleys and in one case, snow was also involved in the failure. This shows a high water condition for all these events.

The last deep failure type in rock structures is toppling which was found only in one case (number 94 in Table 3-1), where the loess scarp material toppled on a deep (~ 60 degrees) slope. Heavy rainfall prior to the earthquake was also a factor involved in this failure.

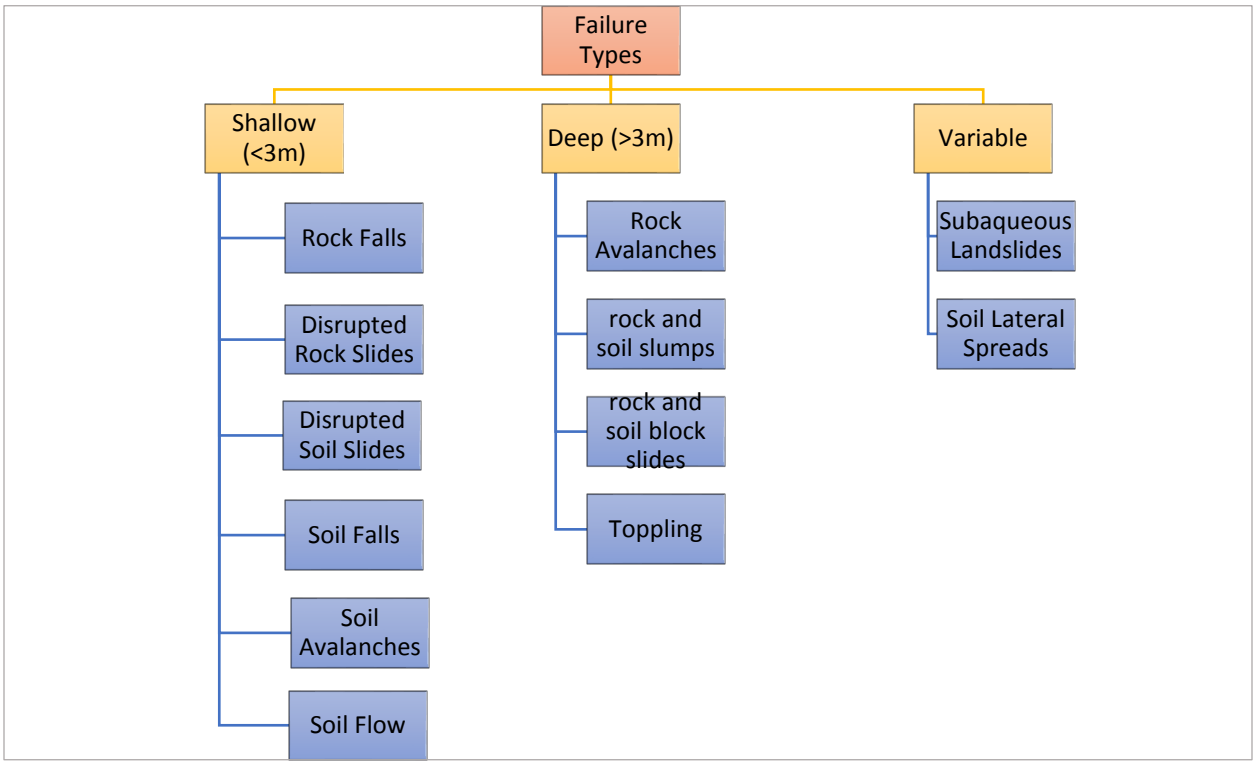

Figure 4-33 landslide classification for different failure modes regarding their failure depth and material type.

The material involved in these deep failure types were mostly weak and highly fractured rock mass with a high water condition. However, these types of material are rarely the major host rock of a mineral and are often found over or around the ore and coal deposits. Moreover, metamorphic and igneous rocks with much higher strength are the host rocks for many minerals in open pit mines [2]. Figure 4-36 (see page 89) presents the distribution of open pit mine commodities from the database in which open pit mines are mostly (> 75%) metal mines with high strength metamorphic and igneous host rock.

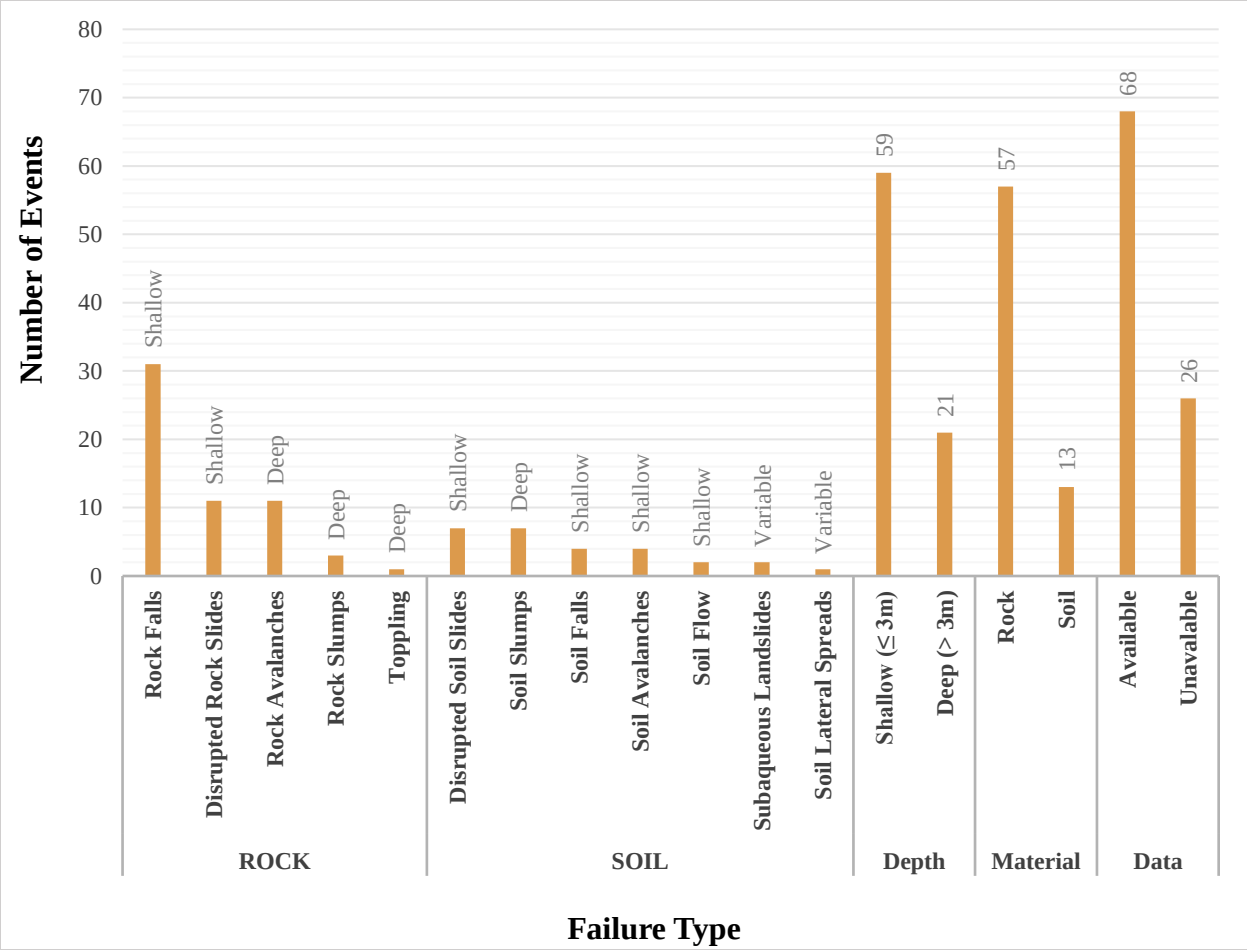

Figure 4-34 Number of failures in different failure modes, failure depths and materials involved.

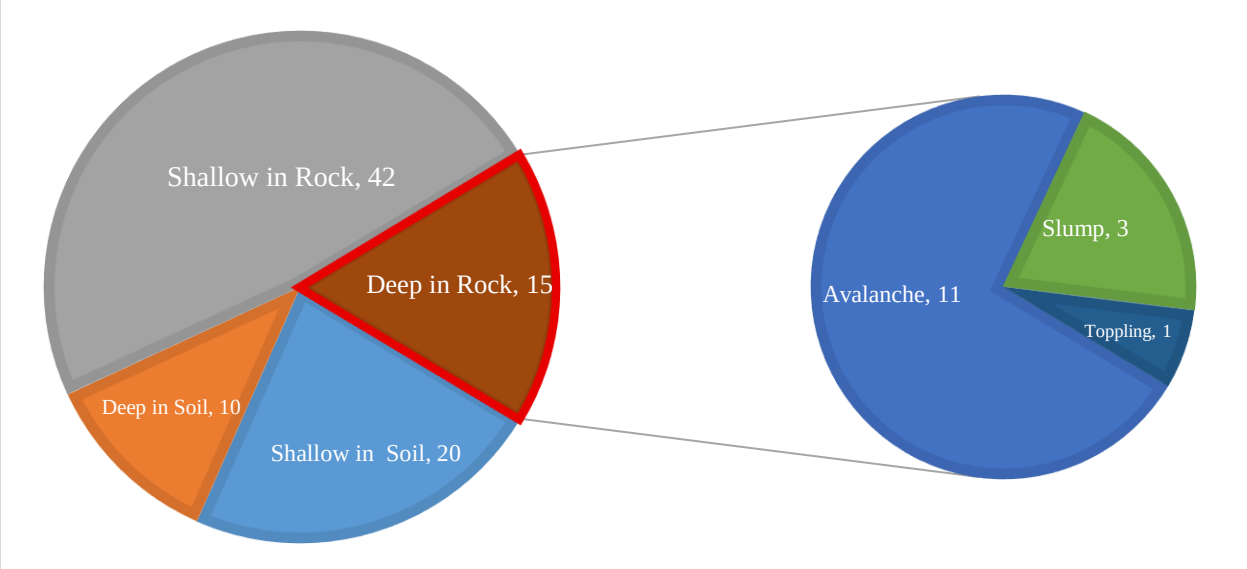

Figure 4-35 Number of Shallow and deep failures in rock and soil structures and number of failure modes in deep rock failures.

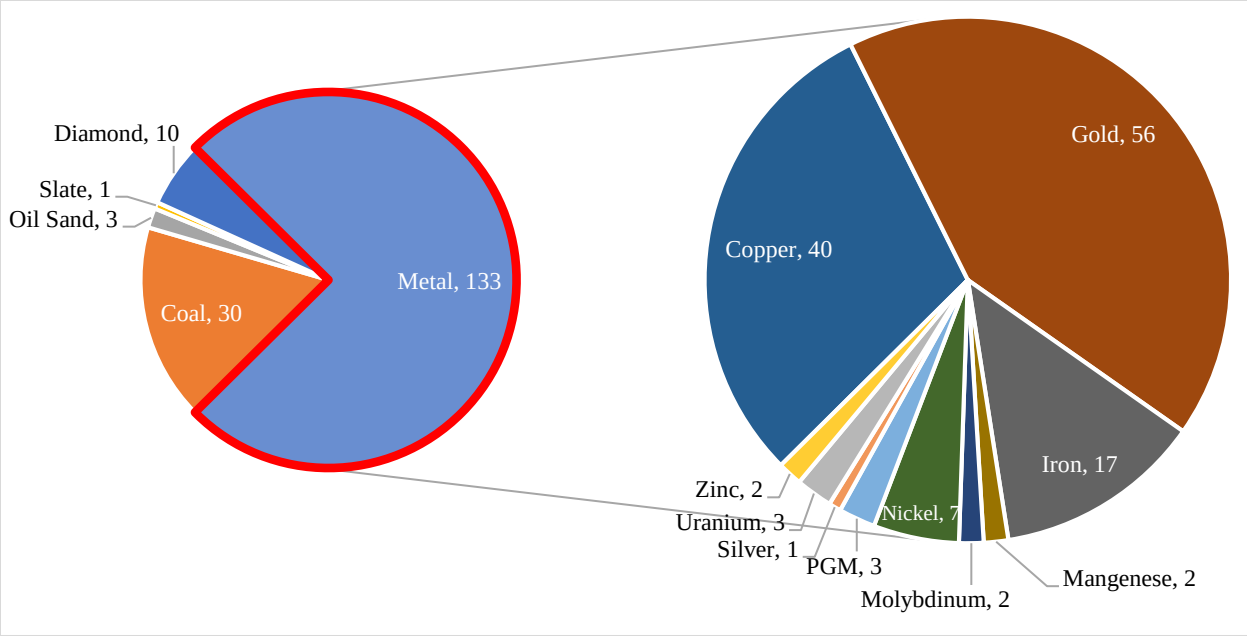

Figure 4-36 Open pit mines commodities distribution.

4.6 Site Effects

As discussed in Chapter 2, in addition to earthquake parameters, site effects are known to control the shaking intensity of slopes. Studies done by researchers show that topographical profile and stiffness contrast of material are the two main site effects. These effects have a significant impact on amplifying the ground shaking on hills, slope ridges and top soil layers [12-15, 31, 127, 151]. The database shows the existence of these two site effects in the natural slope and tailing dam failures. Stiffness contrast phenomenon widely take place, causing failure on the top soil and weathered layer of natural slopes and the unconsolidated material of tailing dams. In contrast, open pit mines are less prone to be affected by this phenomenon because of the cut rock on their slope face. The effect of topography was observed in 12 natural slope events as the main instability factor and on most other failures as a complementary factor of failure. Tailing dams were affected by this phenomenon due to their typical hill shape geometry. In contrast, open pit mines are less

likely to be affected by the topographical effect because of their valley or one-face geometry. Later in Chapter 5, these two site effects are investigated using numerical analysis.

4.6.1 Topographical Effect

Generally, the power of ground shaking during earthquakes is amplified on the slope crests and steep slopes. This amplification is caused by wave focusing and defocusing phenomenon which is controlled by the curvature of the topography. Seismic waves are trapped in hill shape topographies and scattered in valley topography features causing ground shaking amplification and reduction, respectively [152]. A worldwide study by USGS shows that the ground acceleration could be amplified to the factor of 4.0 on slope hills and ridges compared to valleys [153]. According to the database (Table 3-1), topographical effect is one of the failure factors in most natural slope cases and the key factor in 12 of these events. Table 4-6 shows the natural slope failures in which topographical effect was the main instability factor.

According to Table 4-6, New Zealand and California are the two regions that have been the most affected by the topographical shaking amplification as the key failure factor. A study has been done on detecting the topographical amplification factor in these two regions [153]. In this study, the average shear velocity is measured down to 30 meters (V_s^{30}), and correlated with the topographical relief of the region. The V_s^{30} parameter is a factor that indicates the ground motion response at a particular site. Figures 4-37 and 4-38 show the correlation between topography and V_s^{30} of California and New Zealand. The figures illustrate that the shear velocity (V_s^{30}) amplifies on sharp topographical geometries, where all natural slope failures are triggered in these topography zones with amplification factor of 2.0 to more than 4.0.

Studying the effect of topography on the stability of open pit mines shows that, because of the valley-shape or one-face slope geometry of pit slopes, there is a significantly less topographical amplification expected for this type of slope in contrast to natural slopes. The topographical amplification on different geometries of natural slopes and open pit mines is studied in Chapter 5 using numerical methods.

Table 4-6 Natural slope failures in which topographical amplification was the main instability factor.

No.	Name	Country	Year	M	Slope Angle (deg)	Failure	Material	Water Type
2	Marlborough	New Zealand	1848	7.5	-	Topo	Al	RB, Co, Sat
3	Wairarapa	New Zealand	1855	8.2	35-45	RAV, Topo, Cr, Lq	-	-
8	Cape Turnagain	New Zealand	1904	6.8	~ 90 (RF)	Lq, RF, Topo	-	RV
14	Hawke's Bay	New Zealand	1931	7.8	11-20(Lq)	Lq, Sh, RF, Topo	LS, MS, SS	RB
30	Hope Slide BC.	Canada	1965	3.2	45- 80	Topo, RS	Fr, WR, W	Rf, Sn
33	San Fernando Valley	CA, USA	1971	6.5	>60	Topo, Cr	Fr	Sat
37	Panama	Panama	1976	7	-	Topo, Cr, Lq	S, WR	RV
67	Cape Mendocino	CA, USA	1992	7.1	-	RF, Lq Topo	S	RV
68	Suusamyr	Kyrgutzstan	1992	7.3	55	Topo, RF	Gl, W Gr	Ice, RV
72	Fiordland	New Zealand	1993	7	>45	Sh, Topo, SSl, RS	-	LV
74	Ormondville	New Zealand	1993	6.2	-	RF, SF, Lq, Cr, Topo	-	RV
76	Paez	Colombia	1994	6.8	-	Topo	Ash, S	Rf

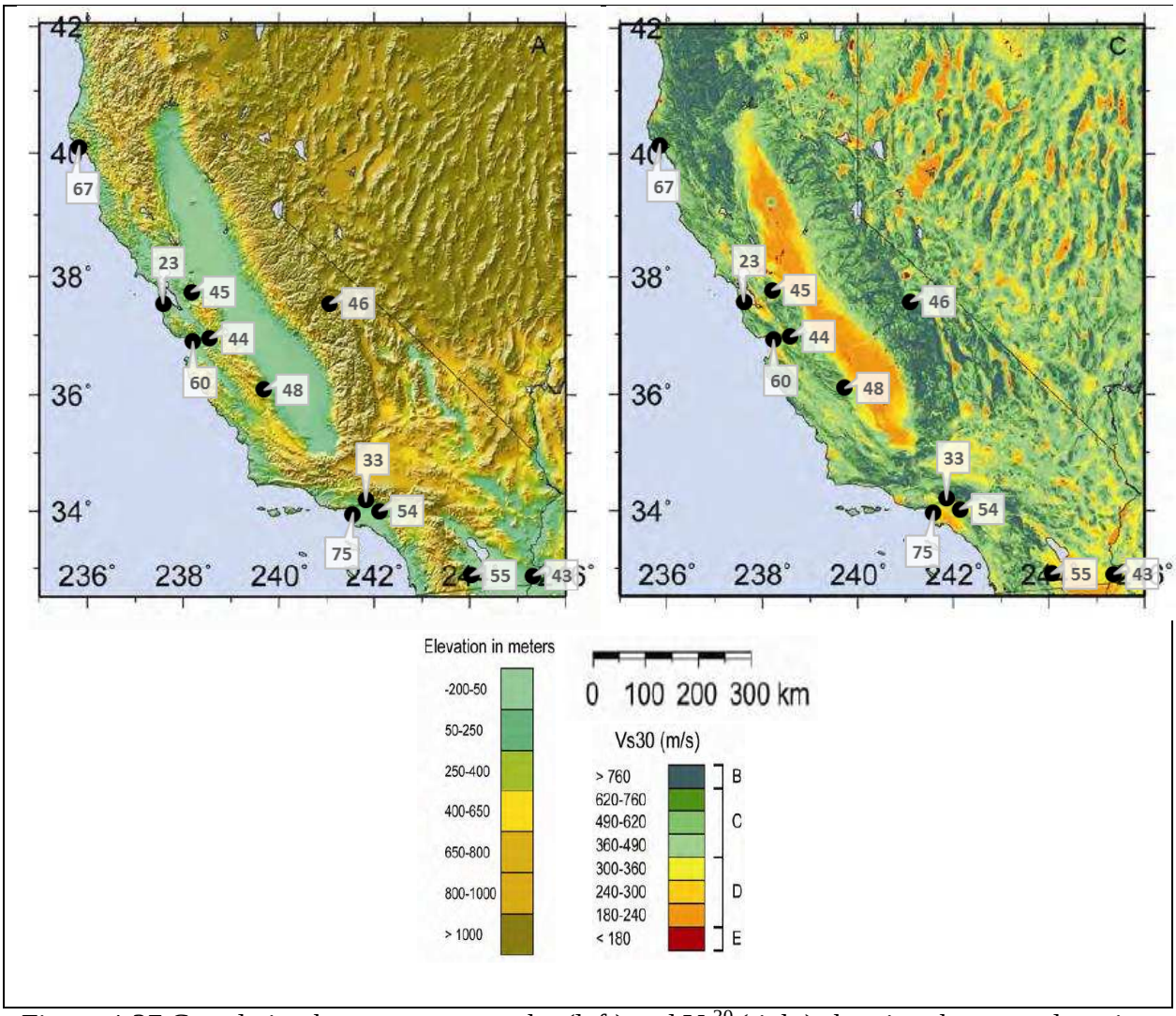

Figure 4-37 Correlation between topography (left) and V_s^{30} (right) showing the ground motion amplification of California, USA.

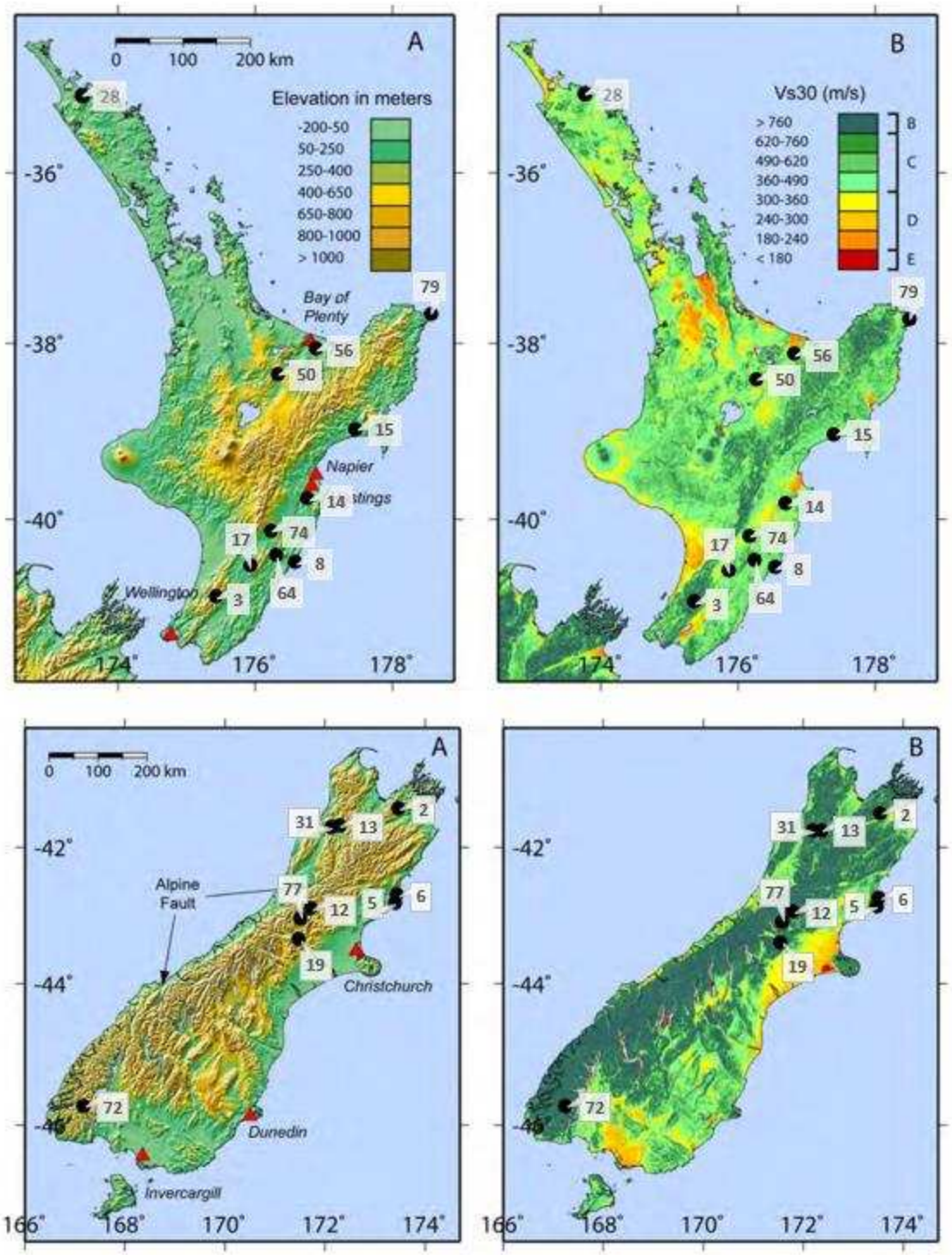

Figure 4-38 Correlation between topography (A) and V_s^{30} (B) showing the ground motion amplification of New Zealand, North Island (top) and South Island (bottom).

4.6.2 Stiffness Contrast

Studies show that when waves travel from hard rock to soft soil, the amplitude of the waves would be increased to carry the same amount of energy, creating stronger shaking intensity [9, 11, 14]. Moreover, the deeper sediment above the bedrock, which means thicker soil layer, creates a stronger amplification [15]. The database shows that this phenomenon widely took place in the top soil layer and weathered material of natural slopes and the unconsolidated top layer of upstream tailing dams. New Zealand and California are the two regions with the most earthquake-triggered natural slope failures, 20 and 12 landslides, respectively. Investigating the geology of these two regions shows that most landslides were triggered in sedimentary rocks and in a few cases, igneous and metamorphic rocks (Figures 4-39 and 4-40). In New Zealand the material involved in all failures except three landslides (numbers 50, 56 and 72 in Table 3-1) were in sedimentary rocks. Generally, sedimentary rocks have a lower stiffness compared to the metamorphic and igneous rocks. These conditions show the significant effect of stiffness contrast in natural slope failures. Tailing dams can also be subjected to the stiffness contrast amplification effect. This effect is widely observed in tailing dam failures constructed by upstream method. This is due to the unconsolidated material on top of the stiff tailing dam core resulting stiffness contrast amplification during earthquake.

In contrast to natural slopes and tailing dams, open pit mines are less prone to getting affected by this phenomenon because of the typical competent material of large open pit mines. Moreover, the top soil layer is mined in the first stages of mining process and after creating the pit slope, the slope face is cut frequently during mining procedure. The effect of stiffness contrast on ground shaking amplification will be discussed in Chapter 5 using numerical methods comparing natural slopes and open pit mine slopes.

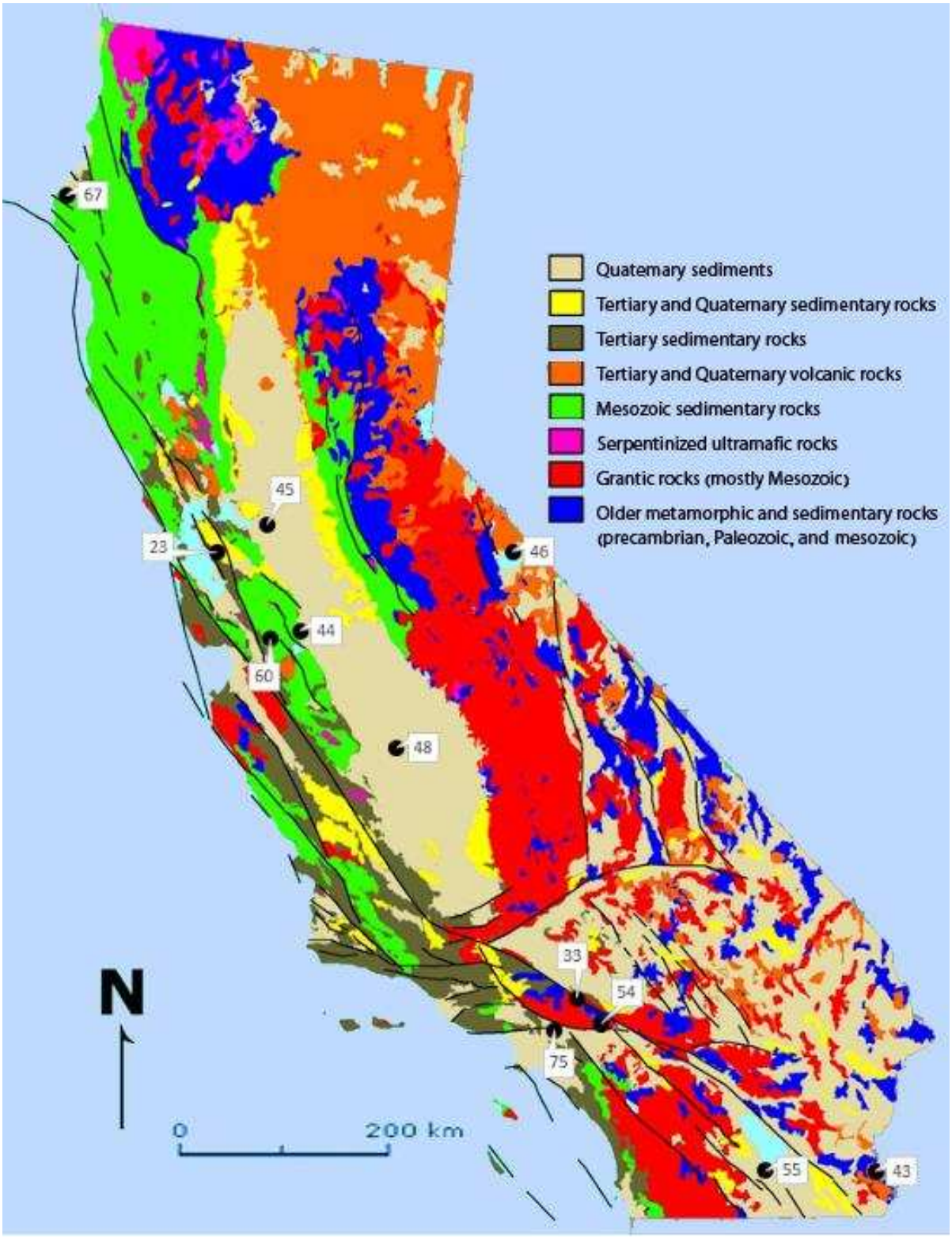

Figure 4-39 Corresponding geology of natural slope failures in California, US.

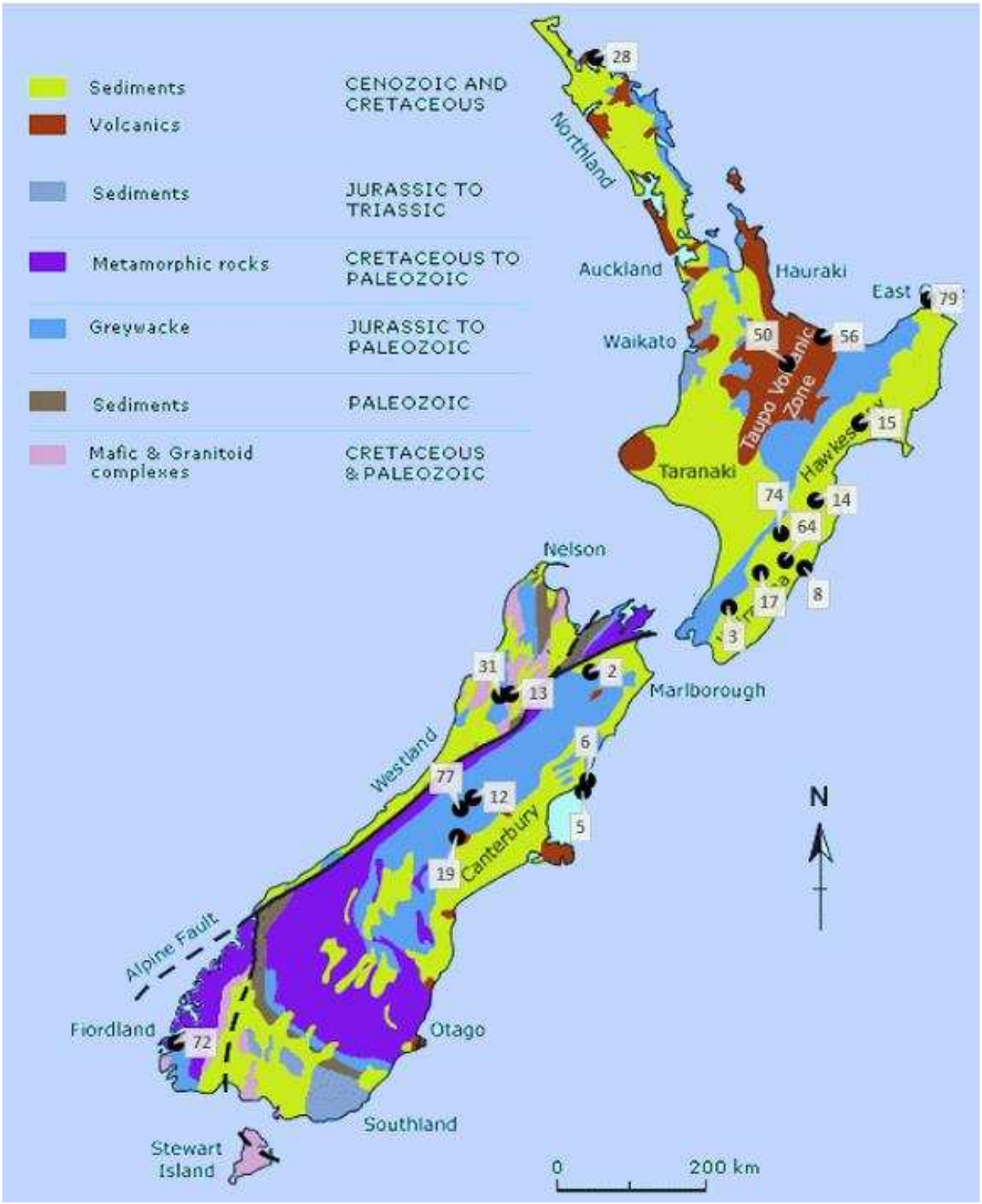

Figure 4-40 Corresponding geology of natural slope failures in New Zealand.

4.7 Conclusion

From the comprehensive comparison between earthquake-triggered natural slopes, tailing dams and earthquake-subjected open pit mine slopes, considering earthquake parameters and geological characteristics, the following conclusions may be drawn:

- All natural slope and tailing dam failures except three cases were triggered by earthquake magnitudes of more than 5.0. Conversely, there were only 30 open pit mines subjected to this range of earthquake magnitudes,
- Triggered natural slope failures are all caused by earthquakes that occur within a range of 200 km epi-center and 70 km depth. Of the 177 open pit mines in this study, only 36 mines (20 percent) are located in such range,
- Tailing dams as a slope structure close to open pit mines are susceptible to failure during earthquakes. In contrast to natural slope failures, number of tailing dam failures do not correlate with the earthquake parameters. This is because tailing dams are prone to liquefaction due to earthquake shaking and may be trigger by smaller shaking intensities,
- According to the intensity analysis, 90 percent of natural slope and tailing dam failures were triggered by earthquake intensities of more than 6.0. Whereas, only 11 percent of open pit mines (20 open pit mine) were subjected to this range of intensities. As such, the response of open pit mines to higher intensity earthquakes in not known,
- Equation 4-1 considers a similar effect for focal depth and epi-central distance on the intensity. However, the analyses on earthquake induced natural slope and tailing dam failures show the greater influence of focal depth compared to epi-central distance on the resultant intensity.

- Most triggered natural slope failures are shallow in thickness, typically less than 3 meters. Often, similar size triggered failures do not have to be recorded as “failure” in open pit mines unless they fall into “reportable” category,
- The presence of water in almost all of the triggered landslides emphasizes the significance of water condition in slope stability. Dewatering of open pit slopes through mining and planned draining is known to increase slope stability,
- Natural slopes are subjected to chemical and biological weathering and degrading during their life period, such as freezing and thawing, floods, earthquakes and winds. This leads to weakening slopes against an external triggering force such as earthquakes. Open pit mines are designed commonly after considering the effect of ice, water and local seismic activities,
- Earthquake caused ground motions amplify on hill tops and ridges, which is a common phenomenon in natural slope failures. In contrast, ground motion reduces in open pit mines due to their one-face and valley geometry, and
- The weak top layers on natural slopes are widely susceptible to failure due to ground motion amplification caused by stiffness contrast between the bedrock and top soil. Open pit mines are less prone to this amplification due to the absence of the top soil layer.

CHAPTER 5

NUMERICAL ANALYSIS OF SITE EFFECTS

5.1 Introduction

As described in Chapter 4, in addition to earthquake parameters, site effects are known to play a significant role in earthquake-triggered natural slopes. This chapter investigates the effect of topography and stiffness contrast on stability of slopes during earthquakes. As discussed in Chapter 2, there are three approaches to analyze the effect of earthquakes on slope stability. However, the two traditional methods, Pseudo-static and Newmark, are subjected to limitations such as assuming a constant earthquake acceleration in Pseudo-static method and the assumption of non-deformable body in Newmark's method. Therefore, the numerical approach is becoming more commonly used in analyzing the stability of slopes under earthquake loads [154-164]. The distinct element method (DEM) proposed by Cundall in 1971 is one of the best approaches to the dynamic analysis for the discontinuum mediums. UDEC is a two dimensional distinct element modelling program that is commonly used to model the behavior of slopes under dynamic loads such as earthquakes [157-164]. The focus of this chapter is to show the effect of topographical conditions and the stiffness contrast of the material as the two main site effects on the behavior of slopes subjected to earthquake loads. A study performed by Lorig in 2016 uses continuous numerical analysis *FLAC* to investigate the effect of heterogeneities and topography of slope on the peak ground acceleration [1]. However, this study did not consider the effect of faults and crest widths on earthquake induced pit slope stability.

This chapter investigates the effect of topography and stiffness contrast, using a spectrum of natural slope geometries and material with different crest widths to simulate the behavior trend of slopes from natural slope to open pit mine geometries. As noted in Chapter 4 (Section 4.6), horizontal velocity is one of the well-defined factors which indicates ground motion response of a particular site to an earthquake. Moreover, Lorig shows that the peak ground velocity has the best correlation with the dynamic safety factor of slopes among other ground motion parameters (i.e. peak ground acceleration) [1]. As a result, models with different topographical geometries and stiffness contrasts are generated to investigate their effect on the horizontal velocity and the results are compared against the available real data derived by USGS (Section 4.6).

Four sets of models were created for the analysis. Two sets of models were generated to investigate the effect of topography on the stability of slopes considering continuous and faulted rock mass. The third set of models was created to study the effect of material stiffness. The last set was designed to study the coupled effect of topography and stiffness contrast.

5.2 Dynamic Analysis Considerations in UDEC

For dynamic analysis, after verifying the stability of a model in static conditions, the first step is to apply the dynamic analysis requirements for boundary and damping conditions [22]. These requirements, if calibrated, ensure that the seismic waves travel through the medium in a realistic manner. After applying the dynamic analysis requirements, the last step is to apply the earthquake load on the model.

- **Boundary Conditions**

The fixed boundaries created in the static condition reflects the seismic waves reflect into the model while reaching the boundary. In order to prevent the seismic shear wave from reflecting,

the bottom of the model where the dynamic load is applied, is considered viscous. The other two sides of the model should be set free so that it allows the waves to pass through the boundaries. Figure 5-1 gives a schematic view of the boundary conditions used for the UDEC analysis in this study.

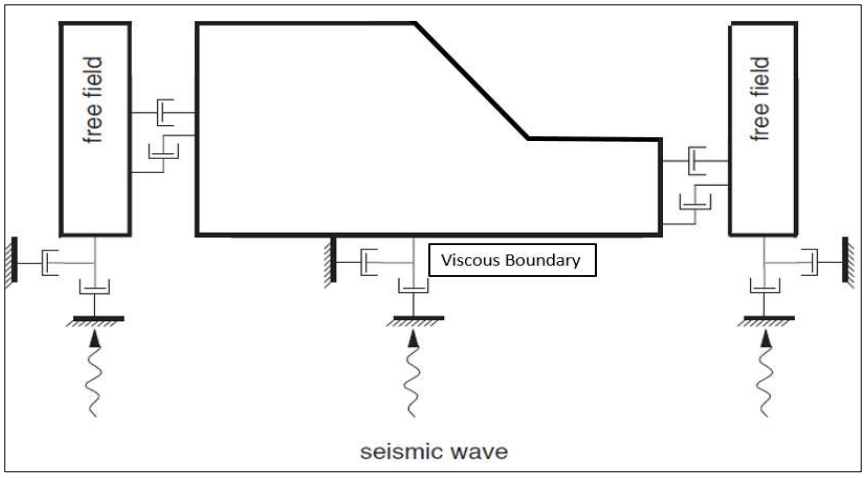

Figure 5-1 Boundary conditions used for UDEC analysis.

- **Wave Transmission Through the Model**

Mesh dimension profoundly influences the wave propagation through the model. A large mesh dimension causes wave reflection in the model whereas infinitesimally small meshing leads to a considerable increment of the calculation time. Therefore, the maximum mesh dimension should be calculated in order to minimize the analysis time and prevent the wave reflection. Equation 5-1 proposes a relation between mesh dimension and wavelength in a way that the accuracy of the wave propagation is not adversely affected from the mesh size, $l_{\max}$ [22], which is given as:

$$l_{\max} = \frac{C_s}{10 f_{\max}} \qquad \text{(Eq.5-1)}$$

where, C_s is shear wave velocity taken as $C_s = \sqrt{\frac{G}{\rho}}$ and $f_{\max}$ is maximum frequency of the waves carrying non-zero energy.

To calculate the maximum mesh dimension, the minimum shear velocity should be considered. Due to the involvement of different materials with different shear modulus (discussed later in the chapter), the minimum shear modulus, 4 GPa, is considered to calculate the maximum mesh dimension. Below is the calculation for the considered mesh dimension:

$$C_s = \sqrt{\frac{G}{\rho}} = \sqrt{\frac{4\ \text{GPa}}{2650\ \frac{\text{kg}}{\text{m}^3}}} = 1228\ \frac{\text{m}}{\text{s}}$$

$$l_{\max} = \frac{C_s}{10 f_{\max}} = \frac{1228\ \text{m/s}}{10(5)\ \text{Hz}} = 24\text{m}$$

Therefore, a mesh dimension of 20 m is used in the analysis.

- **Mechanical Damping**

In principle, natural dynamic systems have some degree of vibration energy damping inside their system, if not, the system would oscillate forever when subjected to a driving force. In order to simulate this phenomenon using numerical methods, artificial damping is considered in dynamic analysis. Damping commonly falls in the range of 2 to 5% of critical damping for geological materials [165]. In this analysis a 5% of critical damping at frequency of 5 Hz is assumed.

- **Seismic Wave Input**

In the analyses for this study a sinusoidal shear wave with velocity amplitude of 3 cm/s and frequency of 5 Hz is applied to the model base for one second. These earthquake properties are selected to fall into a typical range of an earthquake length, magnitude and frequency.

5.3 Topographical Effect in Continuous Rock Mass

As discussed in Chapter 4 (Section 4-6-1), the topography may amplify the shaking intensity in terms of horizontal velocity in sharp natural slope topographies compared to valleys and one-face slopes (Figures 4-33 and 4-34). To study this effect, two different models were

developed, each considering five different model geometries. In the first set, five models were generated with different crest widths. The geometry of these models varies from hill slopes with no crest to one-face pit slope, with gradual increase in the crest width. Figure 5-2 shows the geometry of these five models and Table 5-1 presents the properties considered for the material in these analyses. Model 1 simulates a typical natural slope which is commonly observed among natural slope failures. Intermediate models 2, 3 and 4 simulate the geometries of some natural slope failures which will show the behavior of models from typical natural slopes to open pit mine slopes, defined as Model 5 in Figure 5-2. A one second sinusoidal seismic velocity wave with magnitude of 3 cm/sec and frequency of 5 Hz is applied to the bottom of the model (Figure 5-3) and the horizontal velocity on the slope crest (point B) is recorded and presented in Figure 5-4.

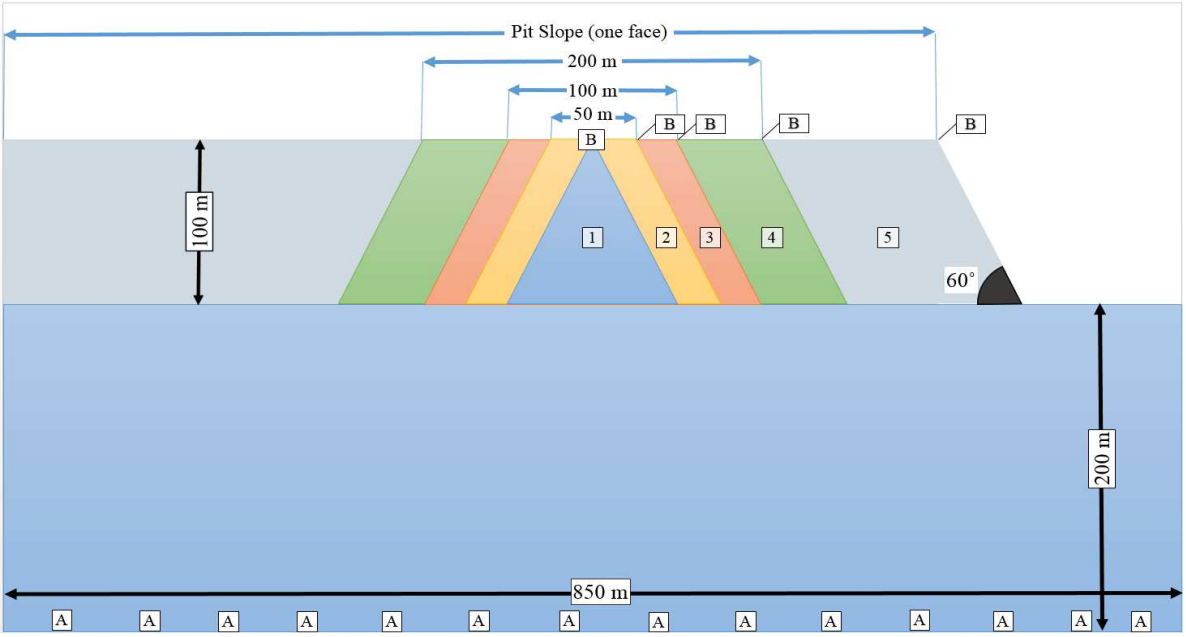

Figure 5-2 Geometry of five models generated with different crest widths.

Table 5-1 Mechanical properties of the slope material.

Mechanical Property	Density (kg/m^3)	Young's Modulus (GPa)	Shear Modulus (GPa)	Bulk Modulus (GPa)	Poison's ratio
Value	2650	50	20	33	0.25

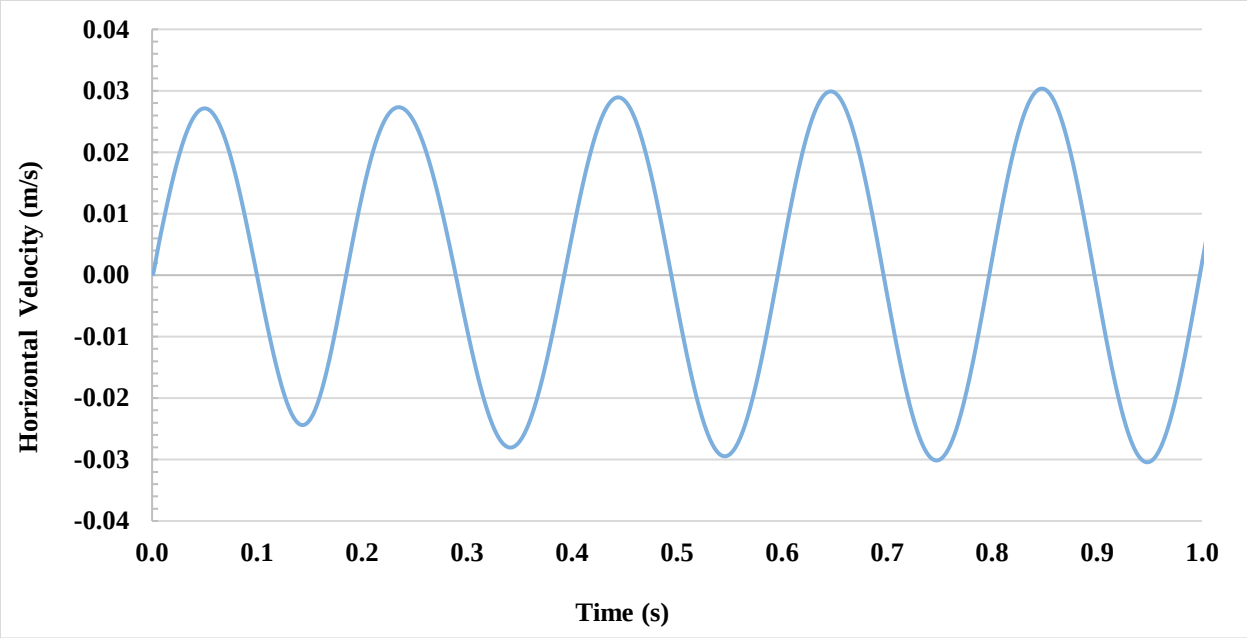

Figure 5-3 Input horizontal seismic velocity applied on the bottom of the model (at Point A on Figure 5-2).

The recorded horizontal velocities on the slope crest (Point B) show that they are amplified compared to the input horizontal velocity. This amplification decreases by increasing the crest width from the hill shape natural slope to the one-face open pit mine slope. The ratio between the recorded horizontal velocity wave (at Point B) and the input horizontal velocity (at Point A) is called the amplification factor. Figure 5-5 shows the mean amplification factor derived from the analysis, in which the velocity is amplified significantly on the hill shape natural slopes up to the factor of 9.0 compared to the open pit mine slopes with an amplification factor of two. These analyses show that the one-face open pit mine slopes are more stable due to the lower topographical amplification factor in comparison with natural slopes. The study done by Lorig, which compares hill, slope and valley topographies, shows an amplification factor of 2.2 and 3.2 for one-face slopes and hill geometries, respectively, in which the topographical amplification result of the one-face slope is very close compared to our results (Figure 5-5). It should be noted that the hill geometry in Lorig's study has a 100 m crest width which is comparable to model 3 in the current analysis.

Moreover, the recorded velocities in the USGS studies for New Zealand and California (Figures 4-33 and 4-34) show a horizontal velocity amplification from less than 180 m/s to more than 760 m/s from valley to hill shape geometries. This gives an amplification factor of more than 4. The derived results from numerical analysis shows a good agreement with the USGS results and the horizontal velocity of hill geometry is 4.5 times more than the one-face pit slope.

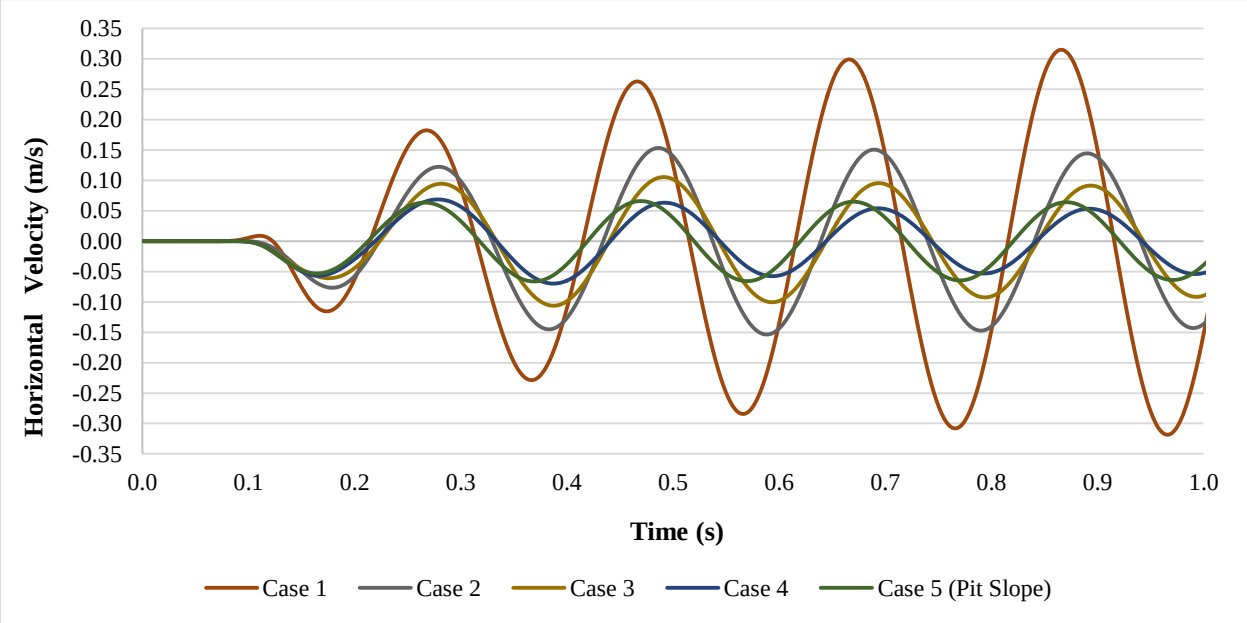

Figure 5-4 Horizontal velocities recorded at Point B on Figure 5-2 for different topographies.

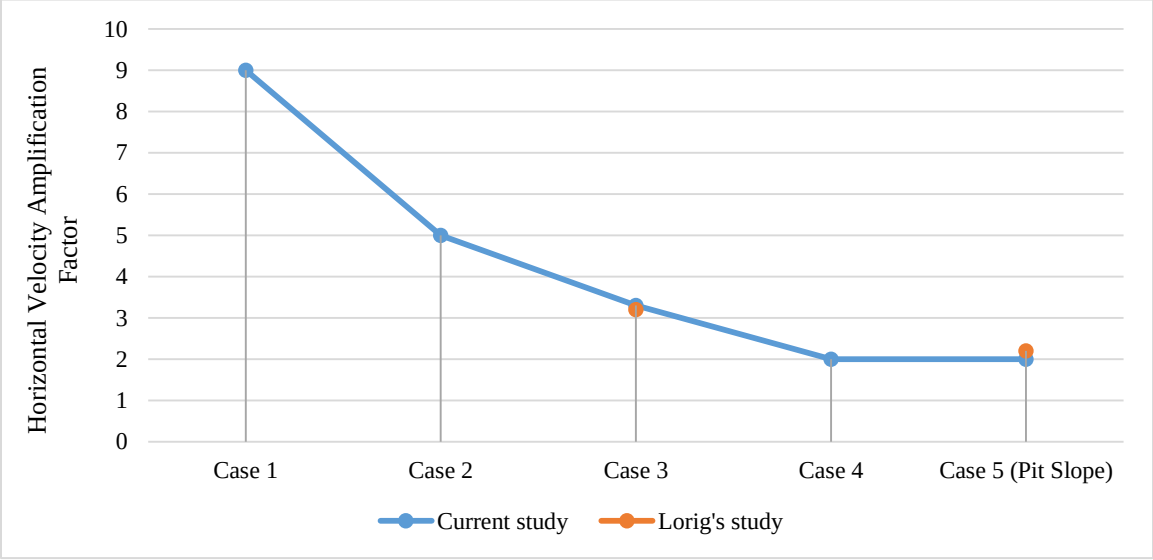

Figure 5-5 Horizontal velocity amplification factors for topographies presented in Figure 5-2.

5.4 Topographical Effect in Faulted Rock Mass

According to the database, some of the natural slope failures were initiated on an outcropping fault on the slope face (i.e. numbers 11, 20 and 24 in Table 3-1). The numerical model developed in the previous section was revised to allow studies of daylighting discontinuity in natural slopes and open pit mine slopes. Figure 5-6 illustrates the models used for this set of analyses. The material properties are the same used for the models in Section 5.3 and the fault is considered cohesionless with a friction angle of 30 degrees. Figure 5-7 illustrates the results derived from these analyses. The results show a similar trend with the ones depicted in the previous section for the continuous models, however, there are two main differences between the results in these two analyses. First, the fault generates an amplified horizontal velocity in the downward direction rather than a symmetric amplification in both directions. Secondly, as shown in Figure 5-8, the amplification factors for the five faulted topographies are less compared to those in the continuous models. These two differences are due to attenuation of wave magnitude propagating through the fault [166, 167]. Even though this attenuation decreases the amplification factor, the amplification factors are still significantly higher, up to 3.0 times, on faulted natural slopes compared to those on pit slopes.

5.5 Stiffness Contrast Effect

According to Chapter 4, a significant number of shallow failures occurred in the weak top layers of rock and soil. Figures 4-35 and 4-36 showed that the majority of failures in California and New Zealand, as regions with abundant failures, where subjected to stiffness contrast effect initiated on the weak top layers. In this section, the effect of stiffness contrast is investigated on a hill shape natural slope (Figure 5-9; see page 109).

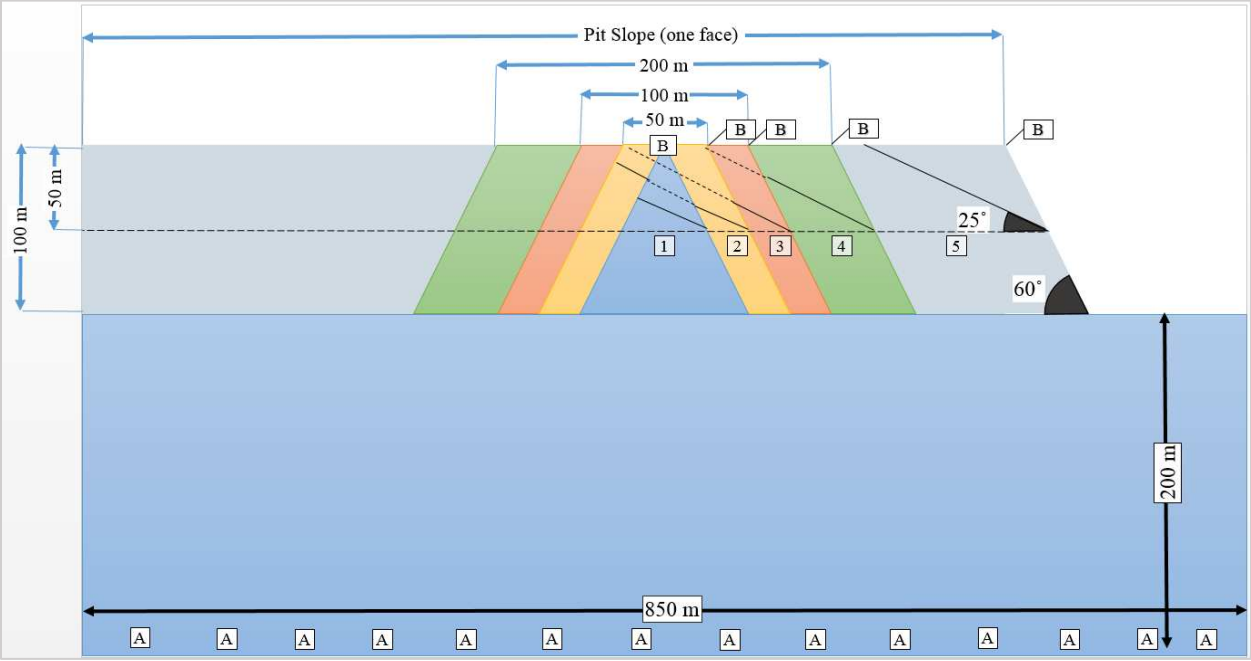

Figure 5-6 Geometry of models considered for the faulted slope analyses.

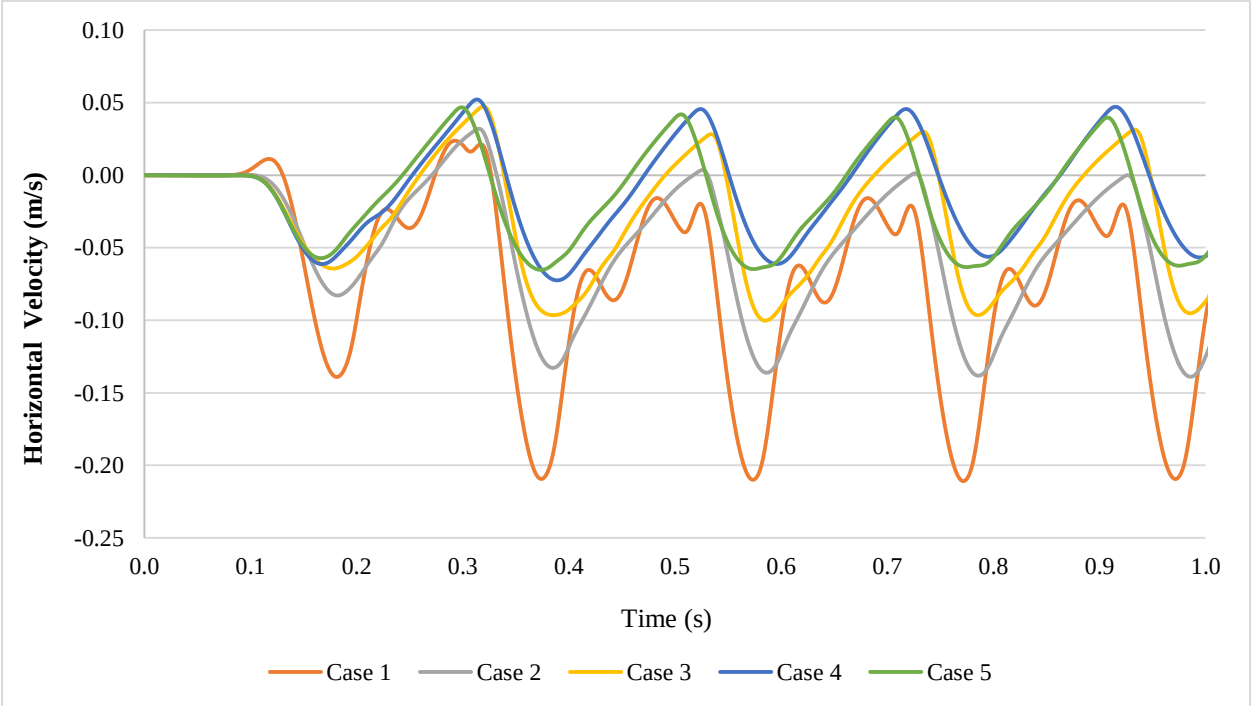

Figure 5-7 Horizontal velocities recorded at Point B on Figure 5-6 for different faulted topographies.

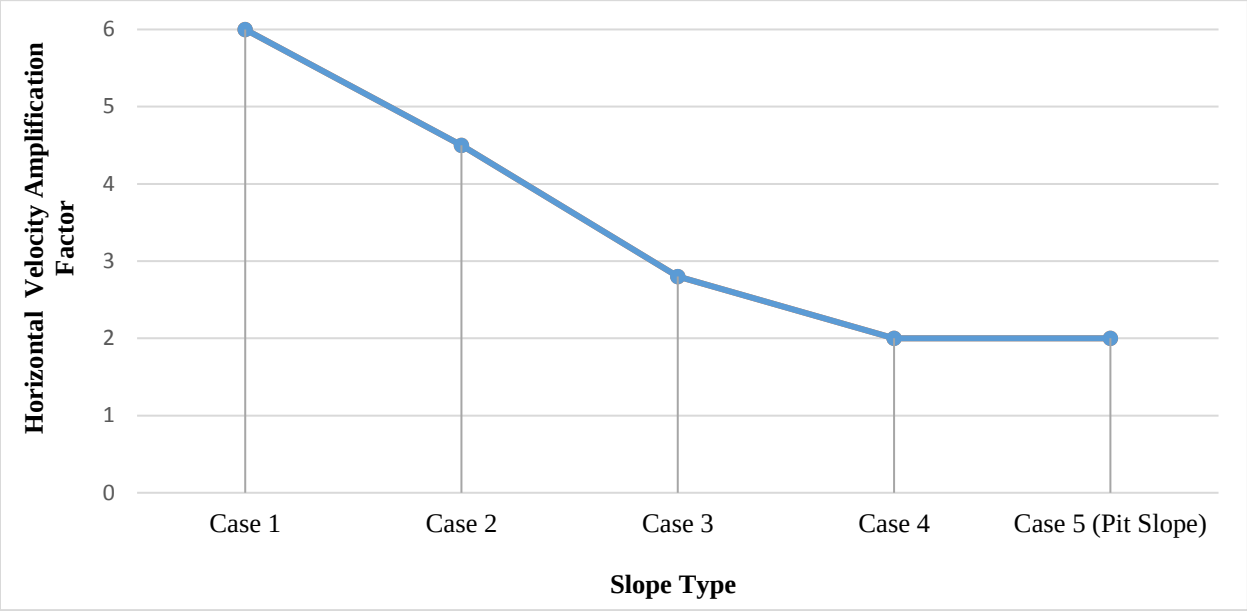

Figure 5-8 Horizontal velocity amplification factors for faulted slope topographies presented in Figure 5-6

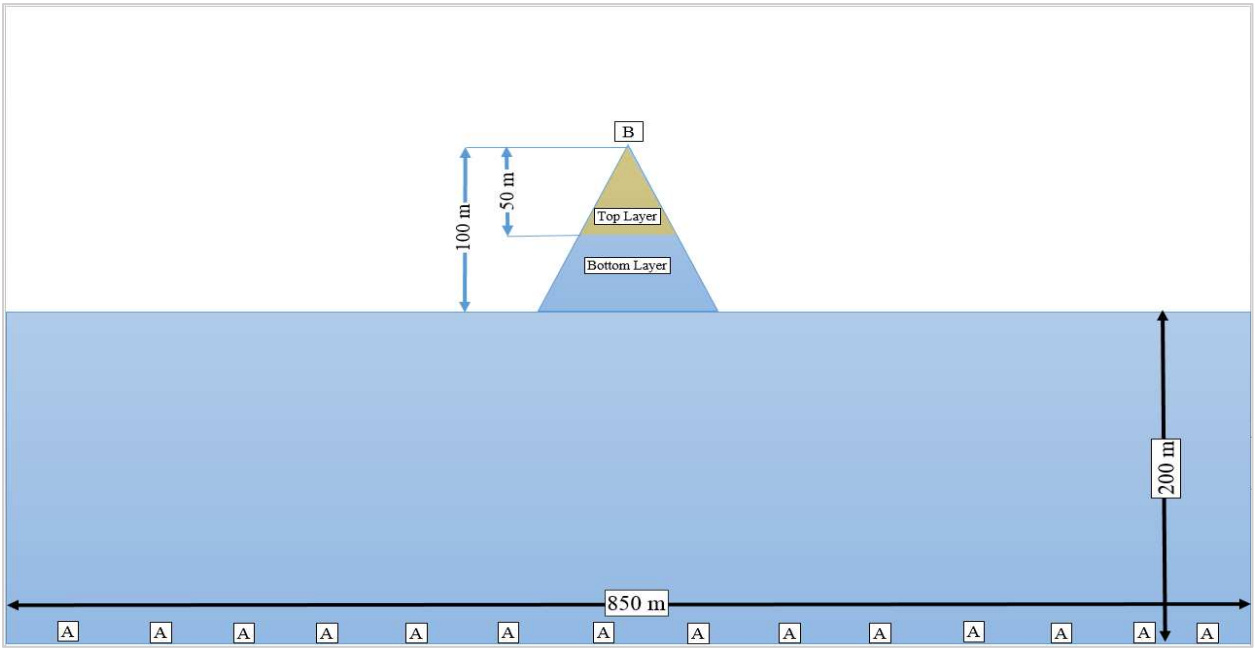

Figure 5-9 Model Generated for hill geometry with stiffness contrast.

A 50 m thick top layer with 1/2 and 1/5 elastic modulus contrast with the bottom layer is considered to simulate a typical greywacke and altered granite material, respectively. These material types are selected as the common failed material according to the database. Table 5-2 presents the properties assumed for the analyses. After defining the geometry and mechanical

properties of the material, the same seismic horizontal velocity for the topographical section is applied to the model bottom (Point A). The horizontal velocity is recorded at Point B for the two stiffness conditions and compared with the continuous model (Figure 5-10) Figure 5-11 shows the amplification factor for the three geology conditions. This figure shows that the horizontal velocity amplifies up to 16 times on lower stiffness top layers, which the amplification factor increases to 11 and 16 for top layers Type 1 to Type 2. This shows how the stiffness contrast in natural slopes and tiling dams could cause failure in contrast to most non-layered and continuous open pit mine slopes.

Table 5-2 Mechanical properties of the slope material with different stiffness contrasts.

Mechanical Property	Density (kg/m^3)	Elastic Modulus (GPa)	Shear Modulus (GPa)	Bulk Modulus (GPa)	Poisson's ratio
Bottom Layer	2650	50	20	33	0.25
Top layer Type 1 (greywacke)	2650	25	10	16.7	0.25
Top Layer Type 2 (altered granite)	2650	10	4	6.7	0.25

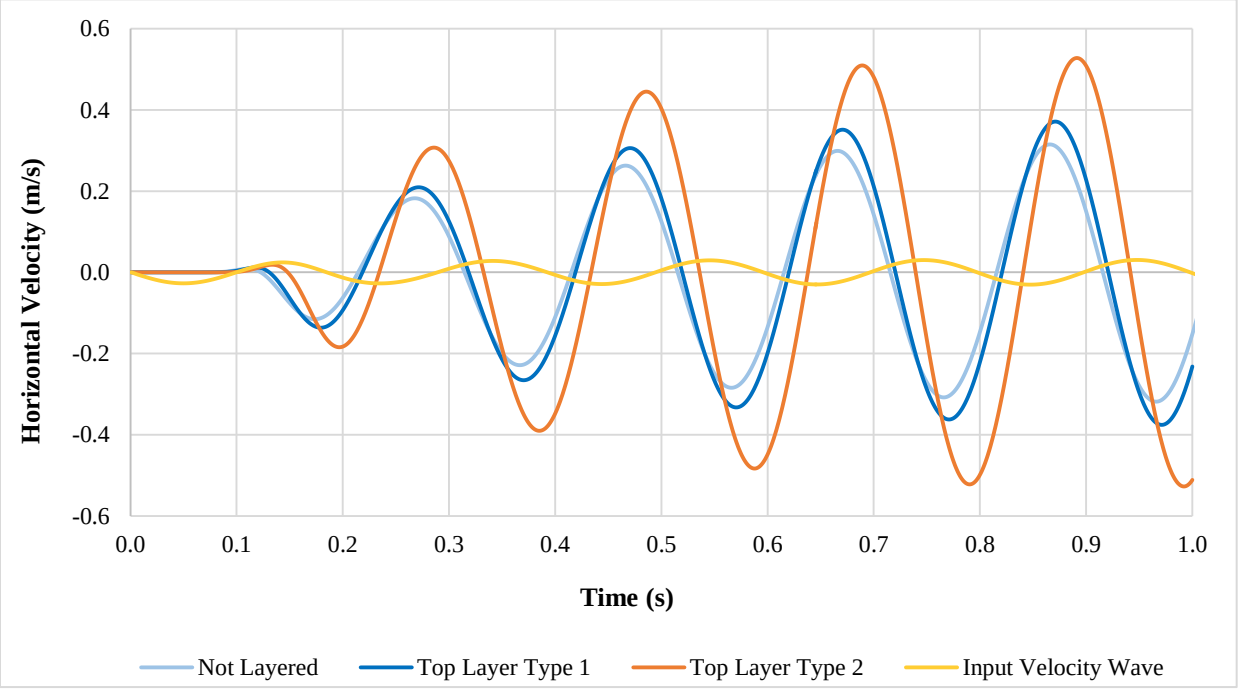

Figure 5-10 Horizontal velocities recorded at Point B on Figure 5-9 for layered hill geometry.

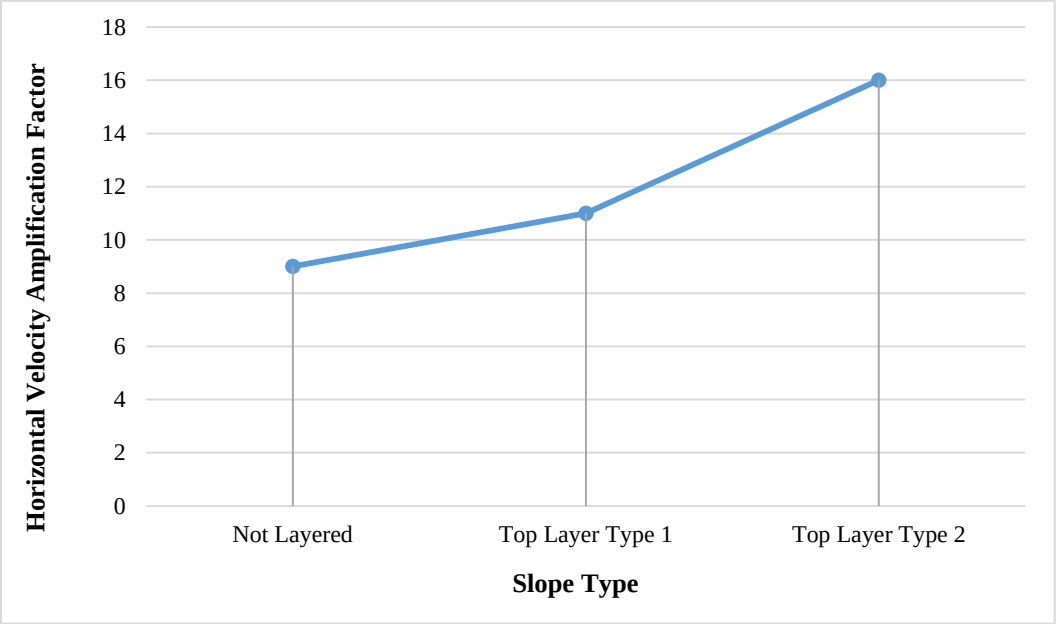

Figure 5-11 Horizontal velocity amplification factor of layered hill geometry.

5.6 Coupled Topography and Stiffness Contrast Effect

The coupled effect is studied to compare the open pit mines with natural slope conditions considering both topographical and stiffness contrast effects at the same time. In order to conduct this study, the top layer of five geometries modelled in the topographical effect analysis (Section 5.4) are subjected to lower stiffness (Figure 5-12). The analyses are performed using the highest stiffness contrast ratio 1/5. Figure 5-13 depicts the horizontal velocity of Point B for five topographies and Figure 5-14 shows the amplification factor derived from each model. The coupled amplification factors show a significant contrast between a typical natural slope with hill shape topography and top weak layer against open pit mine slope geometry with continuous rockmass. The amplification factor on a hill shape natural slope could be up to eight times the amplification factor of a pit slope.

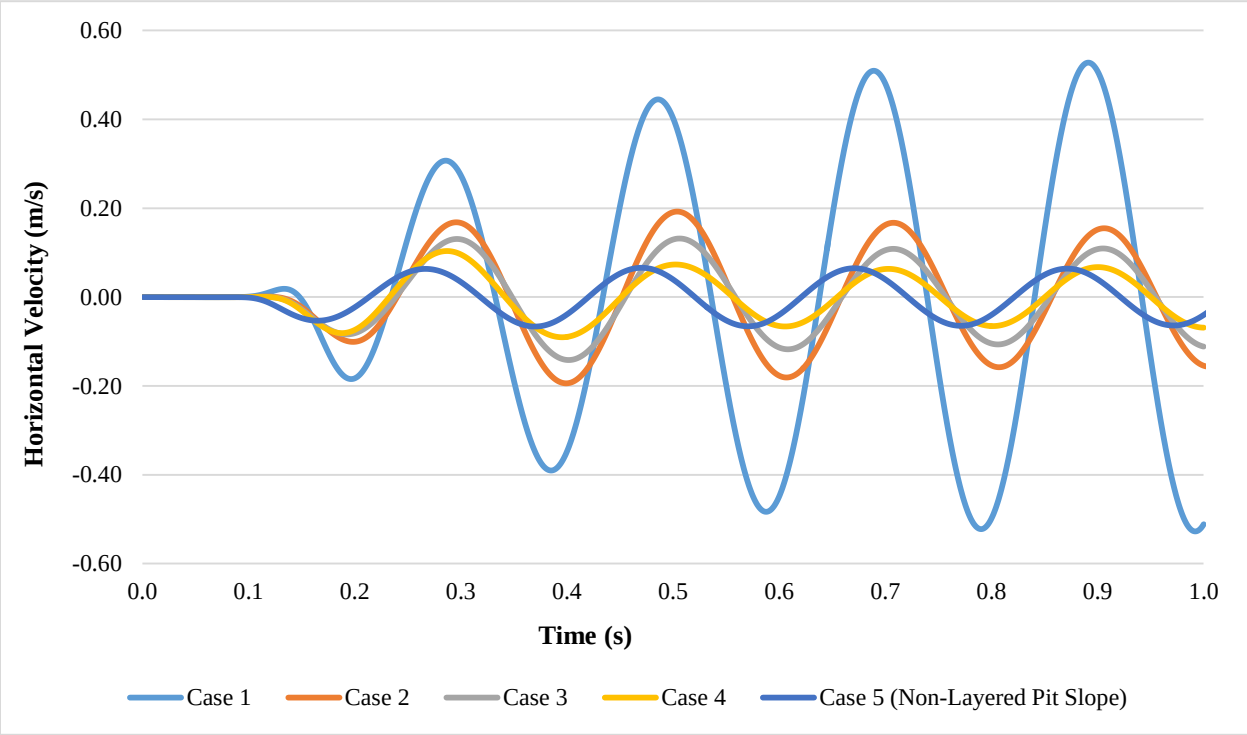

Figure 5-12 Coupled models for topographical and stiffness contrast effects.

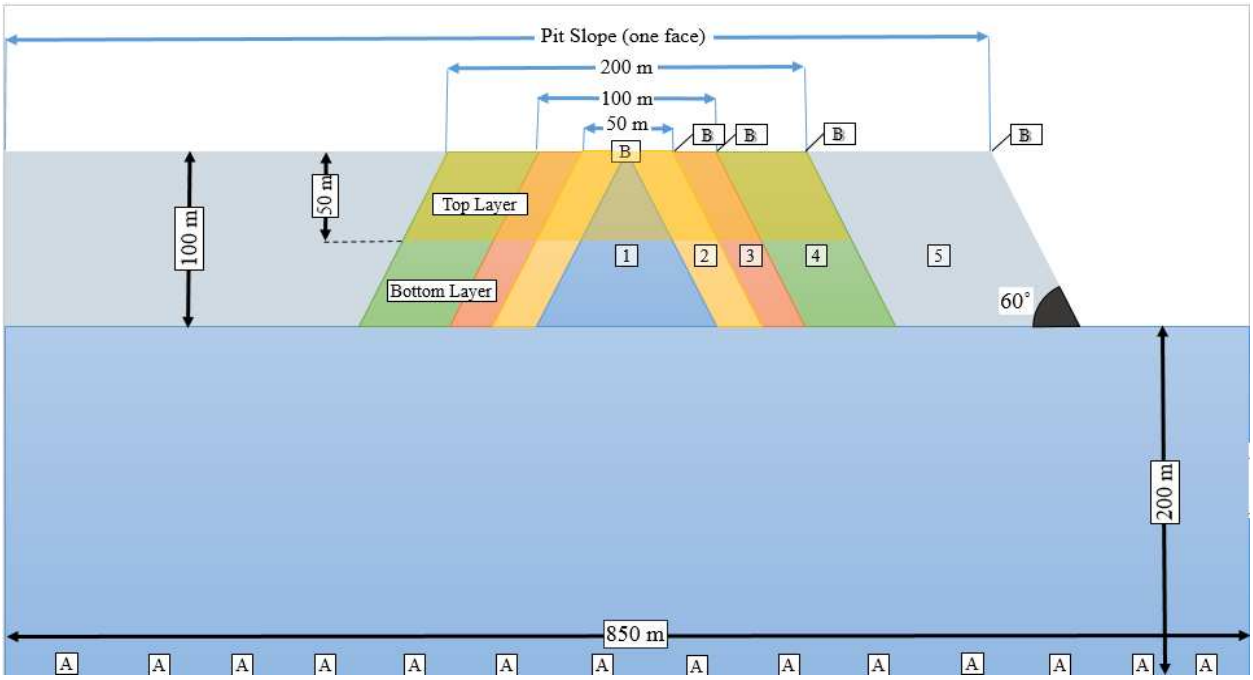

Figure 5-13 Horizontal velocities recorded at Point B on Figure 5-12 for different layered topographies and open pit mine slope.

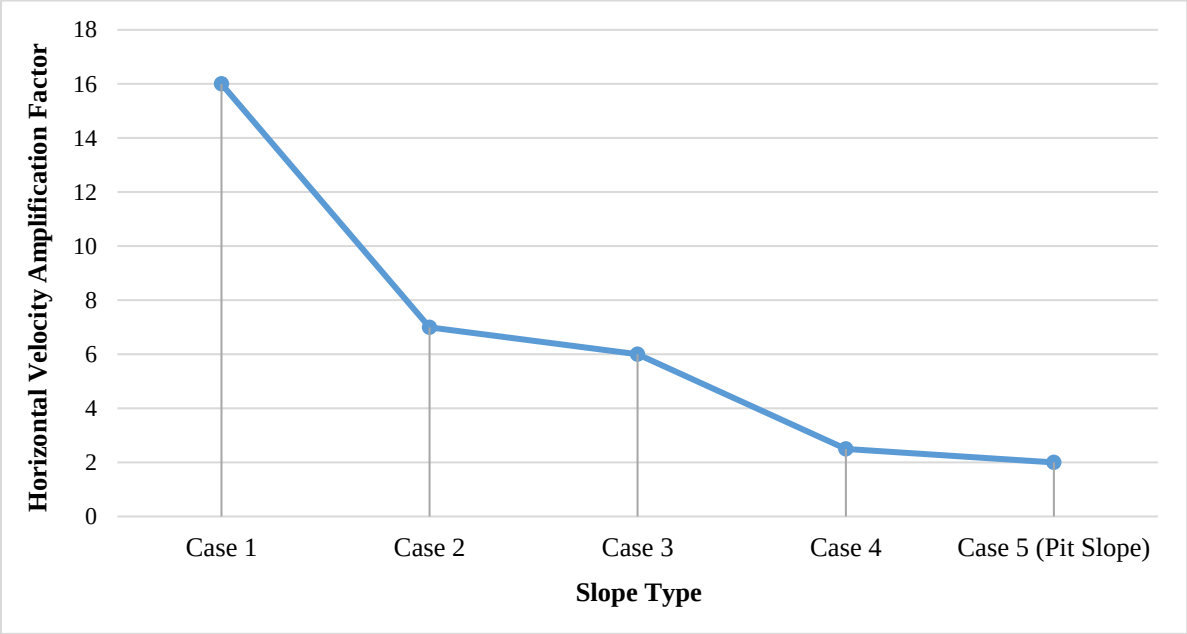

Figure 5-14 Horizontal velocity amplification factor of coupled topography and stiffness contrast effect.

5.7 Conclusions

The effect of topography and stiffness contrast on the horizontal velocity amplification is studied to compare the site effect for open pit mine slopes with natural slopes. Four sets of geometries and material properties are considered to perform the analyses. The first two sets considered the topographical effect of continuous and faulted rock mass. The third set analyzes the effect of stiffness contrast on a hill-geometry natural slope considering two material properties for the top layer. The last set of models is utilized to study the coupled effect topography and stiffness contrast on natural slopes and open pit mine slopes.

The first set of analyses shows a significant difference of topographical effect between natural slope and pit slope geometries. The amplification factor can be increased up to four times from one-face pit slope to two-face hill geometries. An amplification factor of 3.0 is calculated for faulted slopes, which is less than the intact first set of models due to wave power attenuation propagating through the fault. The third set of analyses shows that the horizontal velocity amplifies

up to 12 and 16 times on natural slopes with a stiffness contrast of 1/2 and 1/5, respectively. This phenomenon commonly takes place in earthquake triggered natural slope failures with heterogeneous material, and is rare in competent material for most large open pit mine slopes. The results for the coupled effect of topography and stiffness contrast shows that the different site conditions in natural slopes and open pit mines could amplify the horizontal wave velocity up to eight times on natural slopes compared to the open pit mines. The results derived from the four sets of analyses show the significant influence of site effects on earthquake triggered natural slope failures, and describes how the pit slopes are less prone to these effects.

CHAPTER 6

CONCLUSIONS AND FUTURE WORK

6.1 Main Conclusions

This research studies the potential effects of earthquakes on open pit mines addressing the dichotomy of significant number of natural slope and tailing dam failures versus no reported failures in open pit mines due to earthquakes. A comprehensive comparison of earthquake-triggered natural slope and tailing dam failures against enduring open pit mines is conducted with earthquake parameters and geological characteristics being considered. Following conclusions may be drawn:

- Open pit mines were mostly subjected to relatively distant and deep earthquakes compare to earthquakes that triggered natural slope and tailing dam failures. Natural slope failures are mainly triggered by earthquakes that occur within a range of 100 km epicenter, 40 km depth and magnitudes of more than 5.0. Of the 177 open pit mines considered in this study, only 7 mines were in the vicinity of these earthquake.
- Open pit mines are subjected to lower earthquake intensities than natural slopes and tailing dams that experienced earthquake-triggered failure. This research shows that 90 percent of natural slopes and tailing dam failures were triggered by earthquake intensities of more than 6.0, however, only 11 percent of mines studied were subjected to these intensities. Therefore, the response of open pit mines to higher intensity earthquakes in not well known.
- The equation presented by Barosh [140] in 1969 to predict the earthquake intensity considers an equal effect for epi-central distances and focal depth. However, the data analysis shows that the focal depth has a greater influence upon the resultant intensity.

- Most reported natural slope failures are shallow in thickness, typically less than 3 m. Often, similar size failures in open pit mines do not have to be recorded as “failure” unless they fall into “reportable” category.
- The weak top layers on natural slopes are widely susceptible to failure due to ground motion amplification caused by stiffness contrast between the bedrock and top soil. Open pit mines are less prone to this amplification due to the absence of the unconsolidated top soil layer.
- Presence of water in more than 85% of the triggered landslides emphasizes the significance of water content in slope stability. Dewatering of open pit slopes through mining and surface water control increases slope stability.
- Natural slopes are subjected to chemical, mechanical and biological degradation. These processes reduce the stability of slopes against an external triggering force such as earthquakes. Open pit mines are usually designed considering the effect of water, rock mass strength and local seismic activities, thus increasing stability.
- Earthquake caused ground motions amplify on hill tops and ridges, which is a common phenomenon in natural slope failures. In contrast, ground motion is reduced in open pit mines due to their geometry.

6.2 Future Work

This research was mainly focused on the involvement of earthquake parameters and geological characteristics on stability of the three slope types using the developed database. Although there are numerical analysis performed evaluating the effect of topography and stiffness contrast, further numerical analysis can be performed on other earthquake and geological parameters as listed below:

1. Compare the results from UDEC with the simplified Pseudo-static and Newmark's methods for the faulted slope geometry.
2. Evaluate the effect of different fault properties on stability of slopes subjected to earthquakes.
3. Apply different joint set patterns to the numerical models to investigate the effect of orientation and density of joints on slope stability.
4. Perform sensitivity analysis on earthquake frequency and magnitude parameters to investigate their effect on slope stability.
5. Find the relationship between earthquake frequency and slope crest width and its effect on the stability of hill geometry slopes.
6. Investigate the effect of different fault properties on wave intensity attenuation.
7. Investigate the correlation between earthquake wave orientation and slope dip direction and its effect on slope stability.
8. Study the effect of water and excess pore pressure on slope stability during earthquakes using numerical analysis.
9. Repeat the performed numerical analysis on the faulted slope using strain softening behavior for the discontinuity.
10. Evaluate the effect of different slope angles on topographical amplification.

REFERENCES CITED

[1] Lorig, L., 2016. Designing for extreme events in open pit slope stability. Journal of the Southern African Institute of Mining and Metallurgy, 116(5), pp.387-398.

[2] Read, J. and Stacey, P., 2009. Guidelines for open pit slope design.

[3] Keefer, D.K., 1984. Landslides caused by earthquakes. The Geological Society of America Bulletin, (April), pp.406–421.

[4] Richards, J.P., 2003.Tectono-Magmatic Precursors for Porphyry Cu-(Mo-Au) Deposit Formation. Economic Geology, 98: p. 1515-1533.

[5] Bommer, J.J., Chandler, R.J. & Rodri, C.E., 1999. Earthquake-induced landslides : 1980 – 1997. Soil Dynamics and Earthquake Engineering 18, pp.325–346.

[6] Glass, C.E., 2000. The influence of seismic events on slope stability. Slope Stability in Surface Mining, pp.97-105.

[7] Shebalin N.V. (ed), 1977. Atlas of isoseismal maps for the "New catalogue of strong earthquakes on the USSR territory from ancient times through 1975". Archive of the Institute of Physics of the Earth (IPE), Moscow.

[8] Sep'ulveda, S.A., Murphy, W., R.W., Petley, D.N., 2005. Seismically induced rock slope failures resulting from topographic amplification of strong ground motions: the case of Pacoima Canyon California, Engineering Geology 80, 336-348.

[9] Havenith, H.-B., D. Jongmans, E. Faccioli, K. Abdrakhmatov, and P.-Y. Bard, 2002, Site effect analysis around the seismically induced Ananevo rockslide, Kyrgyzstan, Bulletin of the Seismological Society of America. 92, 3190-3209.

[10] Mavroulis, S, 2009, Fault activity assessment in NW Peloponnesus - Andravida earthquake (08/06/2008). Msc Thesis, National and Kapodistrian University of Athens, Department of Geology and Geoenvironment: 622.

[11] Moore, J. R., V. Gischig, J. Burjanek, F. Amann, and Hunziker M., 2012, Earthquake-triggered rock slope failures: Damage and site effects. In Proceedings 11th International & 2nd North American Symposium on Landslides.

[12] Mavroulis S., Fountoulis I. &. Lekkas E, 2010, Environmental effects caused by the Andravida (08-06-2008, ML=6.5, NW Peloponnese, Greece) earthquake, 11th IAEG Congress New Zealand.

[13] Ma S, Archuleta R. J., Page M. T., 2007, Effects of large-scale surface topography on ground motions, as demonstrated by a study of the San Gabriel Mountains, Los Angeles, California, Bulletin of the Seismological Society of America, Vol. 97, No. 6, pp. 2066–2079.

[14] McColl S. T., Davies T. R. H., McSaveney M. J., 2012. The effect of glaciation on the intensity of the seismic ground motion. Earth Surface Processes and Landforms Earth Surf. Process. Landforms 37, 1290–1301.

[15] Gouveia, F., R. C. Gomes, I. F. Lopes, and A. B. Author, 2012, Influence of stiffness contrast in non-horizontally layered ground on site effects.

[16] Hack, R., Alkema, D., Kruse, G. a. M., Leenders, N., & Luzi, L., 2007, Influence of earthquakes on the stability of slopes. Engineering Geology, 91(1), 4–15.

[17] Biondi G, Cascone E, Maugeri M, Motta E, 2000, Seismic response of saturated cohesionless slopes. Soil Dynamic and Earthquake Engineering 20(1–4):209–215.

[18] Biscontin, G. and Pestana, J.M., 2006. Factors affecting seismic response of submarine slopes. Natural Hazards and Earth System Science, 6(1), pp.97-107.

[19] Strasser, M., Stegmann, S., Bussmann, F., Anselmetti, F.S., Rick, B. and Kopf, A., 2007. Quantifying subaqueous slope stability during seismic shaking: Lake Lucerne as model for ocean margins. Marine Geology, 240(1), pp.77-97.

[20] Newmark, N. M., 1965, Effects of earthquakes on dams and embankments. Geotechnique, 15 (2) 139-160.

[21] Li, a. J., Lyamin, a. V., & Merifield, R. S., 2009, Seismic rock slope stability charts based on limit analysis methods. Computers and Geotechnics, 36(1-2), 135–148.

[22] UDEC Version 4.01, 2008, Itasca Consulting Group Inc. Minneapolis, MN USA.

[23] Mahboubi, A., Aminpour, A. and Noorzad, A., 2008, Conventional and Advanced Numerical Methods of Rock Slope Stability Analysis, A Comparison Study, Gotvand Dam Right Abutment (Iran) Case Study. The 12th International Conference of International Association for Computer Methods and Advances in Geomechanics (IACMAG).

[24] Gheibi, E., and Gassman S.L. (2015). "Magnitudes of prehistoric earthquakes at the Hollywood, South Carolina, site." International Foundations Congress and Equipment Exposition (IFCEE), San Antonio, TX. 1246-1256, DOI: 10.1061/9780784479087.112.

[25] Gheibi, E., and Gassman S.L. (2014). "Reassessment of prehistoric earthquake accelerations at Sampit and Gapway sites in the South Carolina Coastal Plain." Proc. 10th US National Conference on Earthquake Engineering (10NCEE), Paper, DOI:10.4231/D3PV6B73Z.

[26] Keefer D.K., 2002. Investigating landslides caused by Earthquakes– A historical review, Surveys in Geophysics 23: 473–510.

[27] Villavicencio, G., Espinace, R., Palma, J., Fourie, A. and Valenzuela, P., 2013. Failures of sand tailings dams in a highly seismic country. Canadian geotechnical journal, 51(4), pp.449-464.ICOLD, 2001

[28] How does BGS classify landslides?, 2014, British Geology Survey, Natural Environment Research Council. Available from: http://www.bgs.ac.uk/landslides/how_does_BGS_classify_landslides.html

[29] Management of Tailing Storage Facilities, Energy and Earth Resources, 2015, Available from: http://www.energyandresources.vic.gov.au/earth-resources-regulation/licensing-and-approvals/minerals/guidelines-and-codes-of-practice/management-of-tailings-storage-facilities

[30] Ghosh, G.K. and Mahajan, A.K., 2011. Interpretation of intensity attenuation relation of 1905 Kangra earthquake with epicentral distance and magnitude in the northwest Himalayan region. Journal of the Geological Society of India, 77(6), pp.511-520.

[31] Rautian, T. and Leith, W., 2002. Composite regional catalogs of earthquakes in the Former Soviet Union. US Geological Survey Open File Report, 2, p.500.

[32] Khademian, Z. Poeck, E. Garvey, R. and Ozbay U., 2016. Studies of Seismicity Generated by Unstable Failures around Circular Excavations. 50th US Rock Mechanics/Geomechanics Symposium, American Rock Mechanics Association.

[33] Poeck, E.C., Khademian, Z., Garvey, R. and Özbay U., 2016. Modeling unstable rock failures in underground excavations. 2016 ISRM International Symposium.

[34] USGS, 2016, Earthquake Facts, Available from: http://earthquake.usgs.gov/learn/facts.php

[35] Nelson, S A, 2013, Tulane University, Available from:http://www.tulane.edu/~sanelson/Natural_Disasters/slopestability.htm

[36] Gheibi, E., Bagheripour M.H., and Gheibi, A. (2011). "Soil liquefaction potential assessment using nonlinear site response analysis." Proc. 6th International Conference of Seismology and Earthquake Engineering (SEE6). Paper, DOI: 10.13140/RG.2.2.29961.44641

[37] Shafique, M., Anggraeni, D., Bakker, W. and van der Meijde, M., 2010, May. Modeling the impact of topography on seismic amplification at regional scale. In EGU General Assembly Conference Abstracts (Vol. 12, p. 8452).

[38] Ashford, S.A., Sitar, N., Lysmer, J. and Deng, N., 1997. Topographic effects on the seismic response of steep slopes. Bulletin of the seismological society of America, 87(3), pp.701-709.

[39] Ashford, S.A. and Sitar, N., 1997. Analysis of topographic amplification of inclined shear waves in a steep coastal bluff. Bulletin of the seismological society of America, 87(3), pp.692-700.

[40] Khademian, Z., Shahriar K. and Nik M. G. 2012. "Developing an algorithm to estimate in situ stresses using a hybrid numerical method based on local stress measurement." International Journal of Rock Mechanics and Mining Sciences 55: 80-85.

[41] Gheibi, E., and Bagheripour M.H. 2011. "Alterations of equivalent number of cycles in depth of soil profile." *Proc. 6th International Conference of Seismology and Earthquake Engineering (SEE6).* Paper, DOI: 10.13140/RG.2.2.16539.67360.

[42] Terzaghi K., 1950, Mechanisms of Landslides. Engineering Geology (Berkeley) Volume, Geological Society of America.

[43] Hack, R., Alkema, D., Kruse, G. a. M., Leenders, N., & Luzi, L., 2007, Influence of earthquakes on the stability of slopes. Engineering Geology, 91(1), 4–15.

[44] Liu YQ, Li HB, Zhao J, Li JR, Zhou QC., 2004, UDEC simulation for dynamic response of a rock slope subject to explosions. Int J RockMech Mining Sci;41(3):474.

[45] Marcato, G., Fujisawa, K., Mantovani, M., Pasuto, A., Silvano, S., Tagliavini, F., & Zabuski, L., 2007, Evaluation of seismic effects on the landslide deposits of Monte Salta (Eastern Italian Alps) using distinct element method, 695–701.

[46] Bhasin, R. et al., 2004, Insights Into the Deformation Mechanisms of a Jointed Rock Slope Subjected to Dynamic Loading, Int. J Rock Mech. Min. Sci, 41(3), Paper No. 2B.

[47] Kveldsvik, V., Kaynia, A. M., Nadim, F., Bhasin, R., Nilsen, B., & Einstein, H. H., 2009, Dynamic distinct-element analysis of the 800m high Åknes rock slope. International Journal of Rock Mechanics and Mining Sciences, 46(4), 686–698.

[48] Bozzano, F., Lenti, L., Martino, S., Montagna, A., & Paciello, A., 2011, Earthquake triggering of landslides in highly jointed rock masses: Reconstruction of the 1783 Scilla rock avalanche (Italy). Geomorphology, 129(3-4), 294–308.

[49] Jibson, R. W., 2011, Methods for assessing the stability of slopes during earthquakes—A retrospective. Engineering Geology, 122(1-2), 43–50.

[50] New Madrid 1811-1812 Earthquakes, Historic Earthquakes, USGS, 2014, Retrieved from: http://earthquake.usgs.gov/earthquakes/states/events/1811-1812.php.

[51] Eileen McSaveney. 'Historic earthquakes - The 1848 Marlborough earthquake', Te Ara - the Encyclopedia of New Zealand, updated 13-Jul-12, Retrieved from: URL: http://www.TeAra.govt.nz/en/historic-earthquakes/page-2

[52] Graham Hancox, 2005, Landslides and liquefaction effects caused by the 1855 Wairarapa earthquake: then and now, The 1855 Wairarapa Earthquake Symposium.

[53] Geological Hazards of the South Carolina Coastal Plain, 2012, Department of Natural Resourses South Carolina.

[54] Bommer, J.J. & Rodrı, C.E., 2002. Earthquake-induced landslides in Central America. Engineering Geology, 63, pp.189–220.

[55] Downes, G.L., 2006. The 1904 MS =6.8 MW=7.0-7.2 Cape Turnagain , New Zealand , Earthquake. Bulletin of the New Zealand Society for Earthquake Engineering, 39(4), pp.183–207.

[56] Turel, M. 2011, Soft Computing Based Spatial Analysis Of Earthquake Triggered Coherent Landslides Soft Computing Based Spatial Analysis Of. Georgia Institute of Technology, PhD Dissertation.

[57] Chigira, M. et al., 2014, Studies on the 2011 off the Pacific Coast of Tohoku Earthquake.

[58] Robinson, T.R. & Davies, T.R.H., 2013. Review Article: Potential geomorphic consequences of a future great (Mw = 8.0+) Alpine Fault earthquake, South Island, New Zealand. Natural Hazards and Earth System Science, 13(9), pp.2279–2299.

[59] Downs, et al., 1999, The 1934 Pahiatua earthquake sequence: analysis of observational and instrumental data. Bulletin of the New Zealand National Society for Earthquake Engineering, 32(4), pp. 221-245.

[60] Elms L., 2001, Landslide Lake: The 1946 Earthquake. Retrieved from: http://www.beyondnootka.com/articles/landslide_lake.html

[61] Pattle, A. and Wood, J. H, 1994. Ground shaking intensity and damage at Lake Coleridge Power Station in the 18 June Avoca River earthquake. Bulletin of the New Zealand National Society for Earthquake Engineering, 27, 3,227-230.

[62] Yablokov, A., 2000. The Tragedy of Khait : A Natural Disaster in Tajikistan. Mountain Research and Development, 21(1), pp.91–93.

[63] Pacific Northwest geologic mapping and urban hazards, USGS, Retrieved From: http://geomaps.wr.usgs.gov/pacnw/lifeline/eqhazards.html

[64] Historic Earthquakes, Assam-Tiet, 1950 August 15 14:09 UTC 8.6M, USGS, Retrieved from: http://earthquake.usgs.gov/earthquakes/world/events/1950_08_15.php

[65] Historic Earthquakes, Daly City, California 1957 March 22 19:44:21 UTC Magnitude 5.3, USGS, Retrieved from: http://earthquake.usgs.gov/earthquakes/states/events/1957_03_22.php

[66] Miller, B.D.O.N.J., 1960. Giant Waves in Lituya Bay Alaska. Geological Survey Professional Paper 354-C.

[67] Historic Earthquakes, Hebgen Lake, Montana 1959 08 18 06:37:15 UTC (local 08/17) 7.3M, USGS, Retrieved from: http://earthquake.usgs.gov/earthquakes/states/events/1959_08_18.php

[68] Dzierma, Y. et al., 2012. Seismicity near the slip maximum of the 1960 Mw 9.5 Valdivia earthquake (Chile): Plate interface lock and reactivation of the subducted Valdivia Fracture Zone. Journal of Geophysical Research, 117(B6), p.B06312.

[69] Eiby, G. a., 1964. The Northland Earthquakes of 1963 November-December and the Seismicity of Northland. New Zealand Journal of Geology and Geophysics, 7(4), pp.745–765.

[70] Parsons T. et al., Source and progression of a submarine landslide and tsunami: The 1964 Great Alaska earthquake at Valdez, Journal of Geophysical Research: Solid Earth, 119, doi:10.1002/2014JB011514.

[71] Evans, S G. & Couture, R. The 1965 Hope Slide, British Columbia; Catastrophic Failure of a Sagging Rock Slope, Paper No. 16-6, Geol. Society of America meeting in Denver, 2002.

[72] Beck, S.L. & Ruff, L.J., 1989. Great earthquakes and subduction along the Peru trench. Physics of the Earth and Planetary Interiors, (57), pp 199-224.

[73] Douglas M. M. Seismically Triggered Landslides Above San Fernando Valle, Special San Fernando Earthquake Edition, California Geology, April/May 1971, Vol. 24, No. 4-5.

[74] Historic Earthquakes, Island of Hawaii, Hawaii 1973 April 26 20:26:30.6 UTC 6.2M, USGS, Retrieved from: http://earthquake.usgs.gov/earthquakes/states/events/1973_04_26.php

[75] Okubo, C.H., 2004. Rock mass strength and slope stability of the Hilina slump, Kīlauea volcano, Hawai'i. Journal of Volcanology and Geothermal Research, 138(1-2), pp.43–76.

[76] Edwin L. H., 1981, Landslides from 1976. The Guatemala Earthquake of February 4, 1976. Geological Survey Professional Paper 1204-A

[77] L'Heureux, J.S. et al., 2013. Stability, mobility and failure mechanism for landslides at the upper continental slope off Vesterålen, Norway. Marine Geology, 346, pp.192–207.

[78] Berberian M., Papastamatiou D. & Qoraishi M., 1977, Khurgu (North Bandar Abbas-Iran) Earthquake of March 21, 1977: A Preliminary Field Report and a Seismotectonic Discussion, Geological Survey. Iran, 40, pp 7-49.

[79] Ellingwood B., 1980. An Investigation of the Miyagi-ken-oki, Japan, Earthquake of June 12, 1978, Volume 13.

[80] Earthquakes in Southern California, 1979-1989, Geologic Hazards Photos Volume 2, Earthquake Events, National Center for Environmental Information, Retrieved from: ftp://ftp.ngdc.noaa.gov/hazards/cdroms/geohazards_v2/document/647008.htm

[81] Reasenberg, P. & Ellsworth, W.L., 1982. Aftershocks of the Coyote Lake, California, Earthquake of August 6, 1979' A Detailed Study the San. Journal of Geophysical Research, (87) BI3, pp 10,637-10,655.

[82] Jibson R. W., 1993. Predicting Earthquake-Induced Landslide Displacement Using Newmark's Slide Block Analysis, Transportation Research Record 1411.

[83] Area, C.L. & California, E., 2014. Scenario Earthquake Hazards for the Long Valley Caldera-Mono Lake Area, East-Central California USGS Open-File Report 2014 – 1045 CGS Special Report 233.

[84] Capolongo, D., Refice, A. & Mankelow, J., 2002. Evaluating Earthquake-Triggered Landslide Hazard at the Basin Scale through GIS in the Upper Sele River. Surveys in Geophysics, (23), pp.595–625.

[85] The Coalinga Anticline and the Coalinga Earthquake of 1983. 2015. San Joaquin Valley Geology. Retrieved from: http://www.sjvgeology.org/geology/coalinga_earthquake.html

[86] Anon, 1985. Workshop XXVIII on the Borah Peak, Idaho, Earthquake Volume B Convened under Auspices of National Earthquake Prediction and Hazard Programs 3-6 October 1984 Open-File Report 85-290- B Menlo Park, California.

[87] Historic Earthquakes, Offshore Valparaiso, Chile 1985 March 03 22:47:07 UTC, 7.8M., USGS, Retrieved from: http://earthquake.usgs.gov/earthquakes/world/events/1985_03_03.php

[88] El Salvador Earthquake October 1986, International Rescue Corps, Retrieved from: http://www.intrescue.info/hub/index.php/missions/el-salvador-earthquake-october-1986.

[89] Historic Earthquakes, Whittier Narrows, California 1987 October 01 UTC 14:42 5.9M, USGS, Retrieved from: http://earthquake.usgs.gov/earthquakes/states/events/1987_10_01.php

[90] Hauksson, E., 1989. The 1987 Whittier Narrows Earthquake Sequence in Los Angeles, Southern California : Seismological and Tectonic Analysis. , 94, pp.9569–9589.

[91] Disasters, N. Et Al., 1989. Reconnaissance Report on The 21 August 1988 Earthquake In The Nepal-India Border Region. , (March).

[92] Urgeles, R. et al., 2002. The Saguenay Fjord, Quebec, Canada: integrating marine geotechnical and geophysical data for spatial seismic slope stability and hazard assessment. Marine Geology 185 (2002), pp 319-340.

[93] USSR, 1989. Earthquake in Tajikistan Jan 1989 UNDRO Information Report No. 1-5.

[94] Zare, M., 1993. Macrozonation of landslides for the Manjil, Iran 1990 earthquake.

[95] Tang, C. et al., 2011. Landslides induced by the Wenchuan earthquake and the subsequent strong rainfall event: A case study in the Beichuan area of China. Engineering Geology, 122(1-2), pp.22–33.

[96] Goes, S.D.B. et al., 1993. The April 22, 1991, Valle de la Estrella, Costa Rica (Mw - 7.7) Earthquake and Its Tectonic Implications : A Broadband Seismic Study. , 98(93), pp.8127–8142.

[97] Erdik M., et al., 1994. March 13, 1992 Erzincan (Turkey) Earthquake, Earthquake Engineering, tenth World Conference, Balkema, Rottrerdam.

[98] Reagor, B.G. & Brewer, L.R., 1992. The Cape Mendocino Earthquakes of April 25 and 26, 1992.

[99] Jongmans, D. et al., 2000. Geophysical investigations of seismically induced surface effects: case study of a landslide in the suusamyr valley, kyrgyzstan. , pp.349–369.

[100] Mellors, R., 1997. The M s = 7. 3 1992 Suusamyr, Kyrgyzstan, Earthquake in the Tien Shan : 2. Aftershock Focal Mechanisms and Surface Deformation. , (October 2015).

[101] Rodriguez, C.E., 2006. Earthquake-induced Landslides in Colombia.

[102] Lekkas, E.L. et al., 2008. Correlating the Damage Pattern and the Geological Structure. Local Site Effects from the 2006 Mw = 6. 7 Kythira Island Intermediate Depth Event, Sw Greece.

[103] Satake, K. & Tanioka, Y., 1995. Tsunami Generation of the 1993 Hokkaido Nansei-Oki Earthquake. , 145.

[104] Van Dissen, R., Cousins, J., Robinson, R. and Reyners, M., 1994. The Fiordland earthquake of 10 August, 1993: a reconnaissance report covering tectonic setting, peak ground acceleration, and landslide damage. Bulletin of the New Zealand National Society for Earthquake Engineering, 27(2), pp.147-154.

[105] Black, G.L. and Wells, R.E., 1993. Klamath Falls earthquakes, September 20, 1993—including the strongest quake ever measured in Oregon. Oregon Geology, 55(6), p.127.

[106] Harp, E.L. and Jibson, R.W., 1996. Landslides triggered by the 1994 Northridge, California, earthquake. Bulletin of the Seismological Society of America, 86(1B), pp.S319-S332.

[107] Carlos A., 1996. Experiences from the paez Earthquake, Colombia, Eleventh World Conference on Earthquake Engineering, paper No. 103.

[108] Hancox G. T. et al., 1997. Earthquake-Induced landsliding in New Zealand and Implications for Seismic Hazard Assessment, Earthquake Commission Research Foundation, Institute of Geological & Nuclear Sciences Limited.

[109] Kitagawa, Y. and Hiraishi, H., 2004. Overview of the 1995 Hyogo-Ken Nanbu earthquake and proposals for earthquake mitigation measures. Journal of Japan Association for Earthquake Engineering, 4(3), pp.1-29.

[110] Margheriti, S.M., Mele, F., Selvaggi, G., Basili, A. and Boschi, E., 1998. The 1997 Umbria-Marche, Italy, earthquake sequence'. Geophysical Research Letters, 25(15), pp.2861-2864.

[111] Liu, S.H., Lin, C.W. and Tseng, C.M., 2013. A statistical model for the impact of the 1999 Chi-Chi earthquake on the subsequent rainfall-induced landslides. Engineering Geology, 156, pp.11-19.

[112] Mikoš, M. and Ribičič, M., 2006. Sediment production and delivery from recent large landslides and earthquake-induced rock falls in the Upper Soča River Valley, Slovenia. Engineering geology, 86(2), pp.198-210.

[113] Bommer, J.J., Benito, M.B., Ciudad-Real, M., Lemoine, A., López-Menjívar, M.A., Madariaga, R., Mankelow, J., de Hasbun, P.M., Murphy, W., Nieto-Lovo, M. and Rodríguez-Pineda, C.E., 2002. The El Salvador earthquakes of January and February 2001: context, characteristics and implications for seismic risk. Soil dynamics and earthquake engineering, 22(5), pp.389-418.

[114] Gorum, T., Korup, O., van Westen, C.J., van der Meijde, M., Xu, C. and van der Meer, F.D., 2014. Why so few? Landslides triggered by the 2002 Denali earthquake, Alaska. Quaternary Science Reviews, 95, pp.80-94.

[115] Keefer, D.K., Wartman, J., Ochoa, C.N., Rodriguez-Marek, A. and Wieczorek, G.F., 2006. Landslides caused by the M 7.6 Tecomán, Mexico earthquake of January 21, 2003. Engineering Geology, 86(2), pp.183-197.

[116] Kieffer, D.S., Jibson, R., Rathje, E.M. and Kelson, K., 2006. Landslides triggered by the 2004 Niigata Ken Chuetsu, Japan, earthquake. Earthquake Spectra, 22(S1), pp.47-73.

[117] Harp, E.L. and Crone, A.J., 2006. Landslides triggered by the October 8, 2005, Pakistan earthquake and associated landslide-dammed reservoirs (No. 2006-1052).

[118] Chigira, M., Wu, X., Inokuchi, T. and Wang, G., 2010. Landslides induced by the 2008 Wenchuan earthquake, Sichuan, China. Geomorphology, 118(3), pp.225-238.

[119] Baldwin, S.L., Fitzgerald, P.G. and Webb, L.E., 2012. Tectonics of the New Guinea region.

[120] Boyd, O.S., Mueller, C.S. and Rukstales, K.S., 2007. Preliminary earthquake hazard map of Afghanistan. US Geological Survey Open-File Report, 2007, p.1137.

[121] Liu, M., Luo, G. and Wang, H., 2014. The 2013 Lushan earthquake in China tests hazard assessments. Seismological Research Letters, 85(1), pp.40-43.

[122] Xu, C., Xu, X., Shyu, J.B.H., Zheng, W. and Min, W., 2014. Landslides triggered by the 22 July 2013 Minxian–Zhangxian, China, Mw 5.9 earthquake: Inventory compiling and spatial distribution analysis. Journal of Asian Earth Sciences, 92, pp.125-142.

[123] "Ohashi Aso slope and the national highway collapse" (in Chinese). Nikkei Construction. . N.p., 2016. Web. 3 Aug. 2016.

[124] Villavicencio, G. et al., 2014. Failures of sand tailings dams in a highly seismic country. , 464(April 2013), pp.449–464.

[125] Unit, G.H., Reported tailings dam failures. A review of the European incidents in the worldwide context. , pp.1–21.

[126] Li, Q., 2010. Tailings Dam Failures : A Review of the Last One Hundred Years. Waste Geo Technics, December 2010, pp.50-53.

[127] InfoMine Inc., Information on World Mining Operations, Retrieved from: http://www.infomine.com

[128] McGill Research Group Investigating Canadian Mining in Latin America, Maps and spatial data, Retrieved from: http://micla.ca/resources.

[129] Iran Mining & Related Industries Information Center, Mines-Iran, Retrieved from: http://www.iranmining.com/Mines/eindex.asp?Lang=EN&Dir=431.

[130] Mines in Alaska, Retrieved from: http://northern.org/programs/clean-water-mines/hardrock-mines-in-interior-and-arctic-alaska

[131] State-By-State List of Mining Regions, USGS, Retrieved from: http://earthquake.usgs.gov/earthquakes/eqarchives/mineblast/sources.php

[132] CRU Group, Copper Mines list, Retrieved from: http://www.crugroup.com/content/products/30388/coppercostcurve/copper_mine_cost_service_list.pdf

[133] "Global Air Photos Hope Air Photos#9023, Hope Slide - View East". Globalairphotos.com. N.p., 2016. Web. 6 June 2016.

[134] Wetmiller, R.J. and Evans, S.G., 1989. Analysis of the earthquakes associated with the 1965 Hope landslide and their effects on slope stability at the site. Canadian Geotechnical Journal, 26(3), pp.484-490.

[135] Harley M. Benz, Susan Rhea. "Full-size worldwide seismicity map ". Pubs.usgs.gov. N.p., 2016. Web. 2 June 2016.

[136] Harley M. Benz, Susan Rhea. "USGS Open-File Report 2010-1083-I: Seismicity of The Earth 1900–2010 Eastern Margin Of The Australia Plate". Pubs.usgs.gov. N.p., 2016. Web. 2 June 2016.

[137] Hayes, Gavin et al. "Seismicity of The Earth 1900-2013, Seismotectonics of South America (Nazca Plate Region)". Open-File Report (2015): N.p. Web. 2 June 2016.

[138] Harley M. Benz, Susan Rhea. "USGS Open-File Report 2010-1083-A: Seismicity Of The Earth 1900–2010 Caribbean Plate And Vicinity". Pubs.usgs.gov. N.p., 2016. Web. 2 June 2016.

[139] Gutenberg, B. and Richter, C., 1942. Earthquake magnitude, intensity, energy, and acceleration. Bulletin of the Seismological Society of America, 32(3), pp.163-191.

[140] Barosh, P.J., 1969. Use of seismic intensity data to predict the effects of earthquakes and underground nuclear explosions in various geologic settings (No. 1279). US Govt. Print. Off.

[141] Shebalin N.V., Leydecker G., 1998. Earthquake catalogue for central and southeastern Europe 342 BC -1990 AD, European Commission, Final Report to Contract No ETNU-CT93-0087 Brussels.

[142] Strong Quake Kills 2 in Northern Chile 1995, The New York Times, accessed 10 May 2015, http://www.nytimes.com/1995/07/31/world/world-news-briefs-strong-quake-kills-2-in-northern-chile.html.

[143] Geotechnical Report from June 23, 2001 Peruvian Earthquake, 2001, accessed 10 June 2015, http://peer.berkeley.edu/publications/peru_earthquake/Mines/mines2.html.

[144] Gallardo, E 2007, Major earthquake strikes Chile, causing damage, some injuries, Southeast Missourian News, accessed 8 August 2016, http://www.semissourian.com/story/1291071.html.

[145] Jordan, P 2007, Big earthquake kills two in Chile, hits mining, Reuters, accessed 8 August 2016, http://www.reuters.com/article/idUSN14348810._CH_.2400

[146] 2007 Major Copper Disruptions! Will 2008 Be Any Different? FACTBOX-Major copper supply disruptions in 2007, Wordpress, accessed 8 August 2016, https://miningpower.wordpress.com/2008/02/01/2007-major-copper-disruptions-will-2008-be-any-different/.

[147] Gold Stock News 2007, Goldreview, accessed 10 May 2016, http://www.goldreview.com/stocks/index.php?blogid=1&archive=2007-11&catid=3.

[148] Craze, M and Quiroga, J 2014, Bloomberg, Chile Lifts Tsunami Alerts After 8.2-Magnitude Quake, Accessed 10 June 2016, http://www.bloomberg.com/news/articles/2014-04-01/tsunami-alert-issued-after-magnitude-8-0-quake-off-chile-coast.

[149] Buenos Aires Herald 2014, Chile assesses the damage of massive quake, accessed 15 June 2015, http://www.buenosairesherald.com/article/156071/chile-assesses-the-damage-of-massive-quake.

[150] Teck says 'no obvious damage' at Andacollo copper mine after Chile quake 2015, Reuters, accessed 2 May 2015, http://www.reuters.com/article/chile-quake-teckresources-idUSL1N11N09P20150917.

[151] "Slope Stability". Tulane.edu. N.p., 2016. Web. 2 June 2016.

[152] Ashford S. A., Sitar N., Lysmer J., and Deng N., 1997, Topographic Effects on the Seismic Response of Steep Slopes, Bulletin of the Seismological Society of America, Vol. 87, No. 3, pp. 701-709.

[153] Allen, T.I., and Wald, D.J., 2007, Topographic slope as a proxy for global seismic site conditions (VS30) and amplification around the globe: U.S. Geological Survey Open-File Report 2007-1357, 69 p.

[154] Wilson, R.C. and Keefer, D.K., 1983. Dynamic analysis of a slope failure from the 6 August 1979 Coyote Lake, California, earthquake. Bulletin of the Seismological Society of America, 73(3), pp.863-877.

[155] Hughes, T.J., 2012. The finite element method: linear static and dynamic finite element analysis. Courier Corporation.

[156] Dai, M.L. and Li, T.C., 2007. Analysis of dynamic stability safety evaluation for complex rock slopes by strength reduction numerical method. Chinese Journal of Rock Mechanics and Engineering, 26(Suppl 1), pp.2749-2754.

[157] Chuhan, Z., Pekau, O.A., Feng, J. and Guanglun, W., 1997. Application of distinct element method in dynamic analysis of high rock slopes and blocky structures. Soil Dynamics and Earthquake Engineering, 16(6), pp.385-394.

[158] Bhasin, R. and Kaynia, A.M., 2004. Static and dynamic simulation of a 700-m high rock slope in western Norway. Engineering Geology, 71(3), pp.213-226.

[159] Yaqun, L., Haibo, L., Junru, L., Qingchun, Z. and Guangsheng, L., 2004. UDEC Simulation on Dynamic Response of Rock Slope of Huangmailing Phosphorite Mine under Explosion. Chinese Journal of Rock Mechanics and Engineering, 21.

[160] Stead, D., Eberhardt, E. and Coggan, J.S., 2006. Developments in the characterization of complex rock slope deformation and failure using numerical modelling techniques. Engineering Geology, 83(1), pp.217-235.

[161] Li, H.B., Xiao, K.Q. and Liu, Y.Q., 2007. Factor of safety analysis of bedding rock slope under seismic load. Chin J Rock Mech Eng, 26(12), pp.2385-2394.

[162] Zeng, K., Li, J., Liang, X. and Xu, J., 2011. Collapsing Mechanism of Rock Slopes in Wenchuan Earthquake. In Third International Conference on Transportation Engineering (ICTE).

[163] Kainthola, A., Singh, P.K. and Singh, T.N., 2015. Stability investigation of road cut slope in basaltic rockmass, Mahabaleshwar, India. Geoscience Frontiers, 6(6), pp.837-845.

[164] Abdallah, M.A., Shahrour, I. and Chehade, F.H., Stability Analysis of a Rock Mass in Seismic Conditions: Case Study in Lebanon.

[165] Biggs, J.M. and Biggs, J.M., 1964. Introduction to structural dynamics. McGraw-Hill College.

[166] Hudson, J.A., 1981. Wave speeds and attenuation of elastic waves in material containing cracks. Geophysical Journal International, 64(1), pp.133-150.

[167] Pyrak-Nolte, L.J., Myer, L.R. and Cook, N.G., 1990. Transmission of seismic waves across single natural fractures. Journal of Geophysical Research: Solid Earth, 95(B6), pp.8617-8638.

APPENDIX A

MODEL EXAMPLES FOR SITE EFFECT NUMERICAL ANALYSES

This appendix includes the UDEC text file inputs used in Chapter 5 analyzing the effect of topography, stiffness contrast and the coupled condition on seismic stability of slopes. Table A-1 presents the material property units used in these UDEC analyses.

Table A-1 Material properties units used in UDEC input text file

Parameter	**Unit**
Density	kg/cm^3
Distance	m
Young's Modulus	MPa
Bulk Modulus	MPa
Shear Modulus	MPa
Stress	MPa
Time	Sec

- **Topographical Effect**

Figures A-1 is an example for the geometry used in UDEC topographical effect analyses continued with the input text file, discussed in section 5.3.

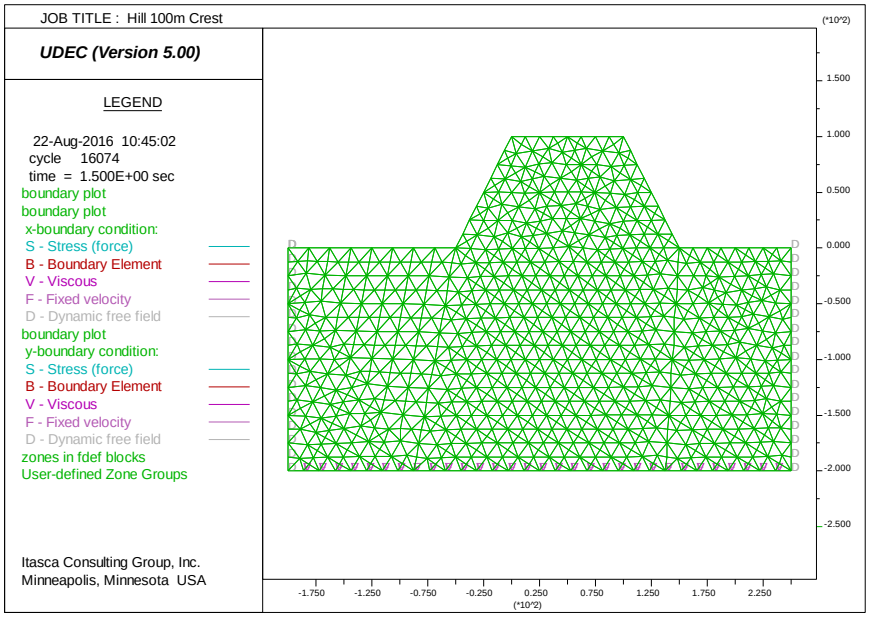

Figure A-1 Hill geometry (model 3) and boundary conditions built in UDEC.

```
;Title:Hill 100 m Crest
; --- insitu stresses (k=0.5)
; --- free-field (20 nodes) --- applied only in phase 3
;
; --- phase 1 --- gravity loading; x-fixed boundaries
;
round 0.5
edge 1
block -200,0 -50,0 0,100 100,100 150,0 250,0 250,-200 -200,-200
gen edge 20
; block properties
zone model elastic density 2.65E-3 bulk 3.333E4 shear 2E4
; boundary conditions : lateral : x-fixed ; bottom : y-fixed
boundary xvelocity 0 range -201,-199 -201,1
boundary xvelocity 0 range 249,251 -201,1
boundary yvelocity 0 range -201,251 -201,-199
; set gravity ; set in-situ stresses (total)
set gravity=0.0 -9.81
insitu stress 0.0,0.0,0.0 xgrad 0.0,0.0,0.0 ygrad 0.017885,0.0,0.02597 szz 0.0 zgrad 0.0,0.017885 ywtable 0.0 range -200,250 -200,0
```

```
solve ratio 1.0E-5 elastic

;;;;;;;;;;;;;;;;;;;;;;;;;;Dynamic;;;;;;;;;;;;;;;;;;;;
; --- phase 3 --- dynamic loading: shear wave at base of model
;  free-field lateral boundaries
;  with constant domain pressures ; no fluid flow by setting flow off
;
damping 0.05 5.0
boundary ffield
boundary xvisc ff_bulk=33333.0 ff_shear=20000.0 ff_density=0.00265 range -201,251 -
201,-199
boundary stress 0.0,0.4,0.0 history=sine(5,10) range -201,251 -201,-199
boundary yvelocity 0 range -201,251 -201,-199
reset history time disp vel
history xvelocity -40.0,100.0
history xvelocity 0.0,-200.0
history xvelocity 0.0 100.0
history yvelocity -40.0,100.0
history xdisplace -40.0,100.0
history ydisplace -40.0,100.0
history ffxvel 0 1
history ffxvel 0 2
history xdisplace -31.765602,-29.082699
history xdisplace -41.061577,100.286316
history xdisplace -39.51225,75.49704
history xdisplace -41.061577,52.25709
history xdisplace -38.737583,23.594501
history xdisplace -38.737583,1.9038887
history xvel -41.061577,52.25709
cycle  time 1.0
```

- **Topographical Effect on Faulted Slope**

Developed geometry of faulted slope is shown in Figure A-3 continued with the input text file.

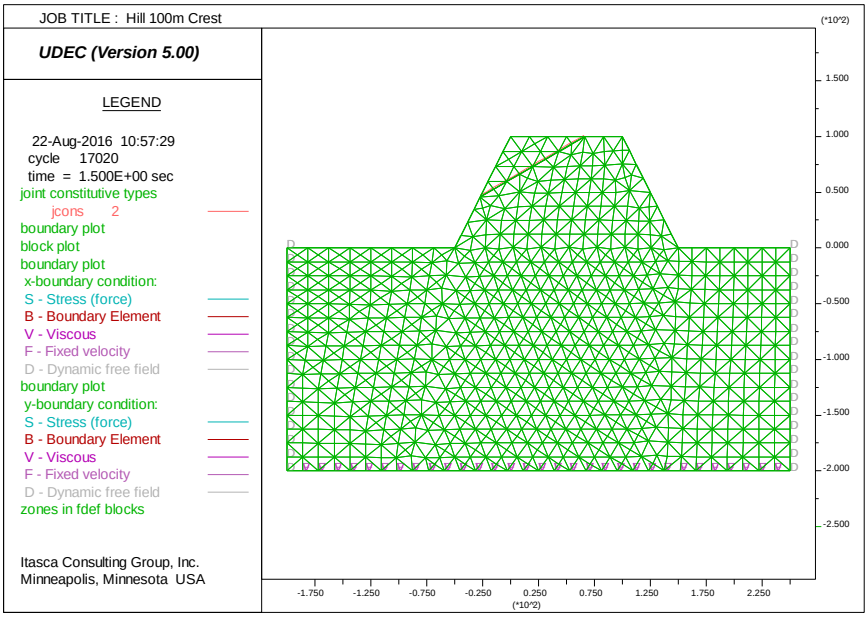

Figure A-3 Geometry and boundary conditions for topographical analyses in faulted slopes.

```
;Title:Faulted Hill 100 m Crest
; --- insitu stresses (k=0.5)
; --- free-field (20 nodes) --- applied only in phase 3
;
; --- phase 1 --- gravity loading; x-fixed boundaries
;
round 0.5
edge 1
block -200,0 -50,0 0,100 100,100 150,0 250,0 250,-200 -200,-200
jregion id 1 -200,0 200,0 200,100 -200,100
jset angle 30 spacing 200 origin -20,50 range jregion 1
gen edge 20
; block and joint properties
zone model elastic density 2.65E-3 bulk 3.333E4 shear 2E4
joint model area jks 1E3 jkn 1E3 jfriction 30 jcohesion 2 jperm 0 ares 5E-4 azero 1E-3
;
; boundary conditions : lateral : x-fixed ; bottom : y-fixed
boundary xvelocity 0 range -201,-199 -201,1
boundary xvelocity 0 range 249,251 -201,1
boundary yvelocity 0 range -201,251 -201,-199
```

```
;
; set gravity ; set in-situ stresses (total)
set gravity=0.0 -9.81
insitu stress 0.0,0.0,0.0 xgrad 0.0,0.0,0.0 ygrad 0.017885,0.0,0.02597 szz 0.0 zgrad 0.0,0.017885 ywtable 0.0 range -200,250 -200,0
solve ratio 1.0E-5 elastic

;;;;;;;;;;;;;;;;;;;;;;;;;Dynamic;;;;;;;;;;;;;;;;;;;;
; --- phase 3 --- dynamic loading: shear wave at base of model
;  free-field lateral boundaries
;  with constant domain pressures ; no fluid flow by setting flow off
;
damping 0.05 5.0
boundary ffield
boundary xvisc ff_bulk=33333.0 ff_shear=20000.0 ff_density=0.00265 range -201,251 -201,-199
boundary stress 0.0,0.4,0.0 history=sine(5,10) range -201,251 -201,-199
boundary yvelocity 0 range -201,251 -201,-199
reset history time disp vel
history xvelocity -40.0,100.0
history xvelocity 0.0,-200.0
history xvelocity 0.0 100.0
history yvelocity -40.0,100.0
history xdisplace -40.0,100.0
history ydisplace -40.0,100.0
history ffxvel 0 1
history ffxvel 0 2
history xdisplace -31.765602,-29.082699
history xdisplace -41.061577,100.286316
history xdisplace -39.51225,75.49704
history xdisplace -41.061577,52.25709
history xdisplace -38.737583,23.594501
history xdisplace -38.737583,1.9038887
history xvel -41.061577,52.25709
cycle  time 1.0
```

- **Stiffness Contrast Effect**

Figure A-3 shows the geometry used for stiffness contrast analyses followed by the input text file for the different stiffness contrast ratios described in section 5.5.

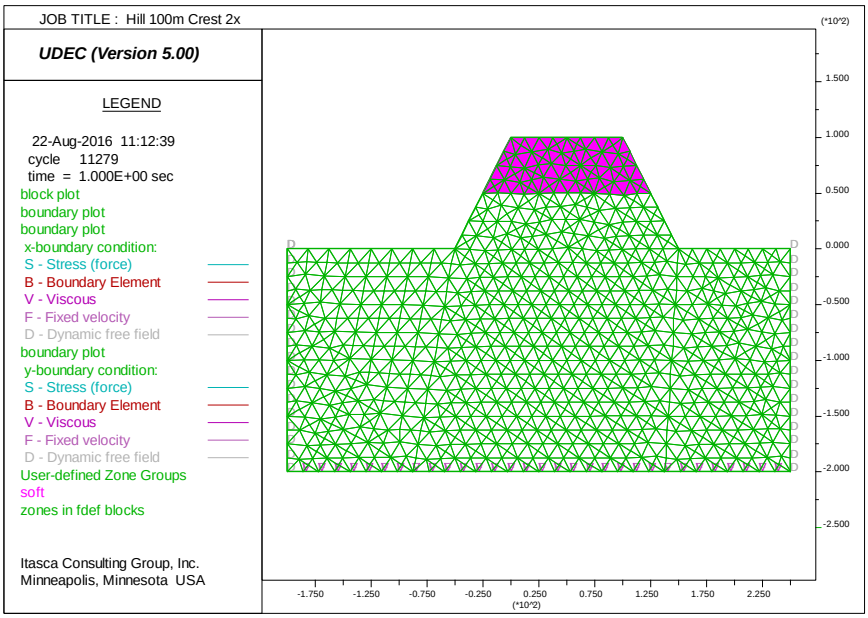

Figure A-3 Geometry and boundary conditions for stiffness contrast analyses.

```
;Title:Hill 100 m Crest
; --- insitu stresses (k=0.5)
; --- free-field (20 nodes) --- applied only in phase 3
;
; --- phase 1 --- gravity loading; x-fixed boundaries
;
round 0.5
edge 1
block -200,0 -50,0 0,100 100,100 150,0 250,0 250,-200 -200,-200
gen edge 20
; block properties
zone model elastic density 2.65E-3 bulk 3.333E4 shear 2E4
group zone 'soft' range -200,200 50,100
zone model elastic density 2.65E-3 bulk 0.33E4 shear 0.2E4 range group 'soft'
; boundary conditions : lateral : x-fixed ; bottom : y-fixed
boundary xvelocity 0 range -201,-199 -201,1
boundary xvelocity 0 range 249,251 -201,1
boundary yvelocity 0 range -201,251 -201,-199
```

```
; set gravity ; set in-situ stresses (total)
set gravity=0.0 -9.81
insitu stress 0.0,0.0,0.0 xgrad 0.0,0.0,0.0 ygrad 0.017885,0.0,0.02597 szz 0.0 zgrad 0.0,0.017885 ywtable 0.0 range -200,250 -200,0
solve ratio 1.0E-5 elastic

;;;;;;;;;;;;;;;;;;;;;;;;Dynamic;;;;;;;;;;;;;;;;;;;
; --- phase 3 --- dynamic loading: shear wave at base of model
;  free-field lateral boundaries
;  with constant domain pressures ; no fluid flow by setting flow off
;
damping 0.05 5.0
boundary ffield
boundary xvisc ff_bulk=33333.0 ff_shear=20000.0 ff_density=0.00265 range -201,251 -201,-199
boundary stress 0.0,0.4,0.0 history=sine(5,10) range -201,251 -201,-199
boundary yvelocity 0 range -201,251 -201,-199
reset history time disp vel
history xvelocity -40.0,100.0
history xvelocity 0.0,-200.0
history xvelocity 0.0 100.0
history yvelocity -40.0,100.0
history xdisplace -40.0,100.0
history ydisplace -40.0,100.0
history ffxvel 0 1
history ffxvel 0 2
history xdisplace -31.765602,-29.082699
history xdisplace -41.061577,100.286316
history xdisplace -39.51225,75.49704
history xdisplace -41.061577,52.25709
history xdisplace -38.737583,23.594501
history xdisplace -38.737583,1.9038887
history xvel -41.061577,52.25709
cycle  time 1.0
```

APPENDIX B

DATABASE ELECTRONIC FILE

This Appendix includes the electronic format of the developed database described in Chapter 3. The electronic file is a KML file type which can be opened using *mymaps.google.com* website or *Google Earth* software downloadable from *Google.com*. As discussed in Chapter 3 the KML file includes the world map with the location of natural slope and tailing dam failure, open pit mines and their corresponding earthquakes. In addition, there is a table attached to each slope presenting the available data for failure characteristics (including figures) and corresponding earthquake parameters. The data presented in this appendix is used for the earthquake parameter analyses in Chapter 4 including, Magnitude, Epi-central distance, Focal Depth and Intensity analyses by creating the network which connects all related earthquakes to each slope. Also, the geological characteristics in this database was implemented in the geological characteristics discussed in Chapter 4, including, water condition, topographical and stiffness contrast effect. Table B-1 describes the organization of the KML database.

Table B-1 Organization of the KML database

Title	**Sections and Descriptions**
Open Pit Mines	**Location** The locations open pit mines are used in the analysis of Chapter 4 on Magnitude, Epi-central distance, Focal Depth and Intensity by relating earthquakes exposed to open pit mines (see Section 4-2)

Table B-1 Continued.

	Commodity Commodities of each open pit mines are used to compare the failure type in open pit mines against natural slopes (see Section 4.5).
	Subjected Earthquakes The table attached to open pit mines section includes three largest earthquakes exposed to each mine which are used in all the earthquake parameter analyses (see Section 4.2).
Natural Slopes and Tailing Dams	**Location** This section includes, the location of all studied the natural slope and tailing dam failures and their available pictures. The location of these failures are used in all earthquake parameters analyses (see Section 4-2) and site effect analysis (see Section 4-6).
	Geological Characteristics This section includes the slope angle, water condition and material type of natural slopes and tailing dam failures. These data are utilized to compare the geological conditions of natural slope and tailing dam failures against open pit mines (see Sections 4-3 to 4-6)

Table B-1 Continued.

	Earthquake Parameters This section includes, magnitude, focal depth, epi-central distance and intensity of the earthquake triggered failure in each natural slope and tailing dam. These data are used in Chapter 4 to compare the earthquake parameters triggered natural slope and tailing dam failures against those exposed to open pit mines (see Section 4-2).
Earthquakes	This section of the database presents the considered earthquakes for earthquake analyses in Chapter 4 (see Section 4-2) classified by date and magnitude as below: - M > 9.0 from 1900 to 2010 - 8 < M < 8.9 from 1900 to 2010 - 7 < M < 7.9 from 1900 to 2010 - 6.5 < M < 6.9 from 1941 to 2010 - 6.5 < M < 6.9 from 1900 to 1941 - 8 < M < 8.9 from 1900 to 2010 - M > 5 from 2015 to 2015